Vancouver Geotechnical Society
A Local Section of the Canadian Geotechnical Society

www.v-g-s.ca

NOTICE OF UPCOMING TECHNICAL PRESENTATION

WEDNESDAY, APRIL 16, 2014

SUBJECT: **Less is more: Step Zero and back of the envelope calculations**

SPEAKER **Professor David Muir Wood**
University of Dundee, UK

David Muir Wood read Mechanical Sciences at Cambridge University, graduating in 1970. He received his PhD there in 1974 for research on the true triaxial behaviour of clays, followed by a lectureship at Cambridge from 1975-1987.

He held the Cormack Chair of Civil Engineering at Glasgow University until 1995 when he was elected to the Chair of Civil Engineering at Bristol University, becoming Dean of the Faculty of Engineering in 2003. He was Professor of Geotechnical Engineering at Dundee University from 2009-2014. He is now Affilierad professor i geoteknik at Chalmers University, Göteborg, Sweden. He was elected a Fellow of the Royal Academy of Engineering in 1998 and Fellow of the Royal Society of Edinburgh in 2012.

David Muir Wood's current research explores themes concerned with the particle continuum duality of soils. He is developing constitutive models for soils with breakable particles, for soils whose finer particles are being transported away by internal flow of water, and for soils whose mechanical response is improved by the addition of short flexible fibres. The ongoing challenge for each of these is to obtain appropriate experimental data to support the modelling hypotheses.

He has written four books: Soil behaviour and critical state soil mechanics (1990), Geotechnical modelling (2004), Soil mechanics: a one-dimensional introduction (2009), Civil engineering: a very short introduction (2012).

CONTENT: Before embarking on complex numerical modelling or physical modelling, Step 0 is 'to write down the answer'. If you have no idea what answer to expect then you will not recognise when the modelling has gone awry. Step 0 estimates are best supported by 'back of the envelope' calculations which may be based on simplified modelling which manages to include the important mechanisms of response. 'System' as opposed to 'element' treatment is often possible.

One example is the use of parabolic isochrones for analysis of consolidation. Such a system model can be used to estimate the progress of consolidation around an embankment on soft clay with vertical drains.

The volume shrinkage that occurs in cement/soil mixtures as the cement hydrates leads to pore pressure changes. Careful consideration of the processes involved leads to a rather simple governing equation for which an analytical solution is available. The problem of an

undersea pipeline sliding on a consolidating interface is also amenable to rather simple treatment.

These are examples in which formulating the problem in terms of dimensionless quantities produces results which may be approximate but are capable of rather general application - particularly in support of Step 0 estimates.

DETAILS

Executive Inn, 4201 Lougheed Highway, Burnaby, BC V5C 3Y6 (Phone: 604-298-2010)
Social Hour: 5:30 to 6:30 pm (drinks available at the hotel bar)
Technical Presentation: 6:30 to 7:30 pm
Dinner: 7:45 pm ($30 will be charged for dinner)
If you would like to stay for dinner please RSVP to ali.amini@shaw.ca or at the door with Robyn Barnett.

Less is more:

Step 0 and back-of-the-envelope calculations

David Muir Wood

Chalmers University, Göteborg, Sweden

(Dundee University, United Kingdom)

d.muirwood@dundee.ac.uk

April 2014

Less is more

- introduction
- consolidation analysis using parabolic isochrones
- application to embankment on soft clay
- behaviour of hydrating cement/soil mixture
- pipeline-seabed interaction
- conclusion

UNIVERSITY OF DUNDEE

Less is more

- introduction
- consolidation analysis using parabolic isochrones
- application to embankment on soft clay
- behaviour of hydrating cement/soil mixture
- pipeline-seabed interaction
- conclusion

UNIVERSITY OF DUNDEE

Less is more

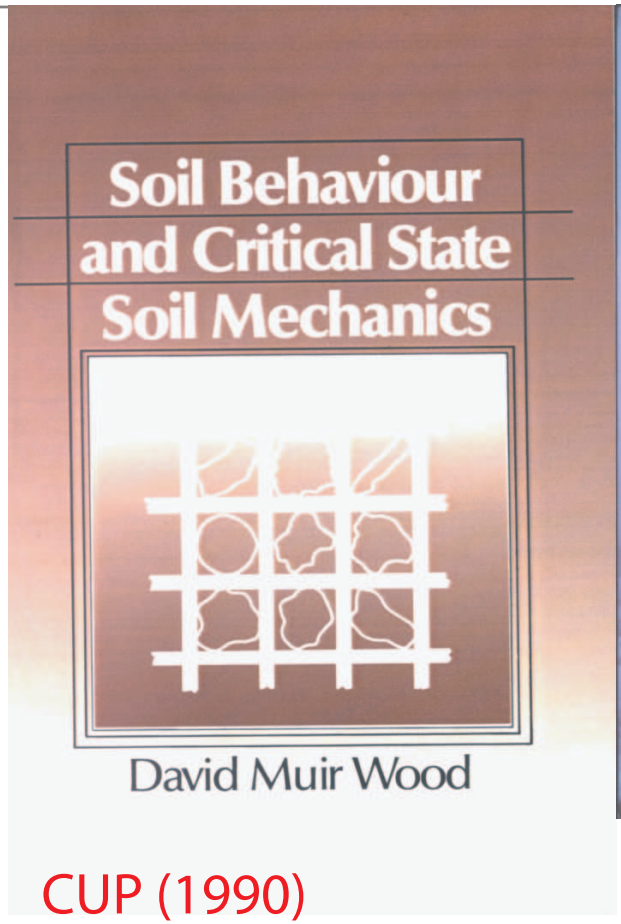

CUP (1990)

Spon (2004)

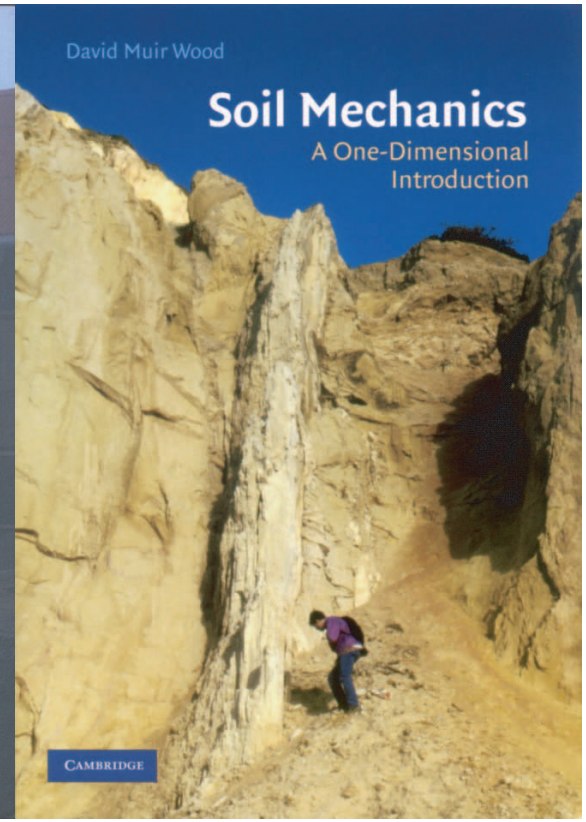

CUP (2009)

UNIVERSITY OF DUNDEE

Less is more

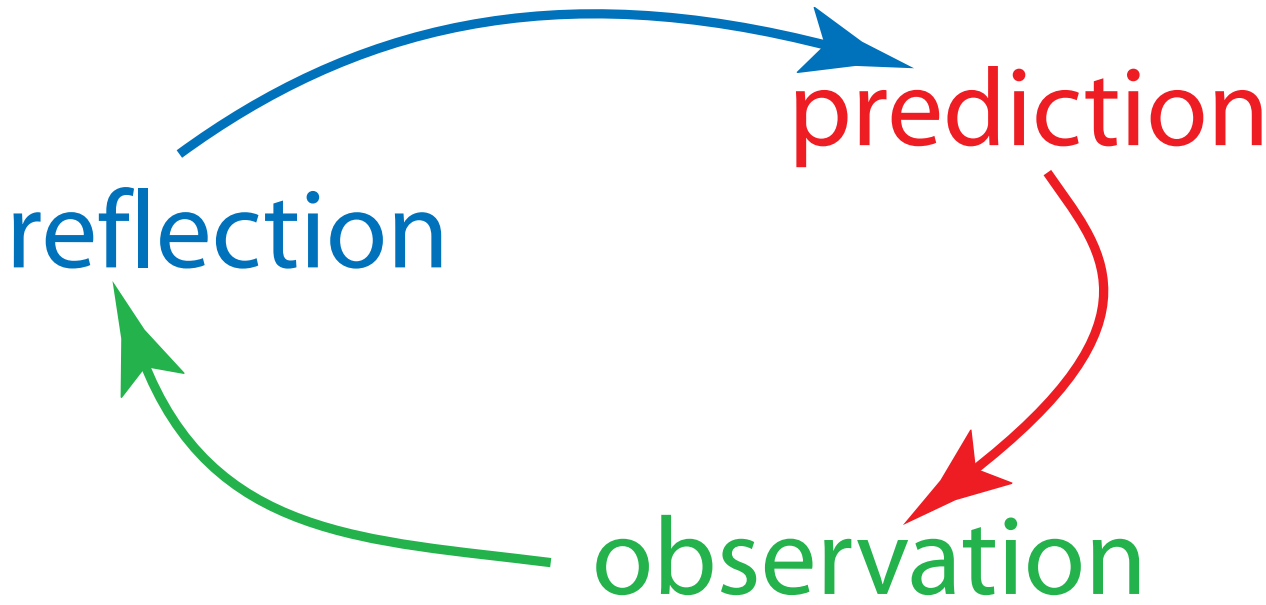

- Soil modelling: **Step 0**: *before you switch on the computer*...
- ...write down the answer!
- always start with *prediction*
- if subsequent *observation* unexpected...
- *reflection* required to improve *prediction* (understanding)

UNIVERSITY OF DUNDEE

Less is more

- closed-form analyses rare (elastic systems)
- numerical analysis possibly heavy-handed way of seeking geotechnical insight
- macroelement: intermediate technique
- rapid estimates; plausible representation of mechanisms; dimensionless (normalised) results - immediately transferable

UNIVERSITY OF DUNDEE

Less is more

- consolidation analysis using parabolic isochrones
- application to embankment on soft clay
- behaviour of hydrating cement/soil mixture
- pipeline-seabed interaction

UNIVERSITY OF DUNDEE

Less is more

- introduction
- consolidation analysis using parabolic isochrones
- application to embankment on soft clay
- behaviour of hydrating cement/soil mixture
- pipeline-seabed interaction
- conclusion

UNIVERSITY OF DUNDEE

Parabolic isochrones

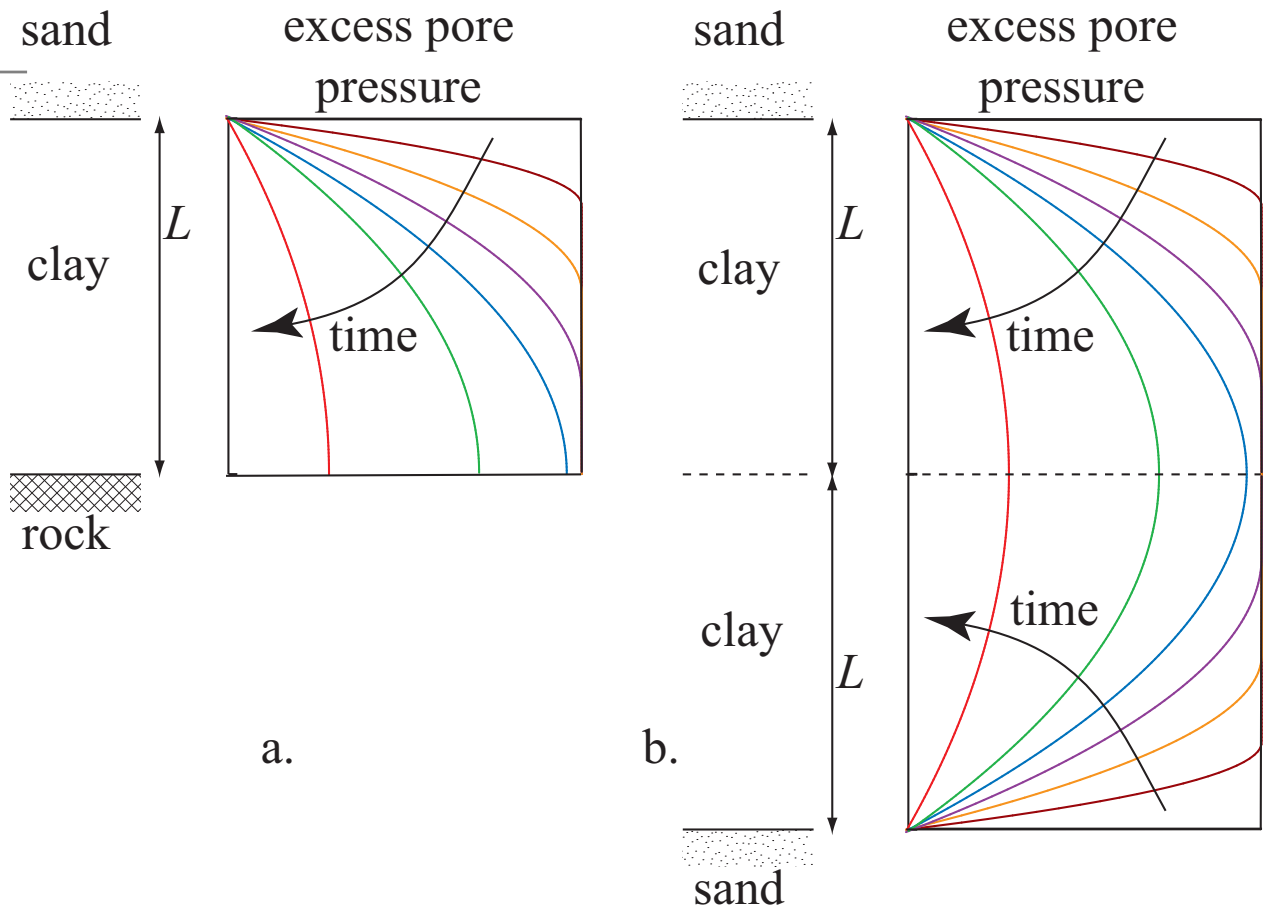

- analysis of consolidation
- boundary conditions applied at *system* (not element) level
- assume parabolic mode shape at all times

Parabolic isochrones

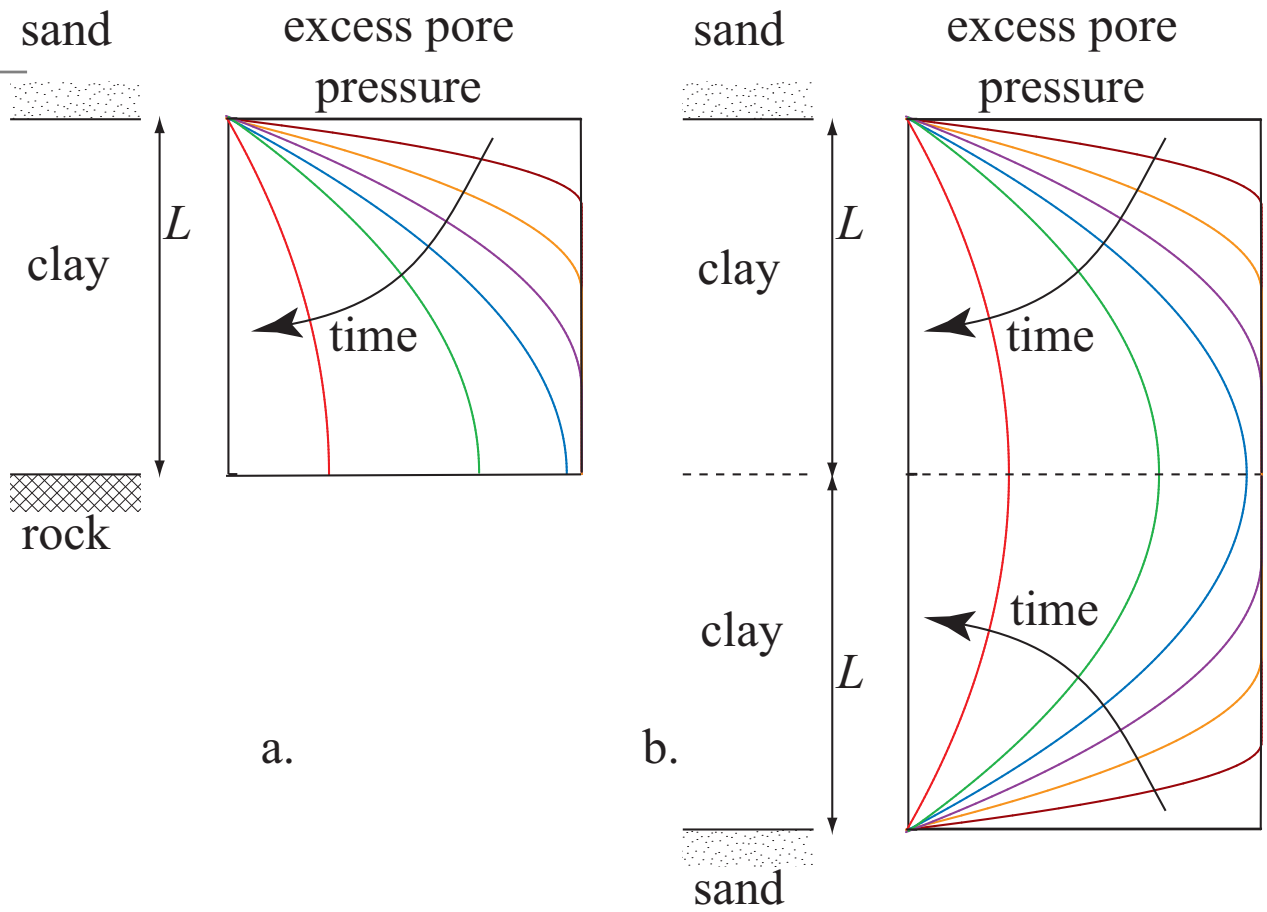

- rate of volume compression through increase of effective stress
- balances rate of outflow of water at drainage boundary
- system analysis

UNIVERSITY OF DUNDEE

Parabolic isochrones

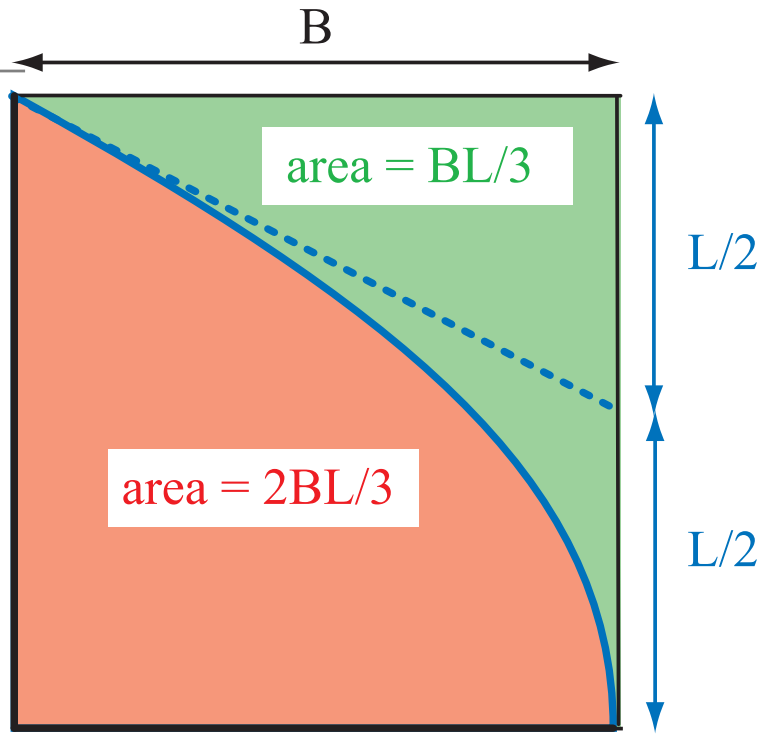

- geometry of parabola
- area = 2/3 enclosing rectangle (transfer of pore pressure to effective stress)
- exit gradient = 2$\times$ diagonal of enclosing rectangle (seepage velocity)

UNIVERSITY OF DUNDEE

Parabolic isochrones: first response regime

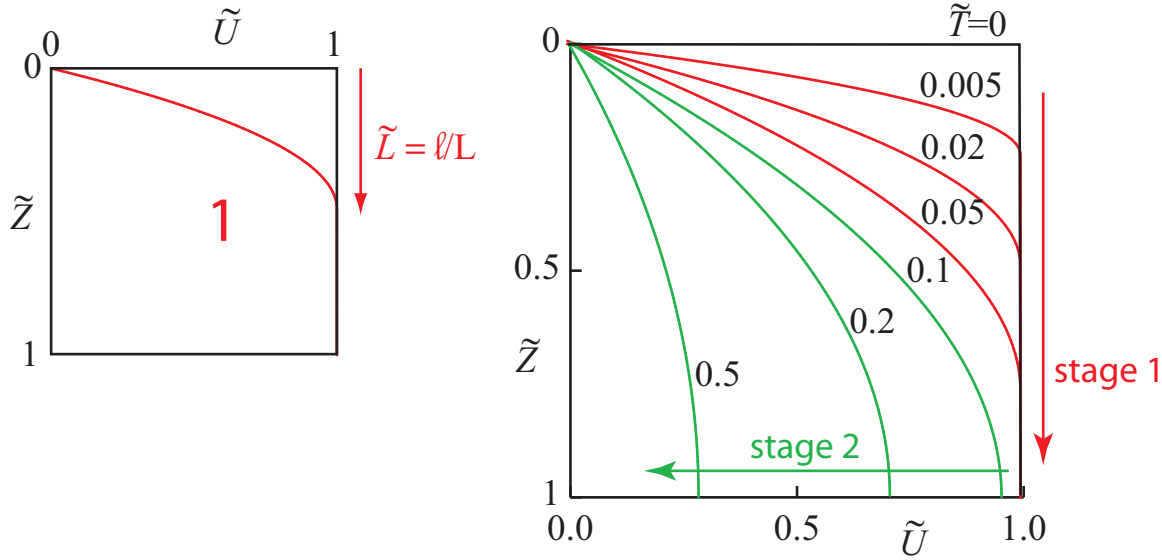

1: consolidation front penetrates layer to depth $\ell = \tilde{L}L$

$$\frac{2ku_i}{\gamma_w \ell} = \frac{\mathrm{d}}{\mathrm{d}t}\left(\frac{u_i \ell}{3E_o}\right); \quad \tilde{L}\frac{\mathrm{d}\tilde{L}}{\mathrm{d}\tilde{T}} = 6; \quad \tilde{L} = \sqrt{12\tilde{T}}$$

until $\tilde{L} = 1$, $\tilde{T} = 1/12$

$\tilde{U} = u/u_i$, $\tilde{T} = kE_o t/\gamma_w L^2 = c_v t/L^2$

UNIVERSITY OF DUNDEE

Parabolic isochrones

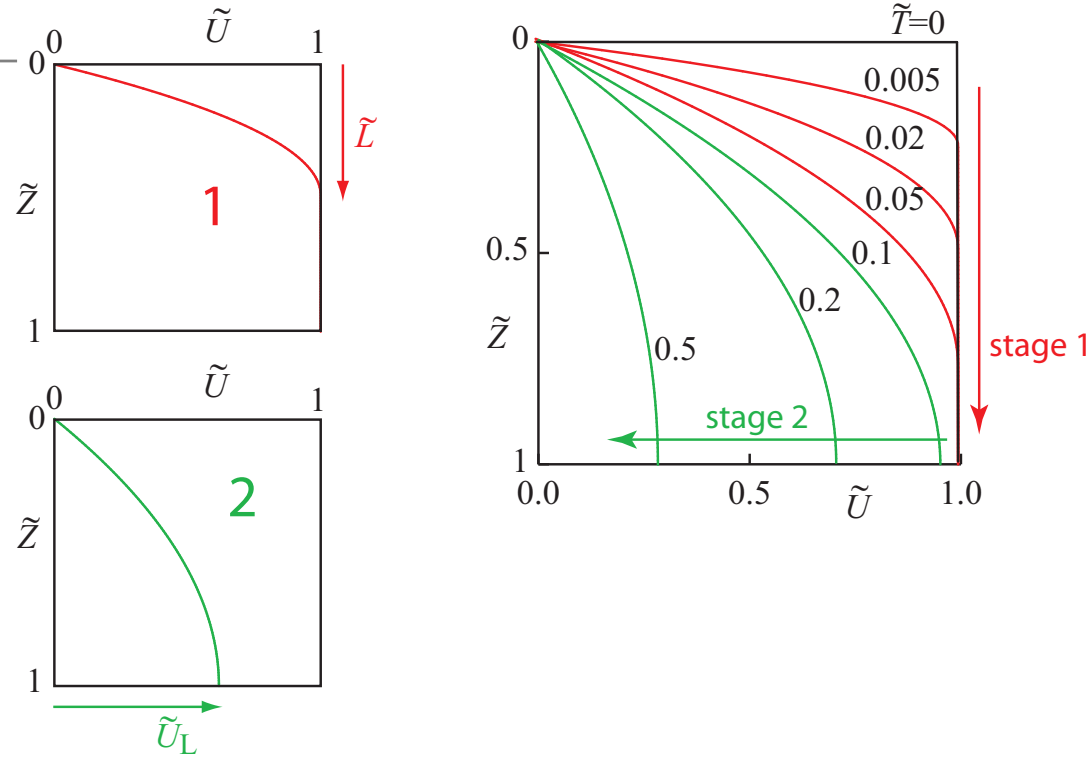

2: pore pressure decays throughout layer

$$\frac{2ku_L}{\gamma_w L} = \frac{1}{E_o}\frac{\mathrm{d}}{\mathrm{d}t}\left(u_i L - \frac{2}{3}u_L L\right); \quad \frac{\mathrm{d}\tilde{U}_L}{\mathrm{d}\tilde{T}} = -3\tilde{U}_L$$

$$\tilde{U}_L = \exp\left[-3(\tilde{T} - 1/12)\right]$$

Parabolic isochrones

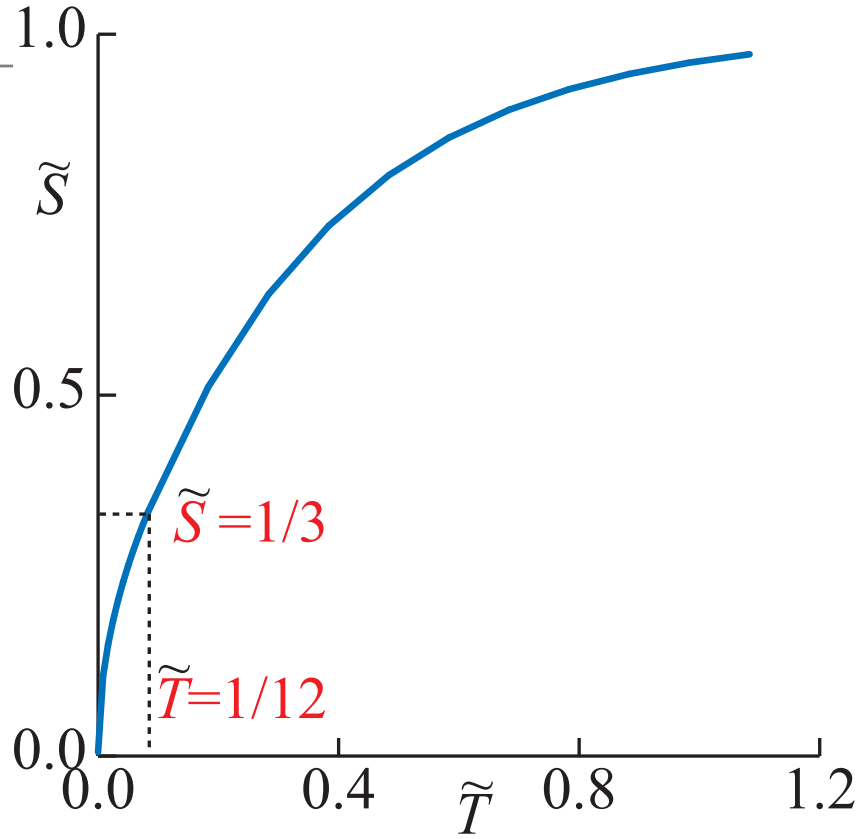

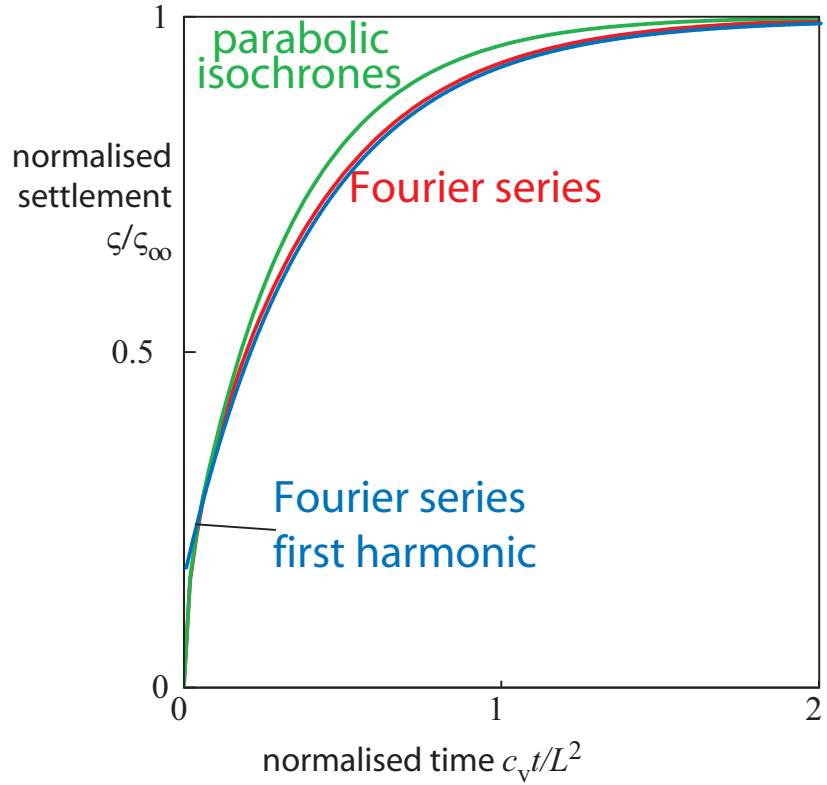

- assumed mode shape (parabola, sine function)
- no further need to consider elemental response within system
- first order ordinary differential equation instead of second order partial differential equation

UNIVERSITY OF DUNDEE

Less is more

- introduction
- consolidation analysis using parabolic isochrones
- application to embankment on soft clay
- behaviour of hydrating cement/soil mixture
- pipeline-seabed interaction
- conclusion

UNIVERSITY OF DUNDEE

embankment on soft clay

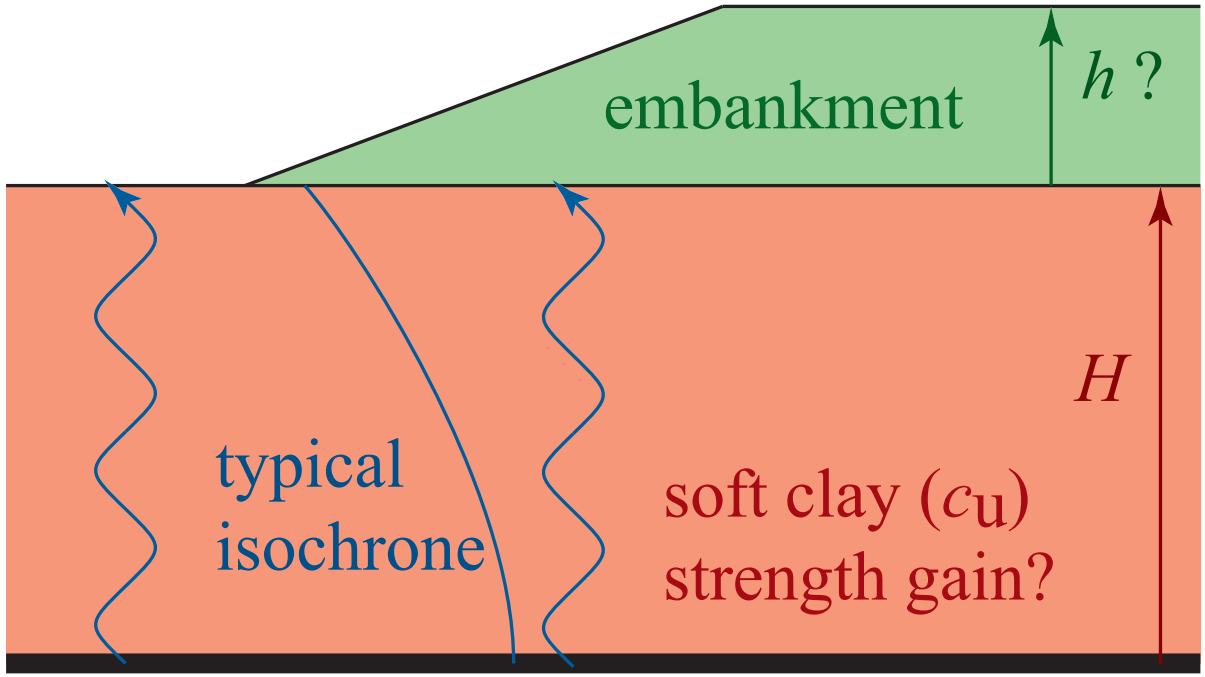

- what is safe height for rapid construction of embankment?
- can we estimate benefit of vertical drains?

UNIVERSITY OF DUNDEE

embankment on soft clay

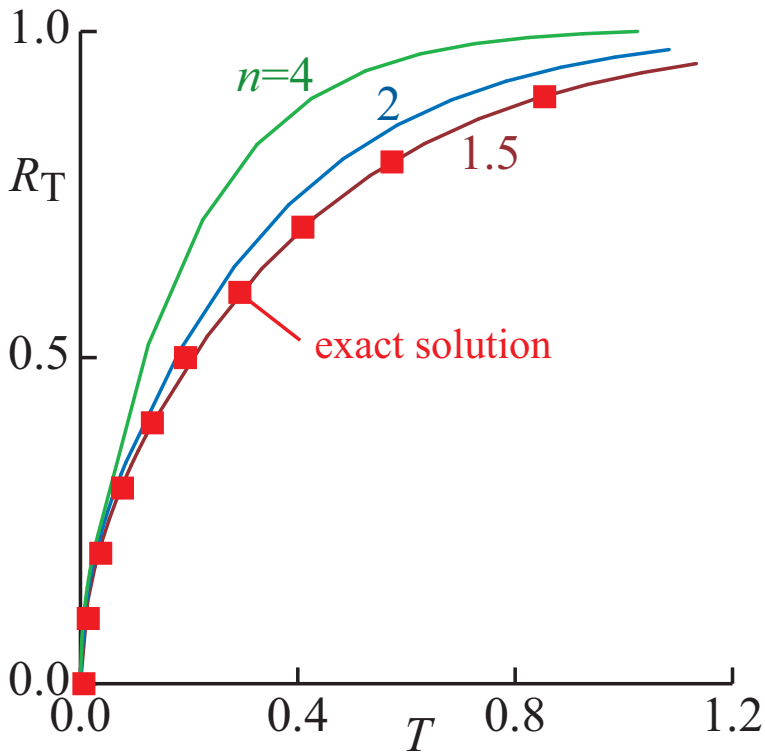

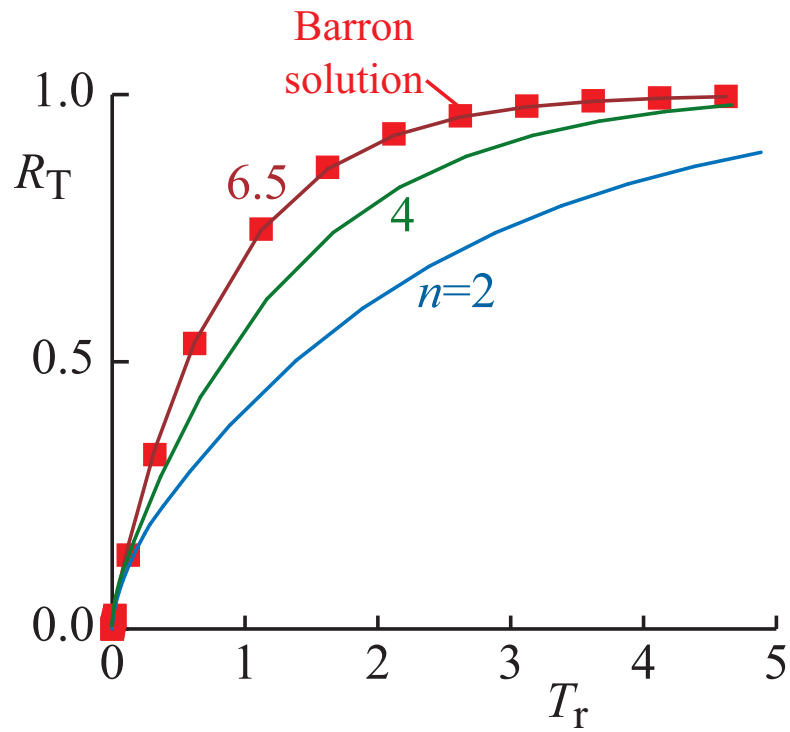

- exponent n in mode shape (=2 for parabola) essentially arbitrary - best fit 1-D: $n \sim 1.5$
- consolidation with radial flow: $n \sim 6.5$ ($r_m/r_o = 10.5$)

UNIVERSITY OF DUNDEE

embankment on soft clay

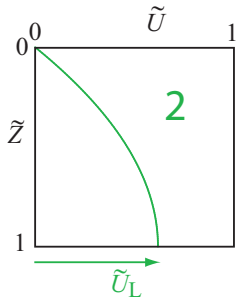

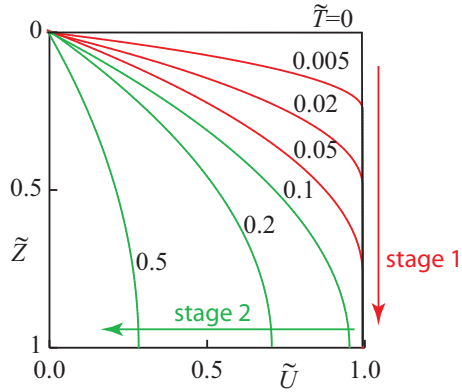

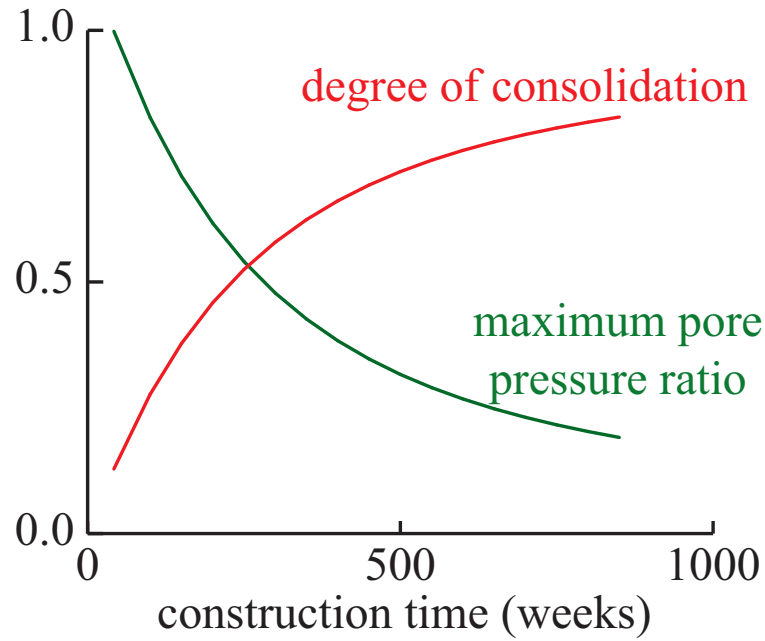

- power-law parabolic consolidation: in stage 2?
- governing equation includes increasing total stress:

$$\frac{n}{n+1}\frac{\mathrm{d}\bar{u}}{\mathrm{d}\bar{t}} + n\bar{u} = \frac{\mathrm{d}\bar{\sigma}_v}{\mathrm{d}\bar{t}} = \text{(constant)} \qquad \bar{u} = \frac{u}{\gamma h}; \bar{t} = \frac{c_v t}{H^2}$$

UNIVERSITY OF DUNDEE

embankment on soft clay

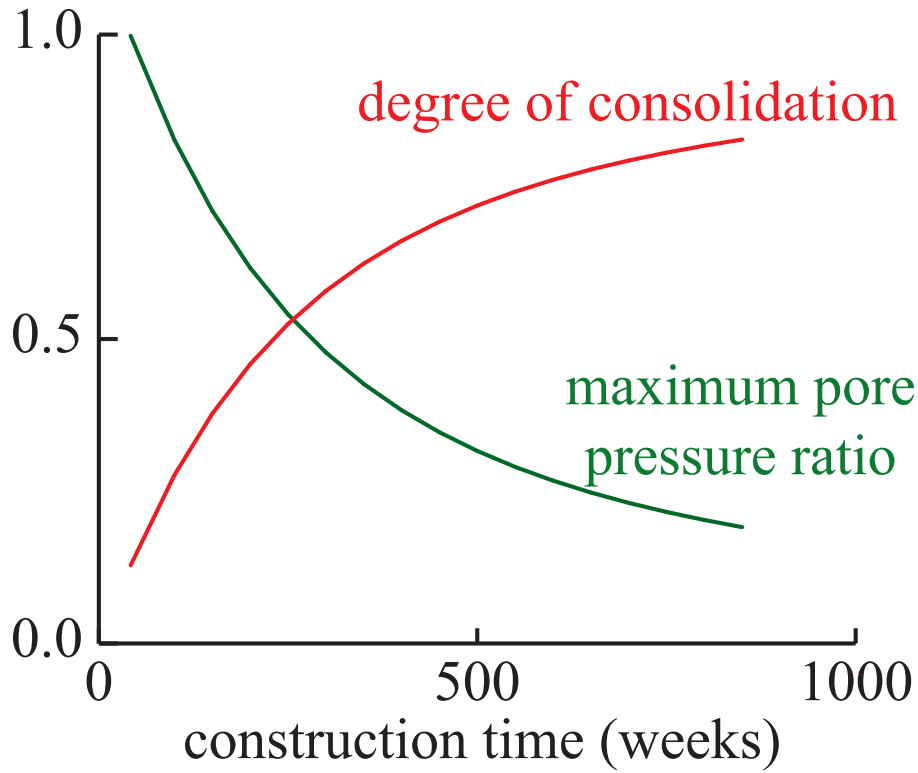

- long construction time for significant consolidation
- time < 40 weeks, assumption of stage 2 pore pressure breaks down
- loading varies with position - strength gain varies with position

UNIVERSITY OF DUNDEE

embankment on soft clay

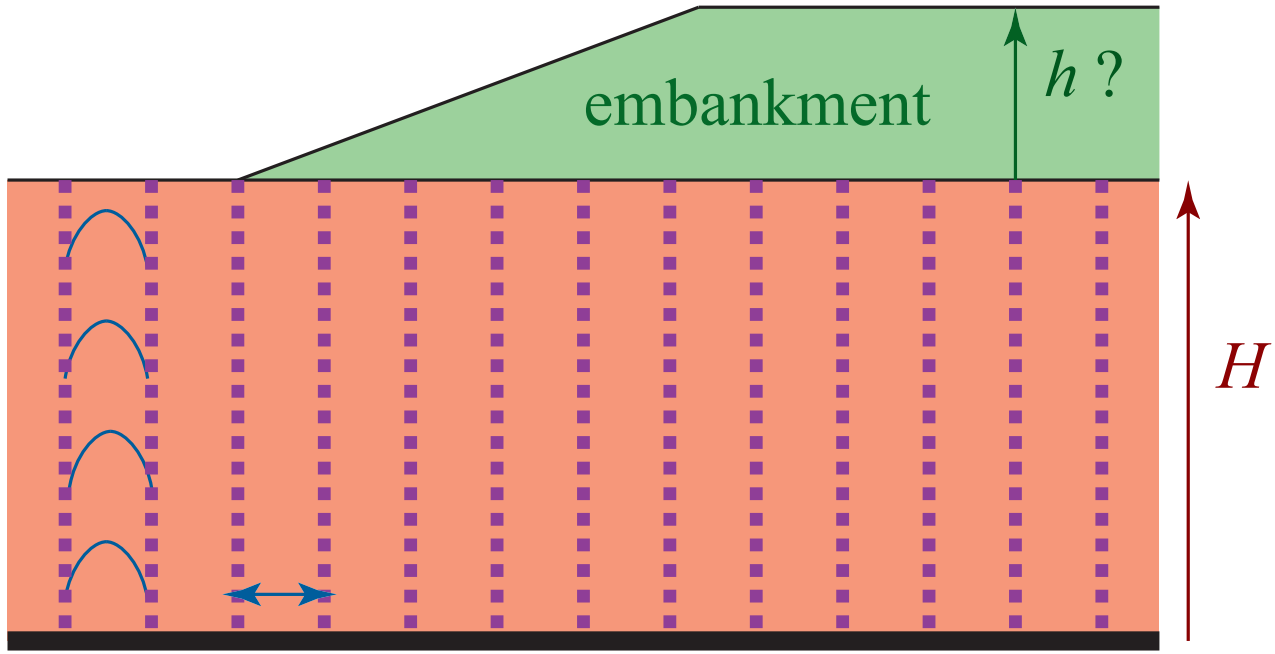

- array of drains reduces flow path
- consolidation essentially uniform over each vertical section
- strength gain from local degree of consolidation and local vertical stress increment

UNIVERSITY OF DUNDEE

embankment on soft clay

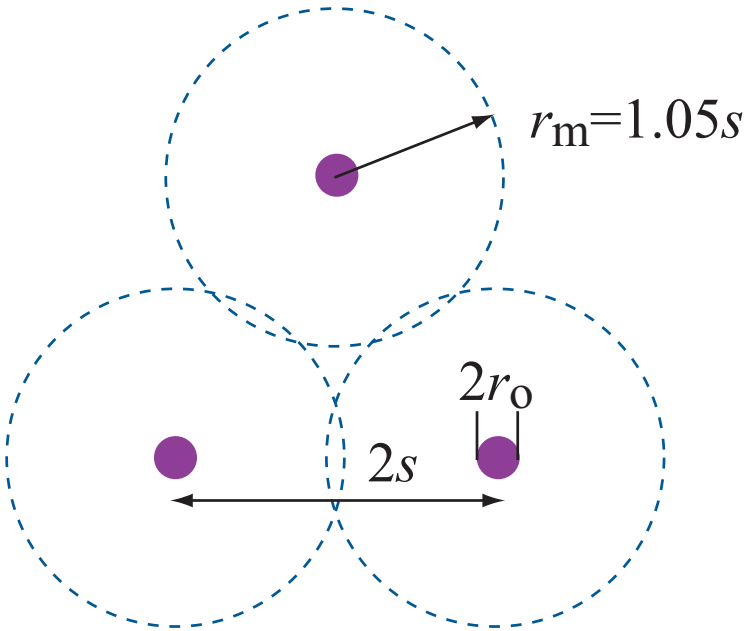

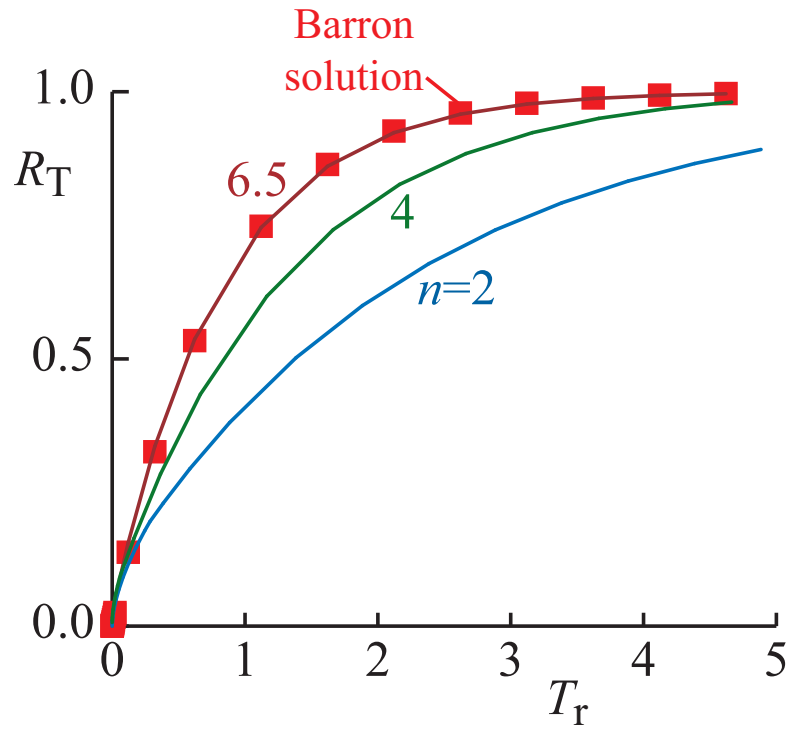

- array of vertical drains - spacing - radius of influence
- consolidation with radial flow: $n \sim 6.5$ ($r_m/r_o = 10.5$)

UNIVERSITY OF DUNDEE

embankment on soft clay

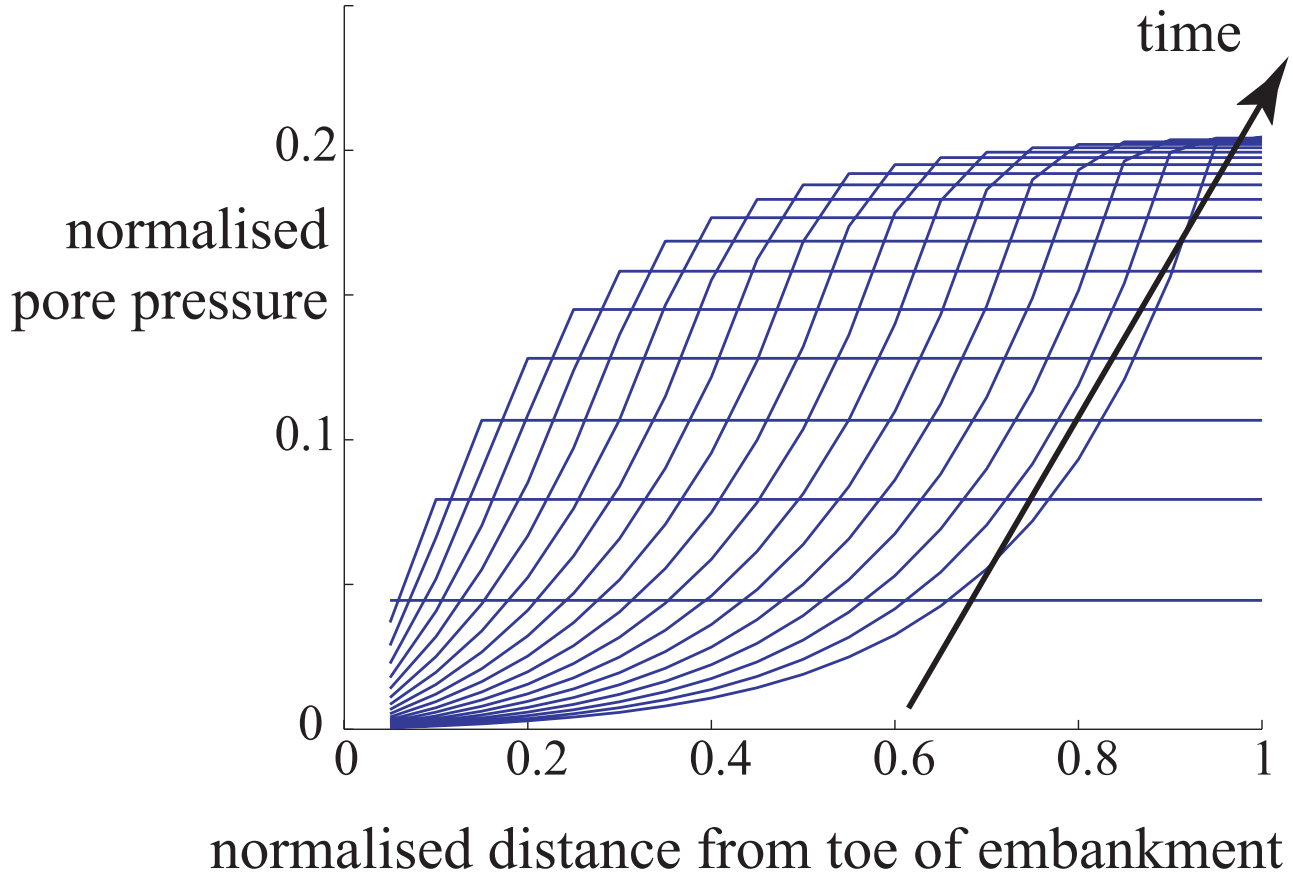

- maximum loading varies with position and time
- nearer toe, pore pressure lower, consolidation more complete

UNIVERSITY OF DUNDEE

embankment on soft clay

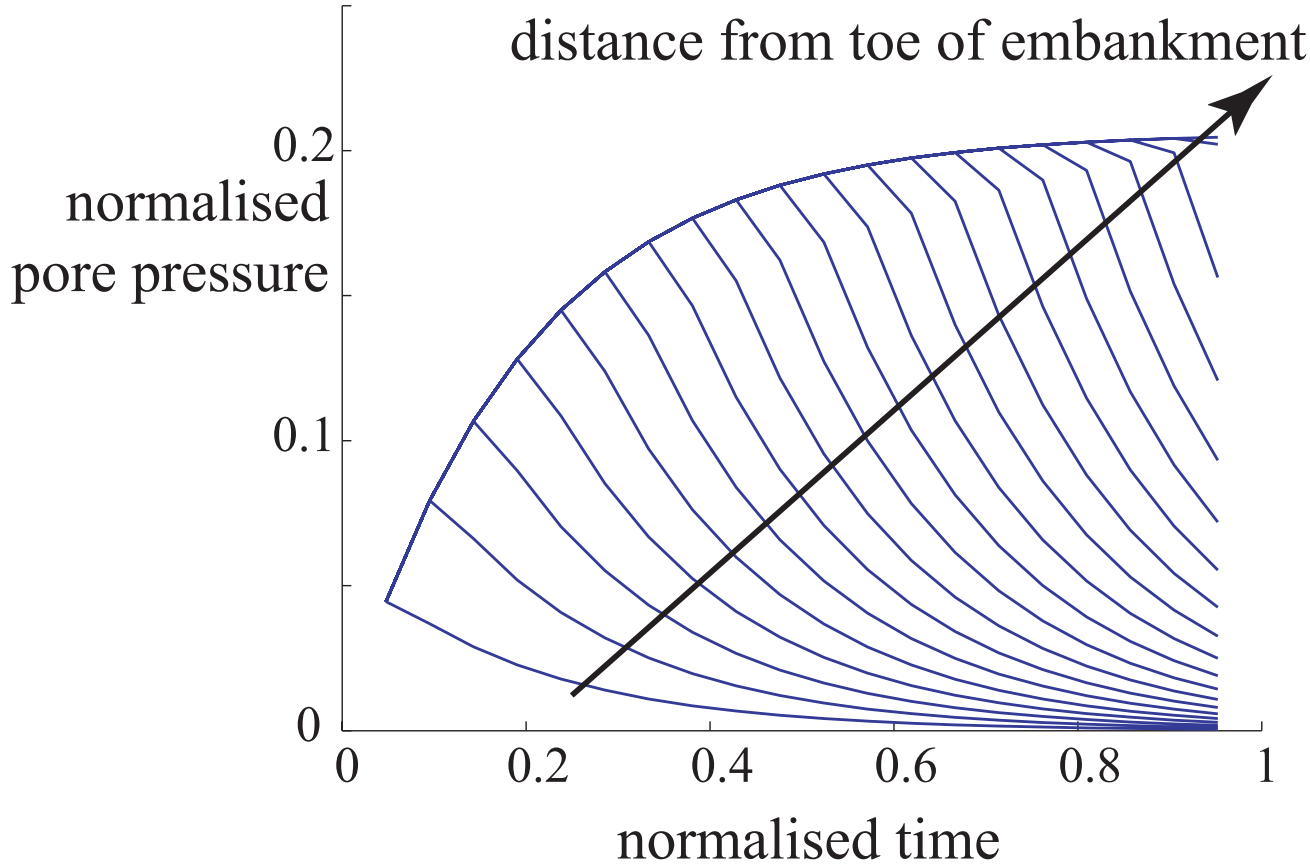

- maximum loading varies with position and time
- nearer toe, pore pressure lower, consolidation more complete

UNIVERSITY OF DUNDEE

embankment on soft clay

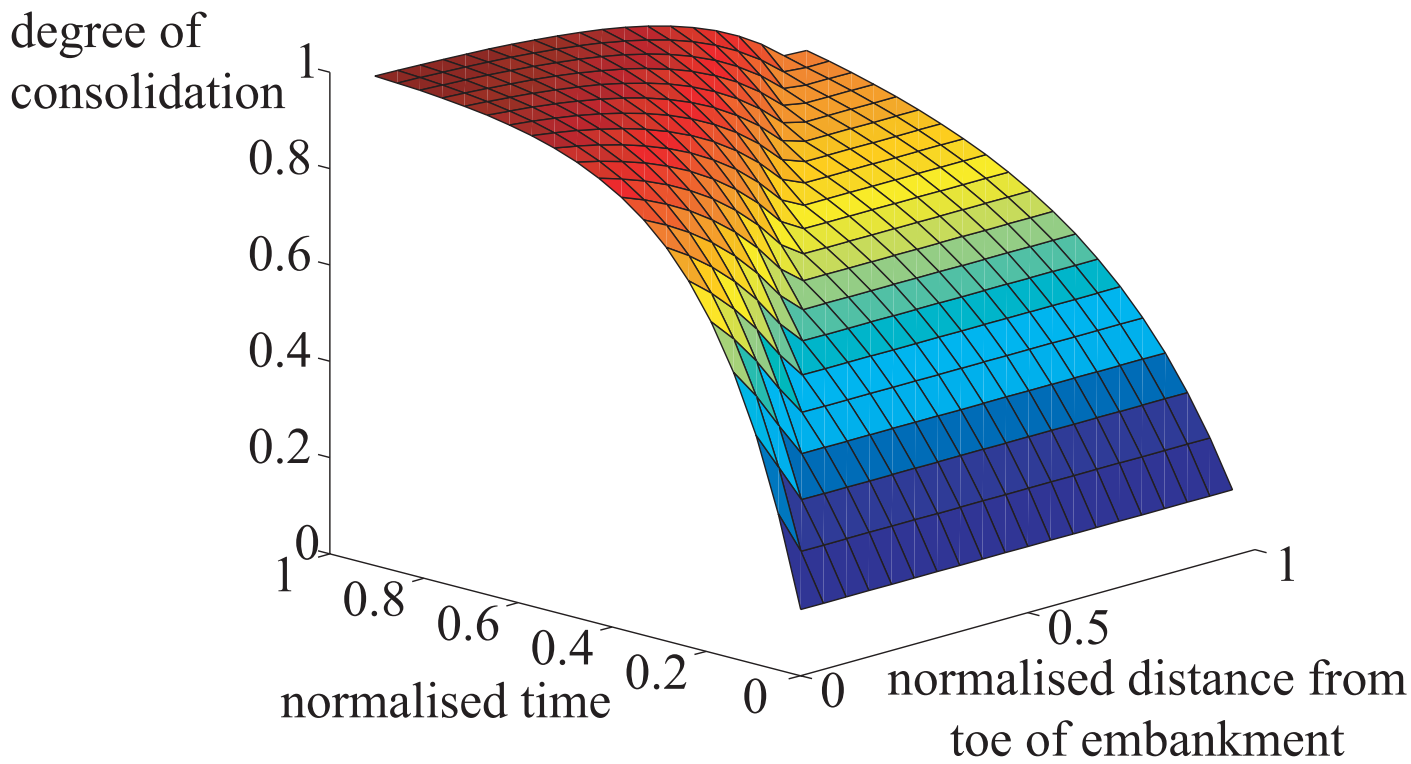

- degree of consolidation - position - time

embankment on soft clay

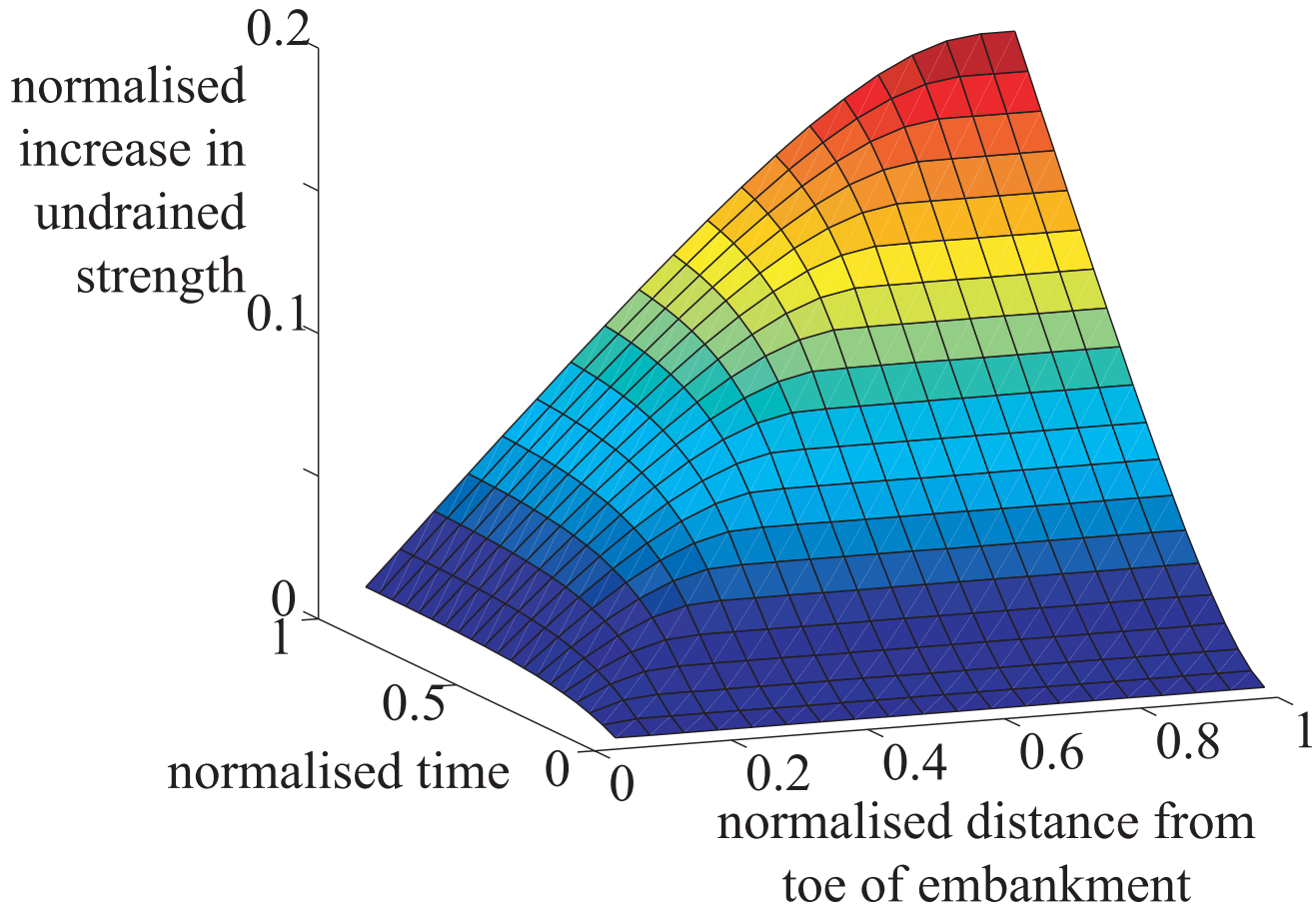

- strength gain - degree of consolidation $\times \alpha \Delta \sigma_v$; $\alpha \sim 0.2$?

embankment on soft clay

- application of ‘power-law’ isochrones (generalisation of parabolic isochrones)
- dimensionless results - wider applicability
- system response - simple equations

UNIVERSITY OF DUNDEE

Less is more

- introduction
- consolidation analysis using parabolic isochrones
- application to embankment on soft clay
- behaviour of hydrating cement/soil mixture
- pipeline-seabed interaction
- conclusion

UNIVERSITY OF DUNDEE

Consolidation of cement paste

- effective stress development in cement-paste mine backfill, bored piles
- cement hydration leads to volume change
- complicated problem - many soil properties
- develop governing dimensionless equation - general solution - one controlling property (non-dimensional group of properties)
- exact solutions for one-dimensional and axisymmetric problems; finite difference solutions - finite element calculations - parabolic isochrone approximation

UNIVERSITY OF DUNDEE

Volume changes in hydrating element

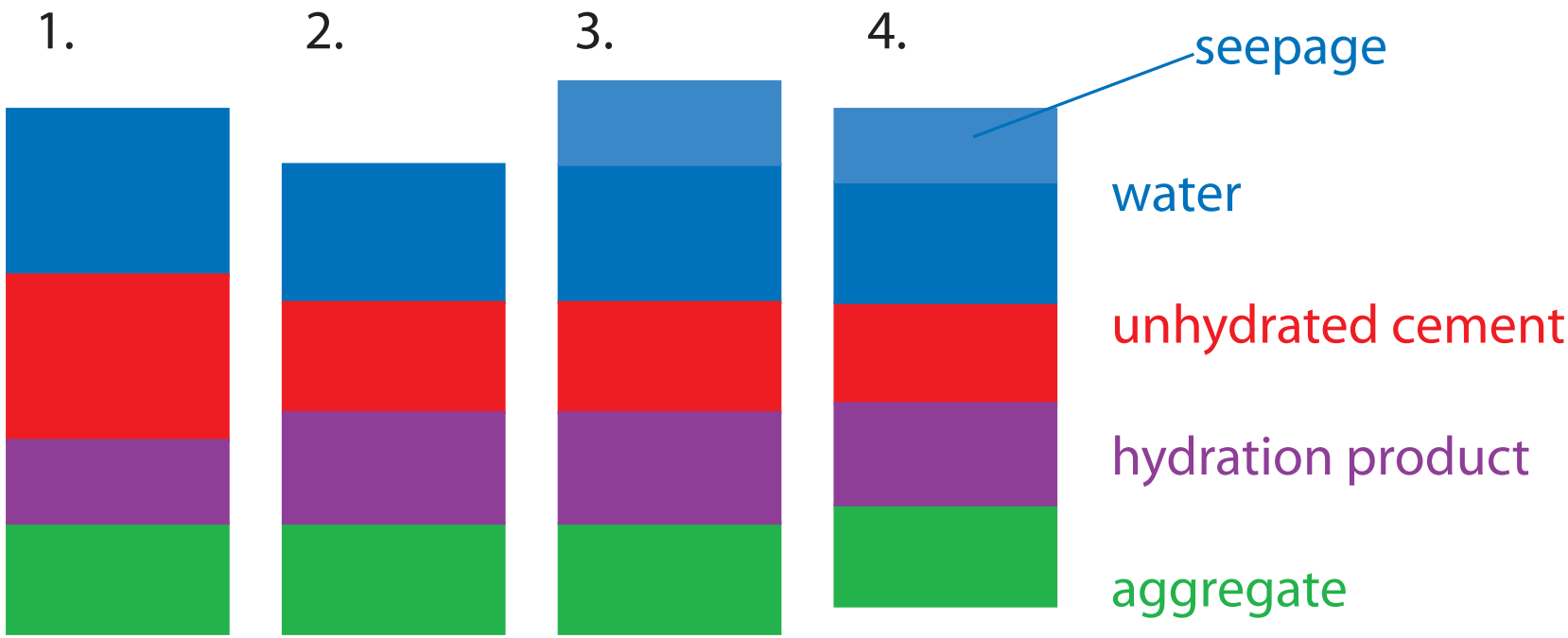

1. initial state
2. volume of hydration products increases; : volume of cement and water decreases
3. volume change resulting from seepage flow
4. pore pressure change: change in effective stress; compression of solid skeleton, compression of pore water

UNIVERSITY OF DUNDEE

Governing equation

finite layer thickness H

dimensionless coordinate $\tilde{x} = x/H$

coefficient of consolidation $c_v = kE^*/\rho_w g$

dimensionless time $\tilde{t} = c_v t/H^2$

dimensionless rate of hydration $\kappa^* = \kappa H^2/c_v$

dimensionless pore pressure $\tilde{u} = u/E^*\alpha\nu_{co}$

$\alpha\nu_{co}$ is eventual volume loss through hydration

$$\kappa^* \exp(-\kappa^* \tilde{t}) - \frac{\partial^2 \tilde{u}}{\partial \tilde{x}^2} + \frac{\partial \tilde{u}}{\partial \tilde{t}} = 0$$

diffusion equation with time-dependent source

UNIVERSITY OF DUNDEE

Finite layer with one impermeable boundary

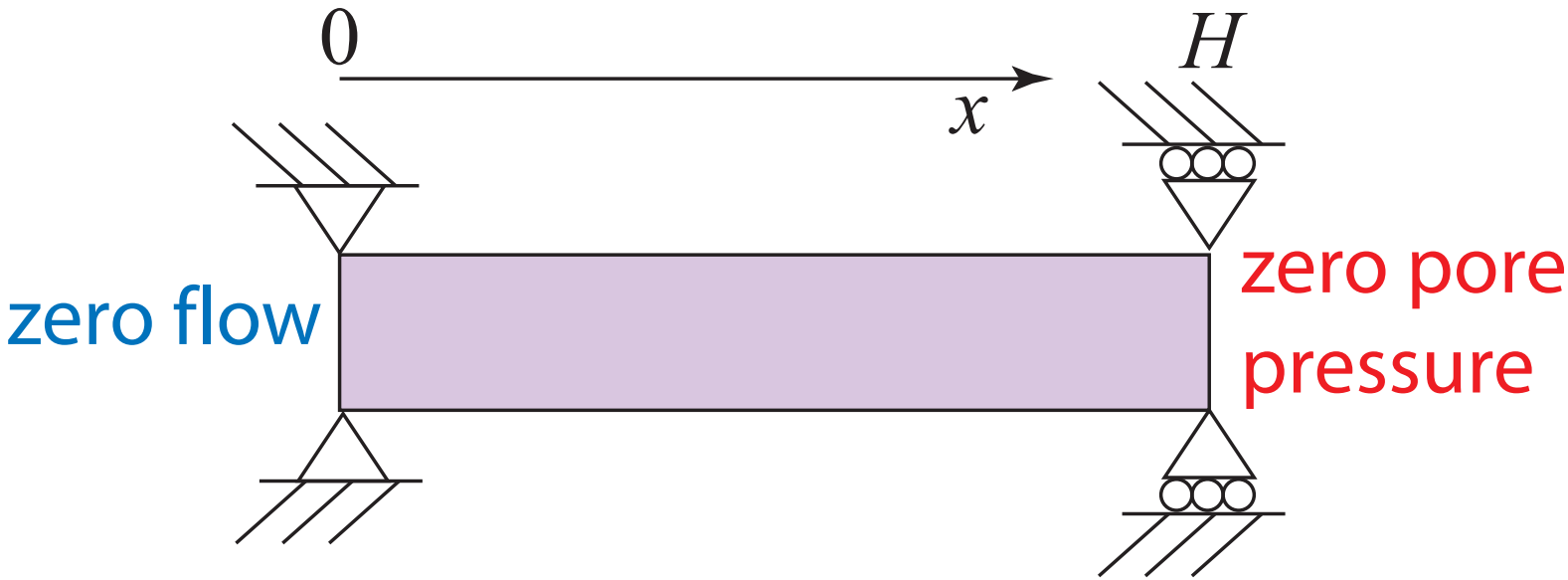

boundary conditions:

$\mathrm{d}\tilde{u}/\mathrm{d}\tilde{x} = 0$ at $\tilde{x} = 0$

$\tilde{u} = 0$ at $\tilde{x} = 1$

$\tilde{u} \to 0$ as $\tilde{t} \to \infty$

at time $\tilde{t} = 0$, $\tilde{u} = 0$ for $0 < \tilde{x} < 1$

Finite layer with one impermeable boundary

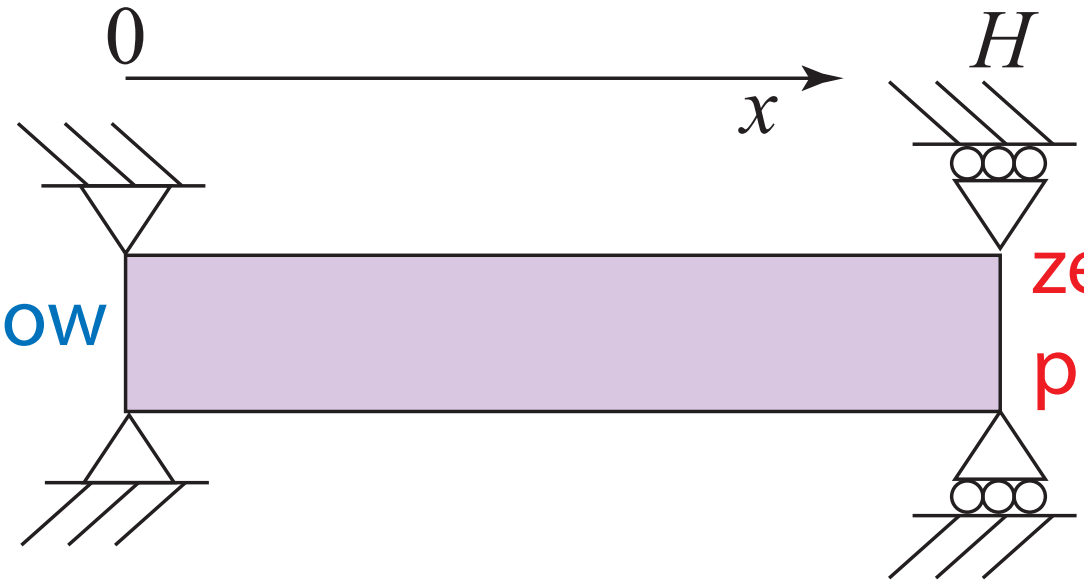

$$\tilde{u} = \frac{4\kappa^*}{\pi} \sum_{m=0}^{\infty} (-1)^{m+1} \cos\left[(2m+1)\frac{\pi}{2}\tilde{x}\right] \times$$

$$\times \frac{1}{(\pi^2(2m+1)^2/4 - \kappa^*)} \left[\exp(-\kappa^*\tilde{t}) - \exp(-\tilde{t}(\pi^2(2m+1)^2/4))\right.$$

(Carslaw and Jaeger)

UNIVERSITY OF DUNDEE

One-dimensional analysis

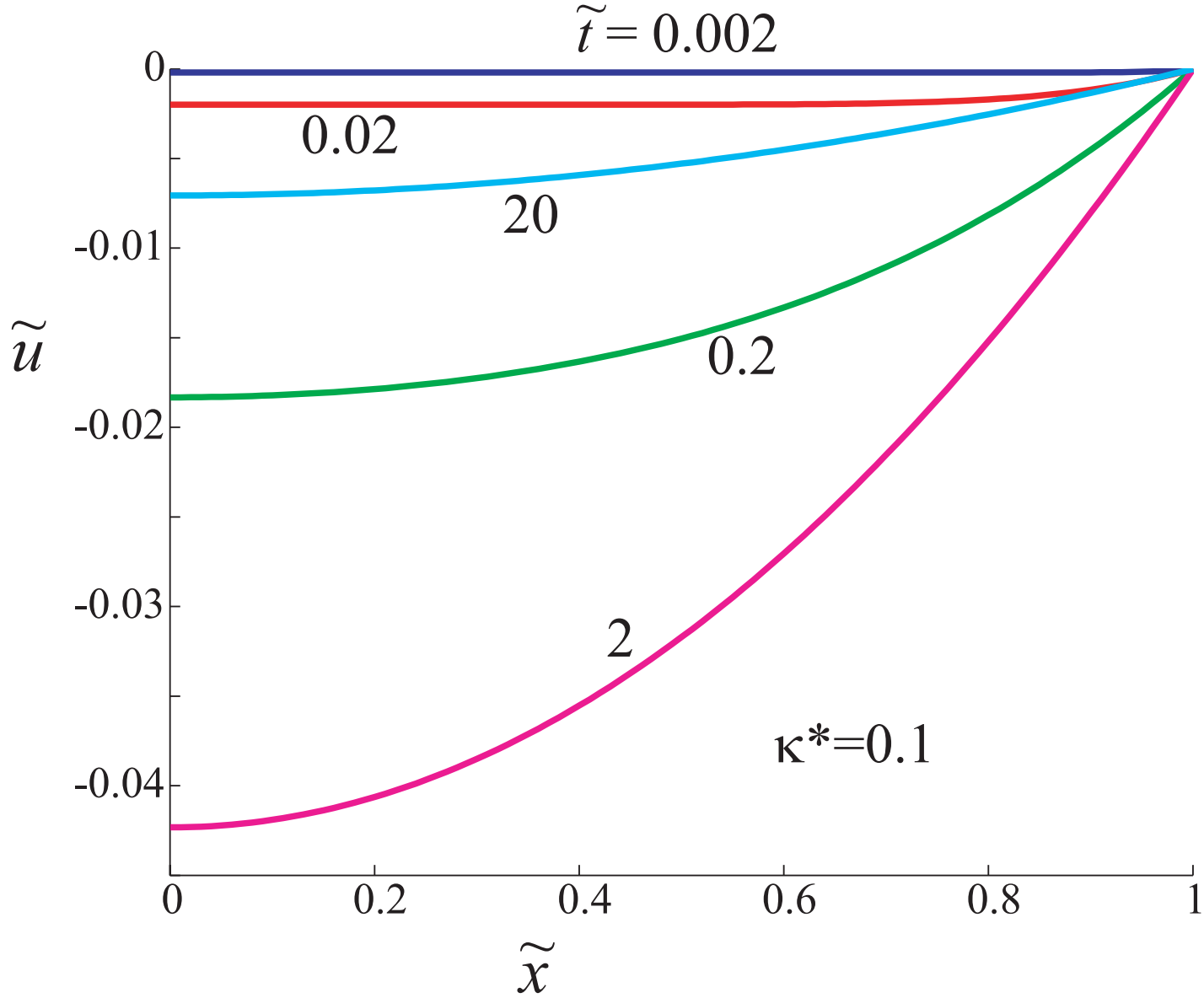

isochrones for pore pressure in concrete

One-dimensional analysis

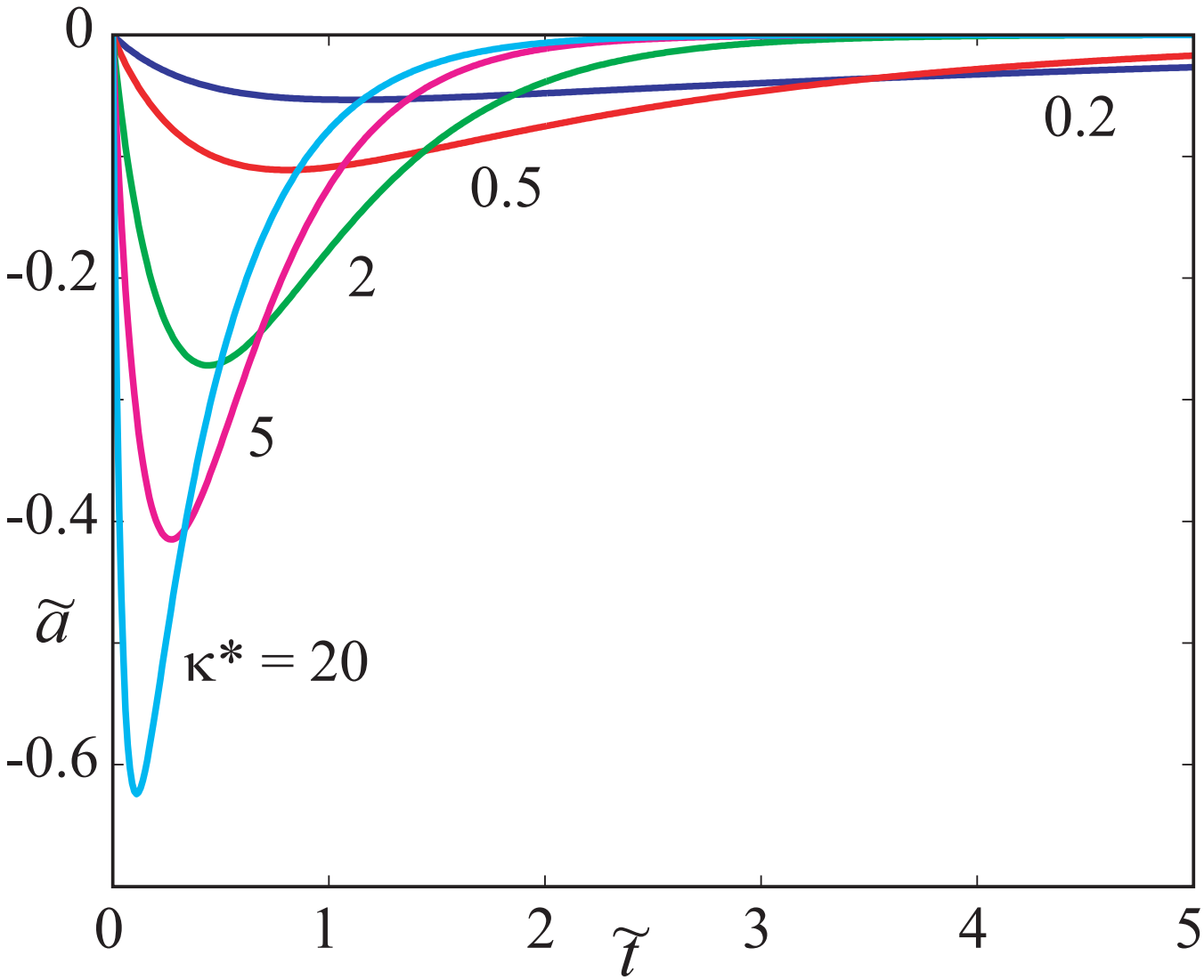

displacement at free boundary

Analytical and ABAQUS solution

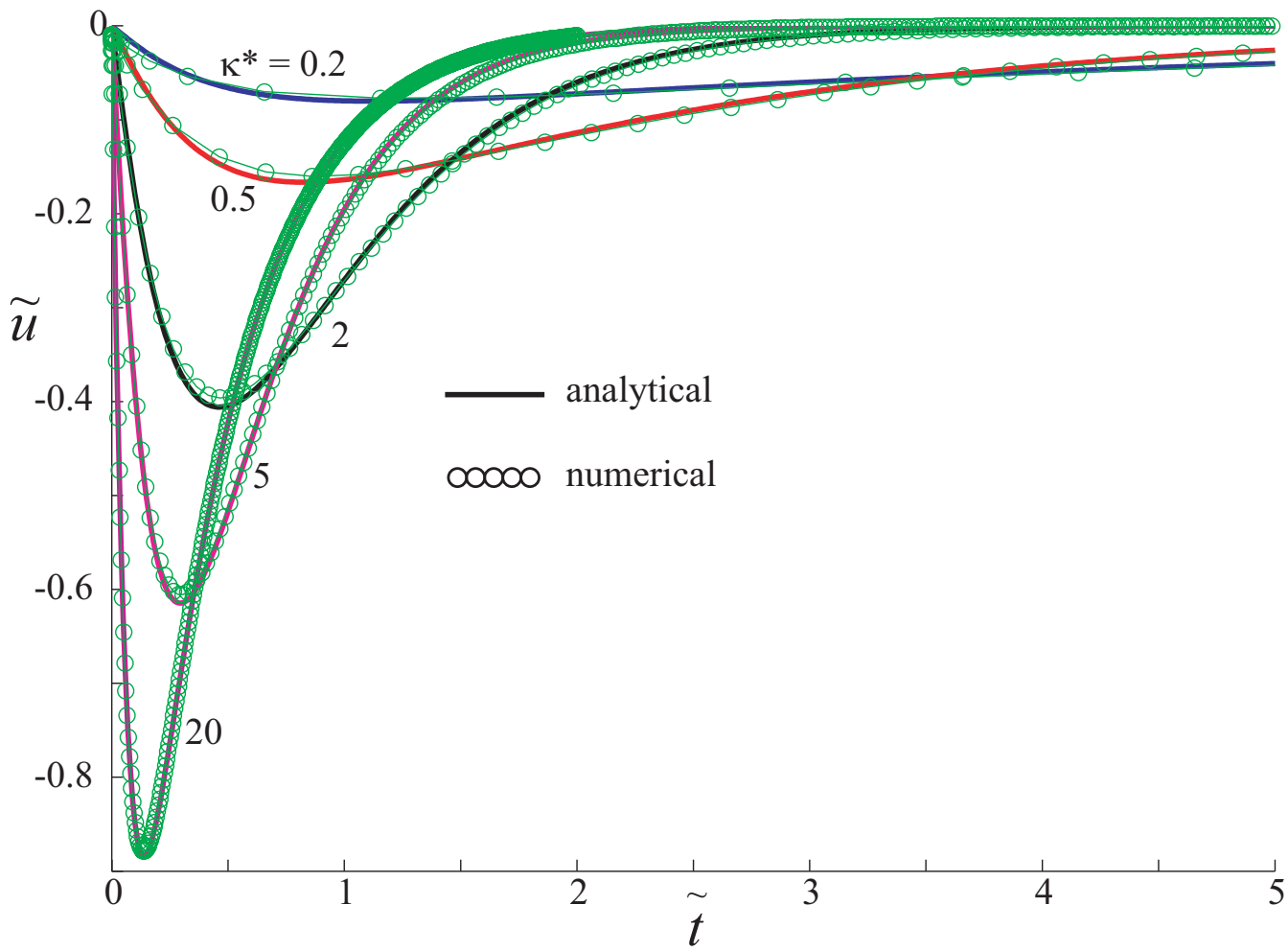

one-dimensional analysis; pore pressure at impermeable boundary

Finite difference solution

central difference formulation in space and time

tridiagonal matrix - simple solution by forward and reverse substitution (no matrix inversion)

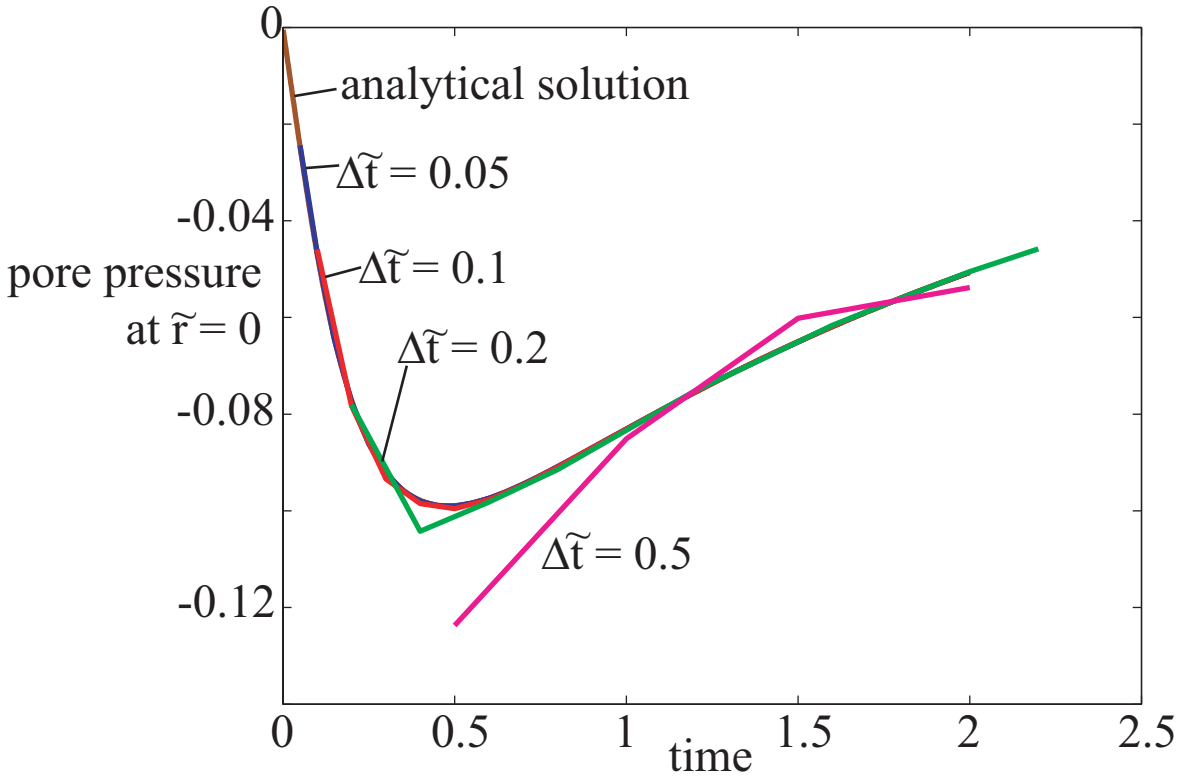

effect of time step (axisymmetric analysis)

UNIVERSITY OF DUNDEE

Analytical and finite difference solution

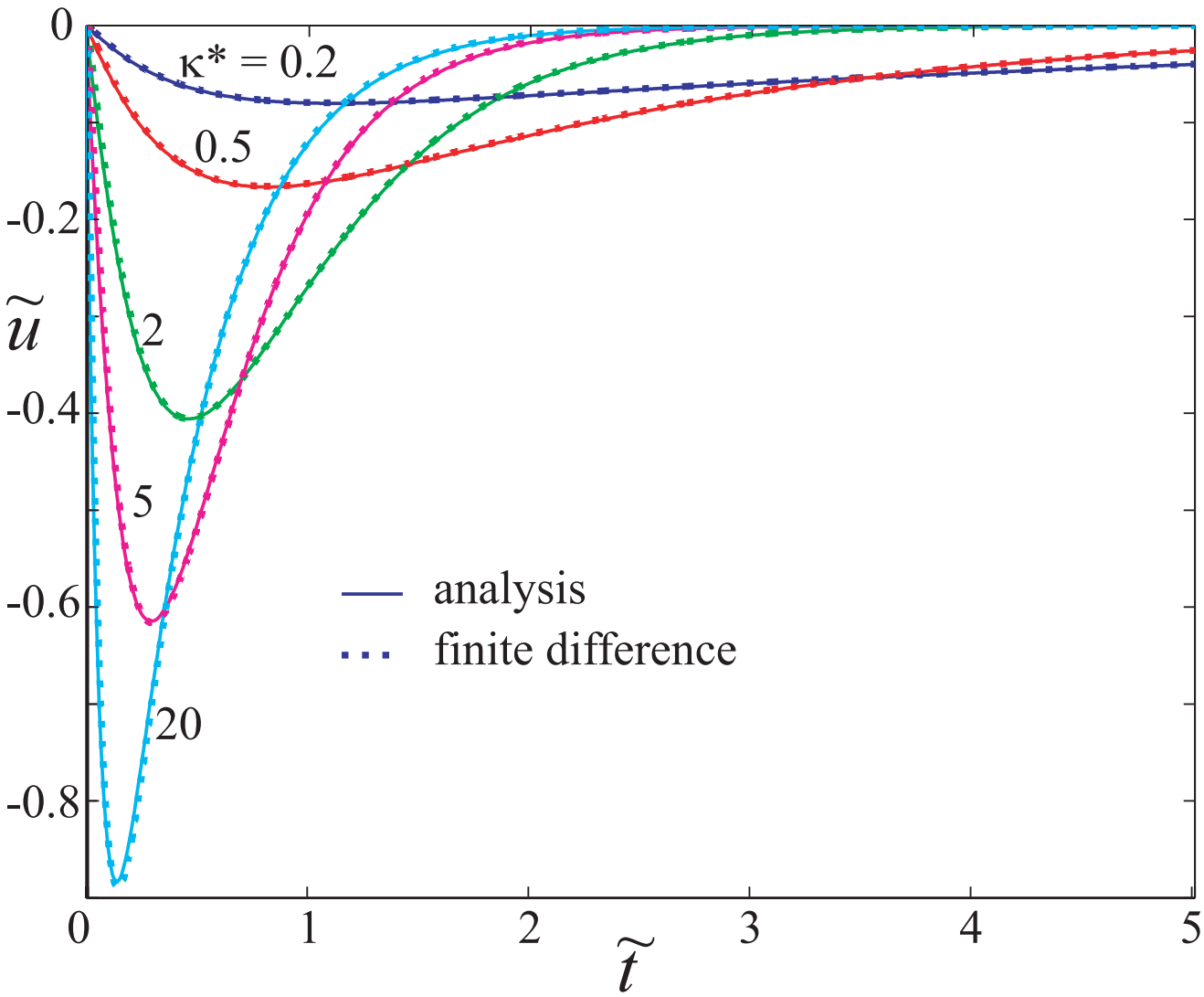

one-dimensional analysis; pore pressure at impermeable boundary

UNIVERSITY OF DUNDEE

One-dimensional analysis: parabolic isochrones

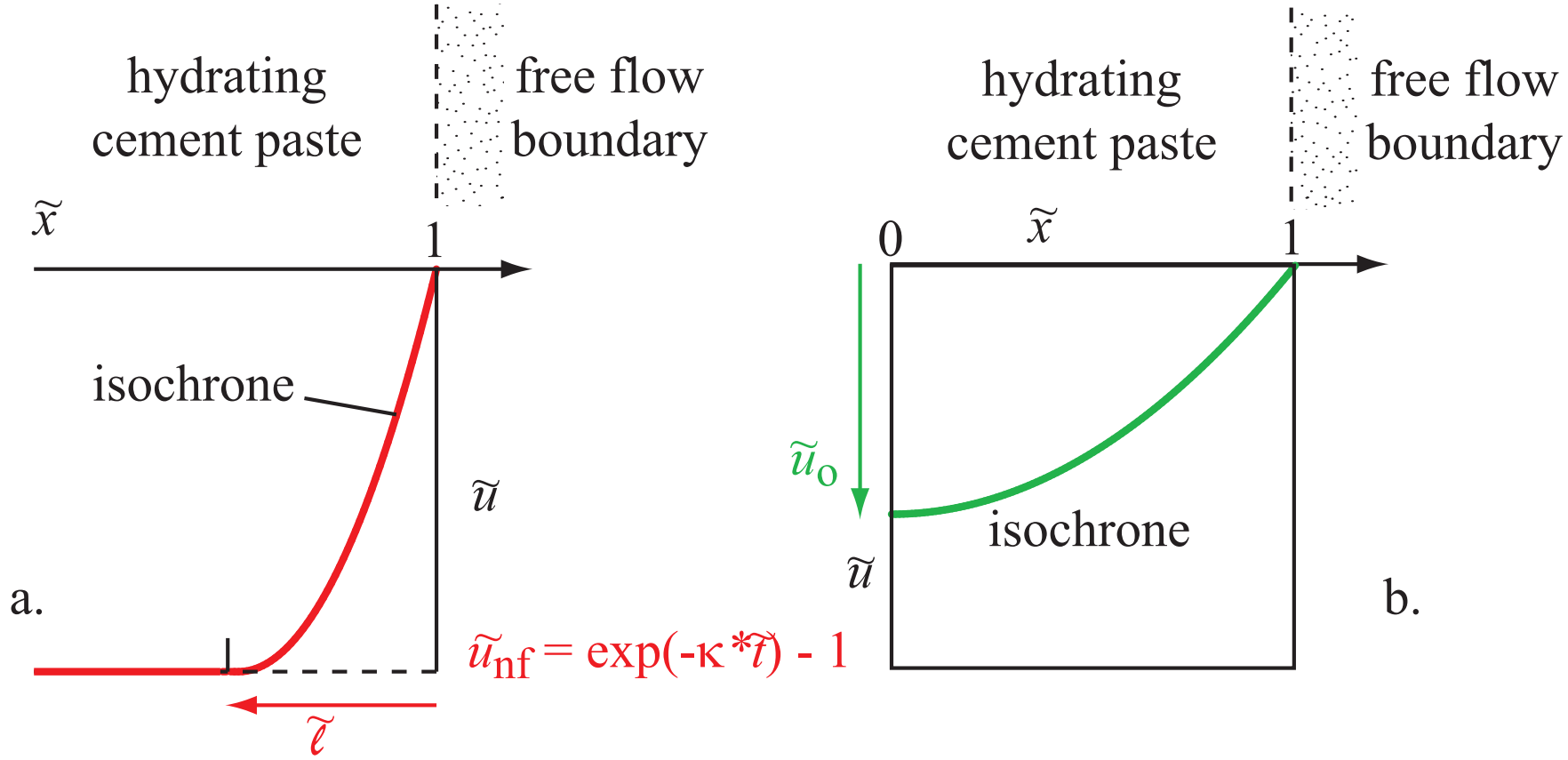

(a) pore pressure build-up and drainage front penetration

(b) pore pressure dissipation

UNIVERSITY OF DUNDEE

One-dimensional analysis: parabolic isochrones

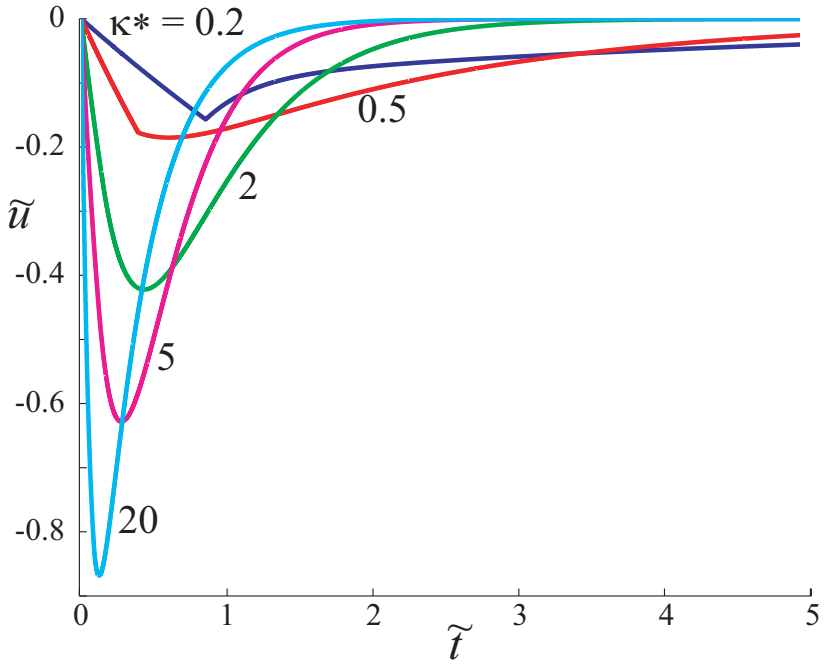

parabolic isochrones

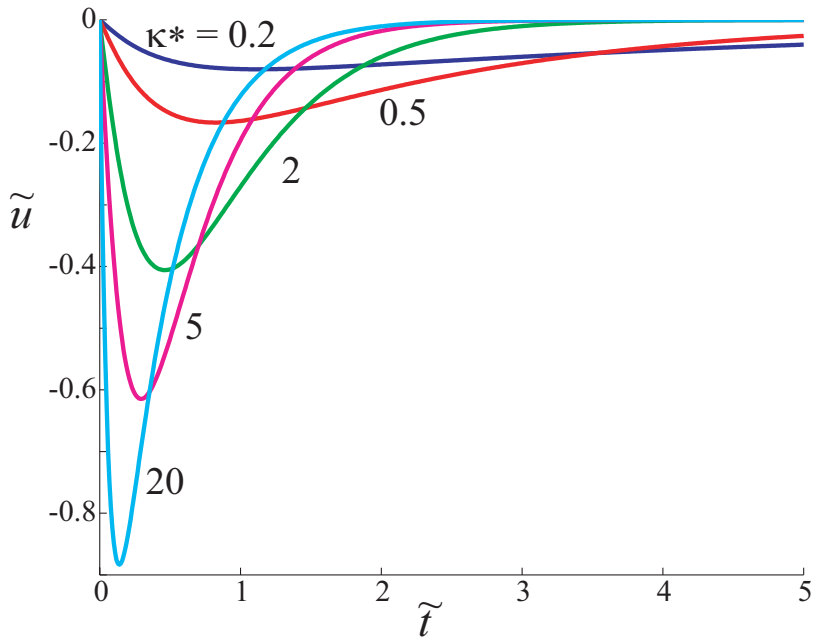

exact analysis

UNIVERSITY OF DUNDEE

One-dimensional analysis

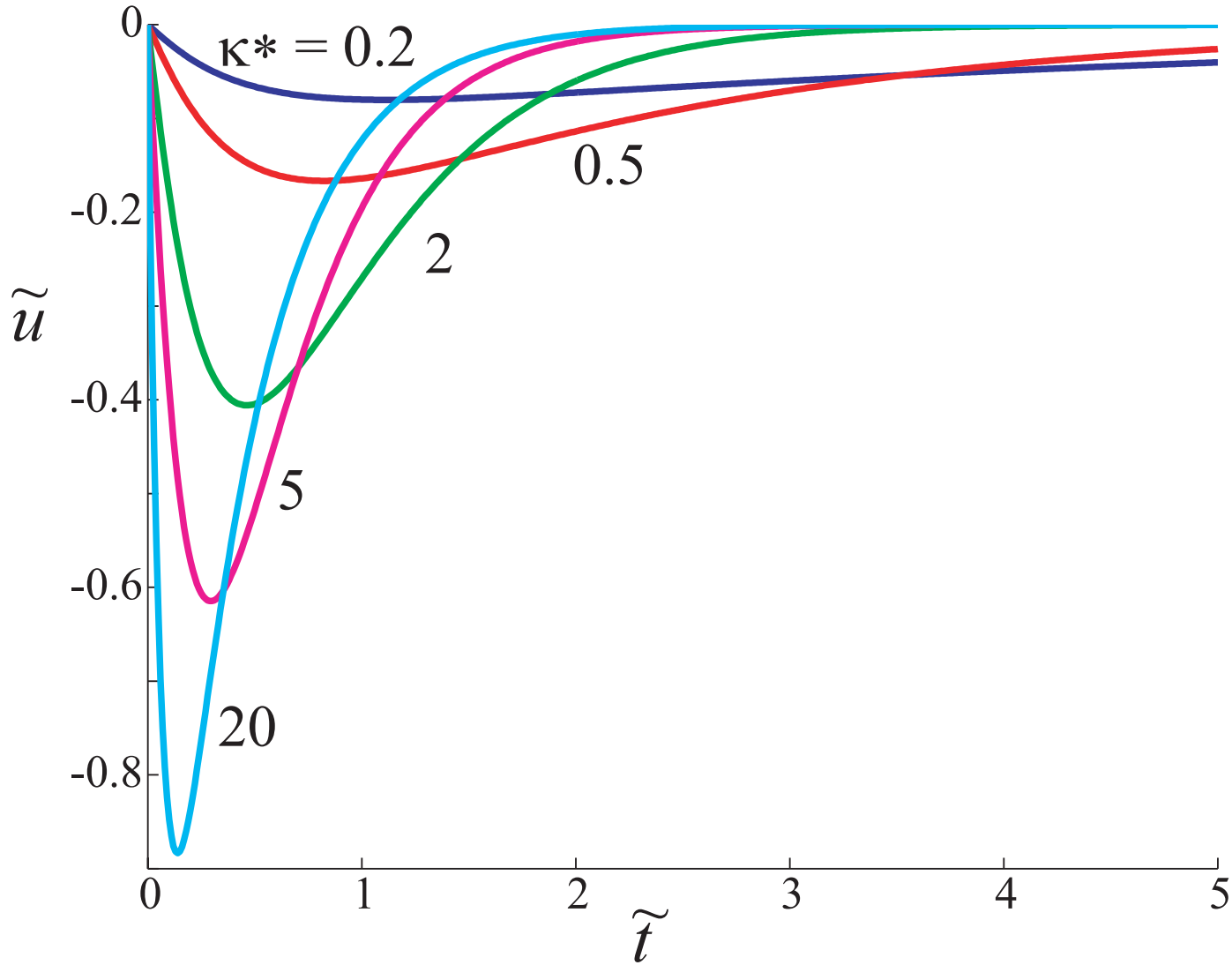

pore pressure at impermeable boundary

UNIVERSITY OF DUNDEE

One-dimensional analysis: parabolic isochrones

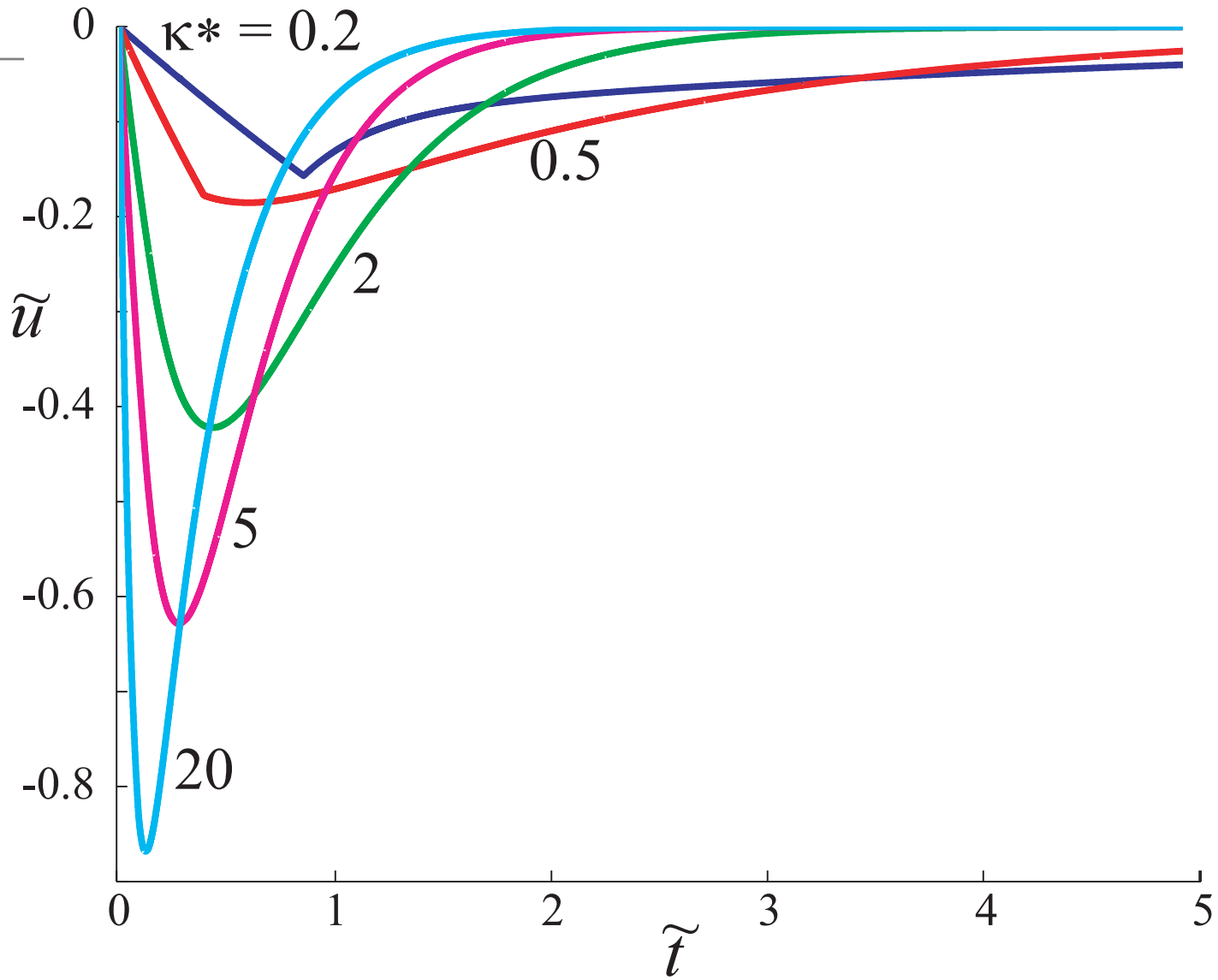

central pore pressure build-up and dissipation

UNIVERSITY OF DUNDEE

Finite difference: more complex problems

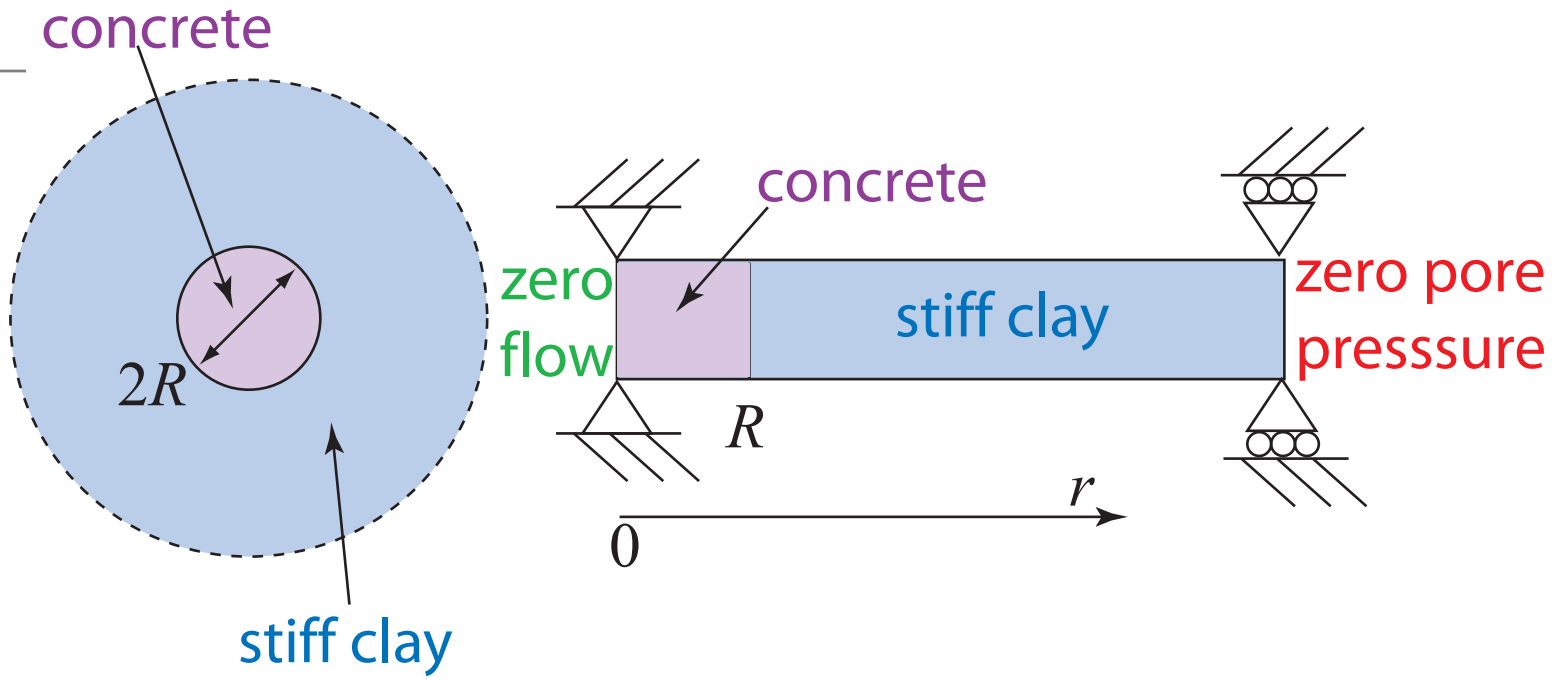

bored pile - concrete poured in

surrounding clay has different properties

need to build in allowance for stiffness of clay beyond (continuity)

ratio of c_v for concrete and soil

Axisymmetric analysis

kappa = 0.1

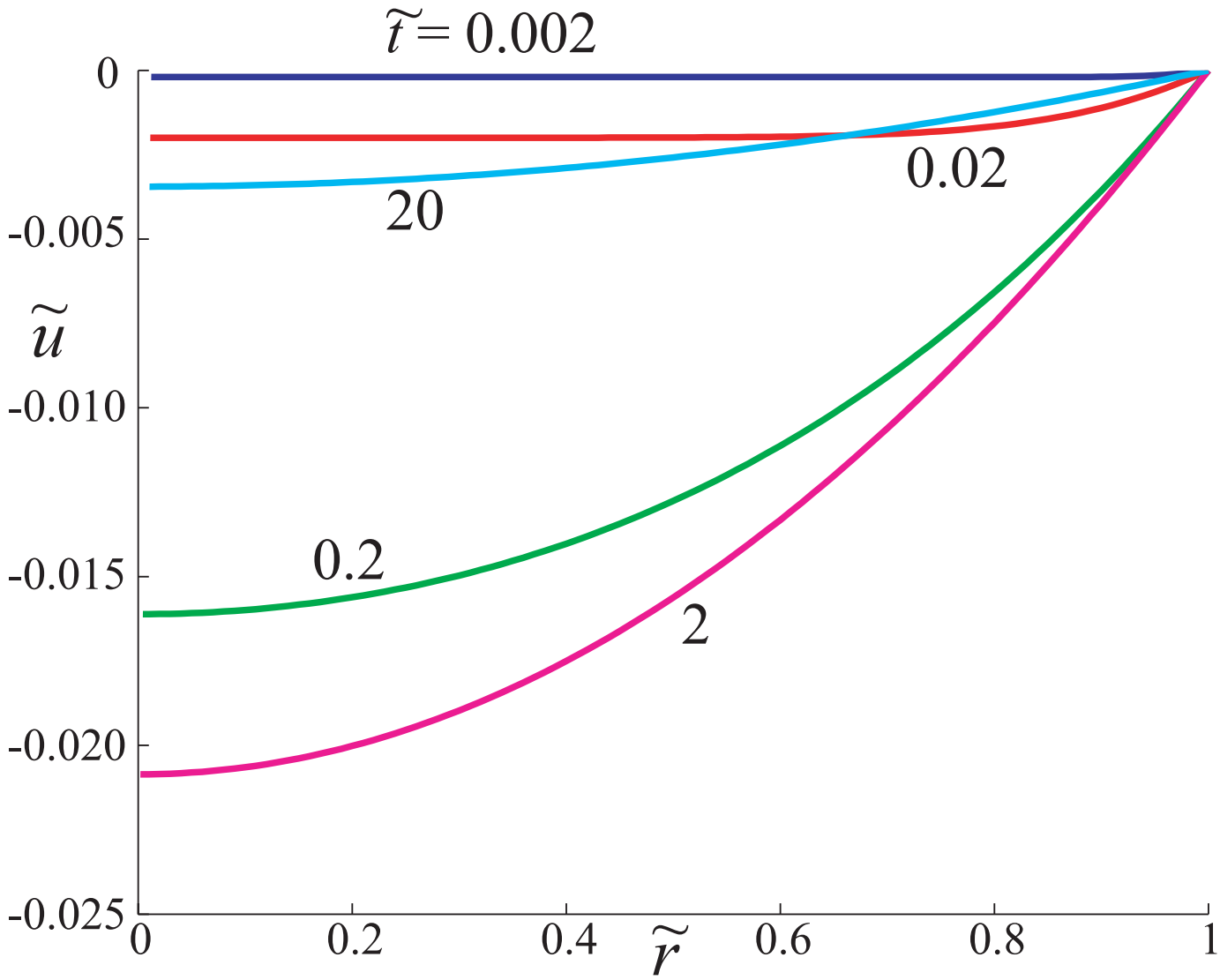

isochrones for pore pressure in concrete

UNIVERSITY OF DUNDEE

Axisymmetric analysis

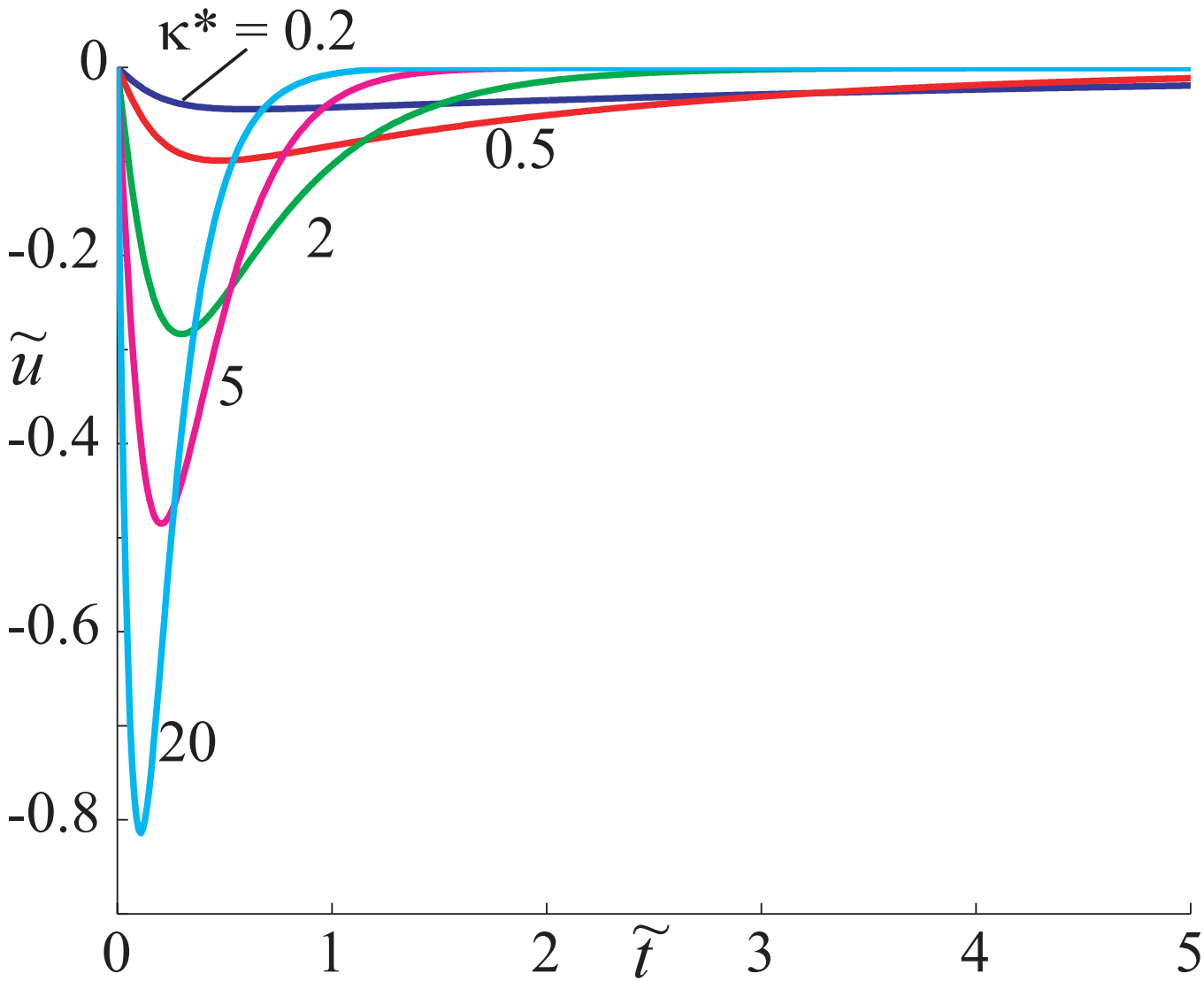

pore pressure at centre

Axisymmetric analysis

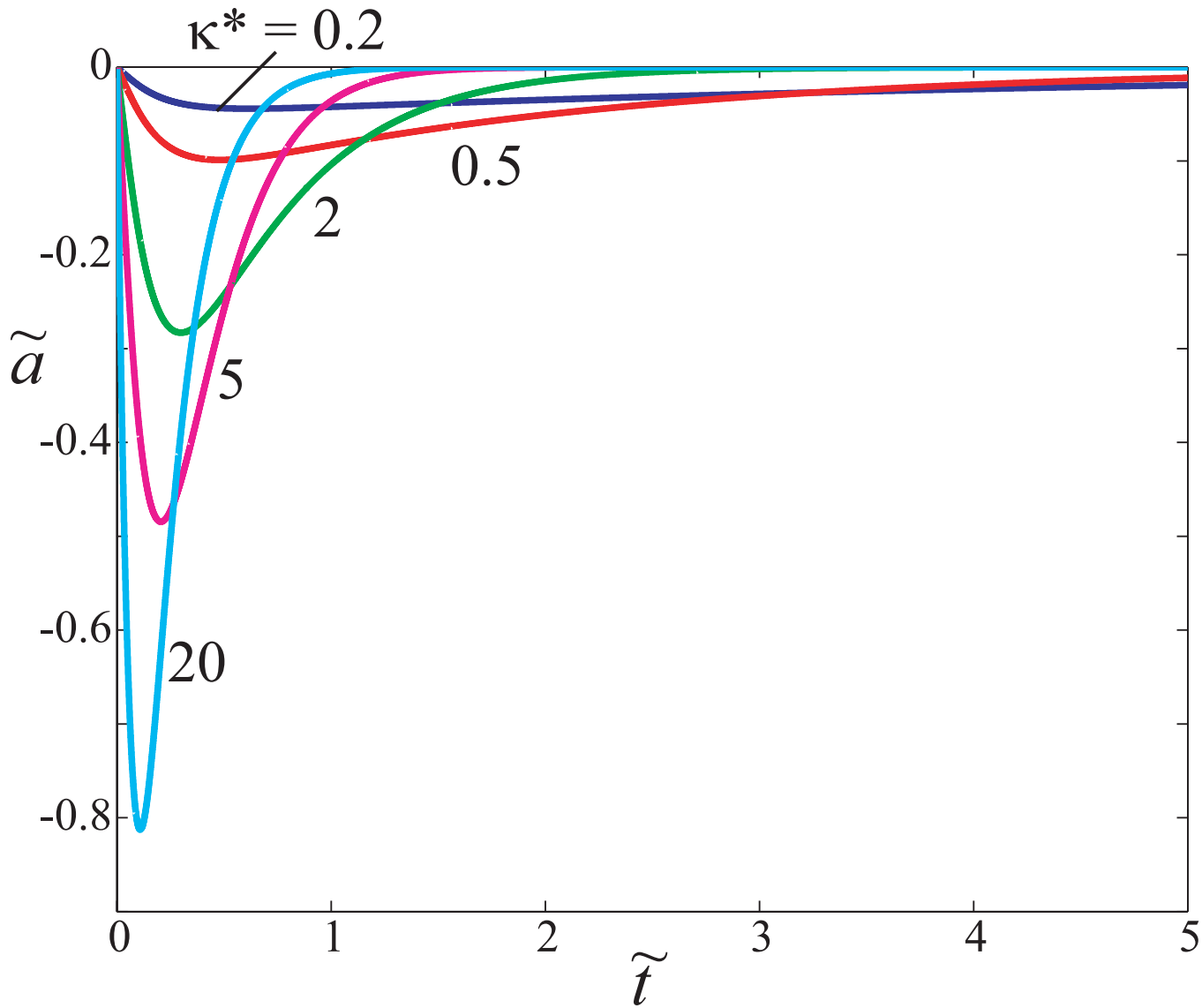

displacement at outer boundary

Finite difference: more complex problems

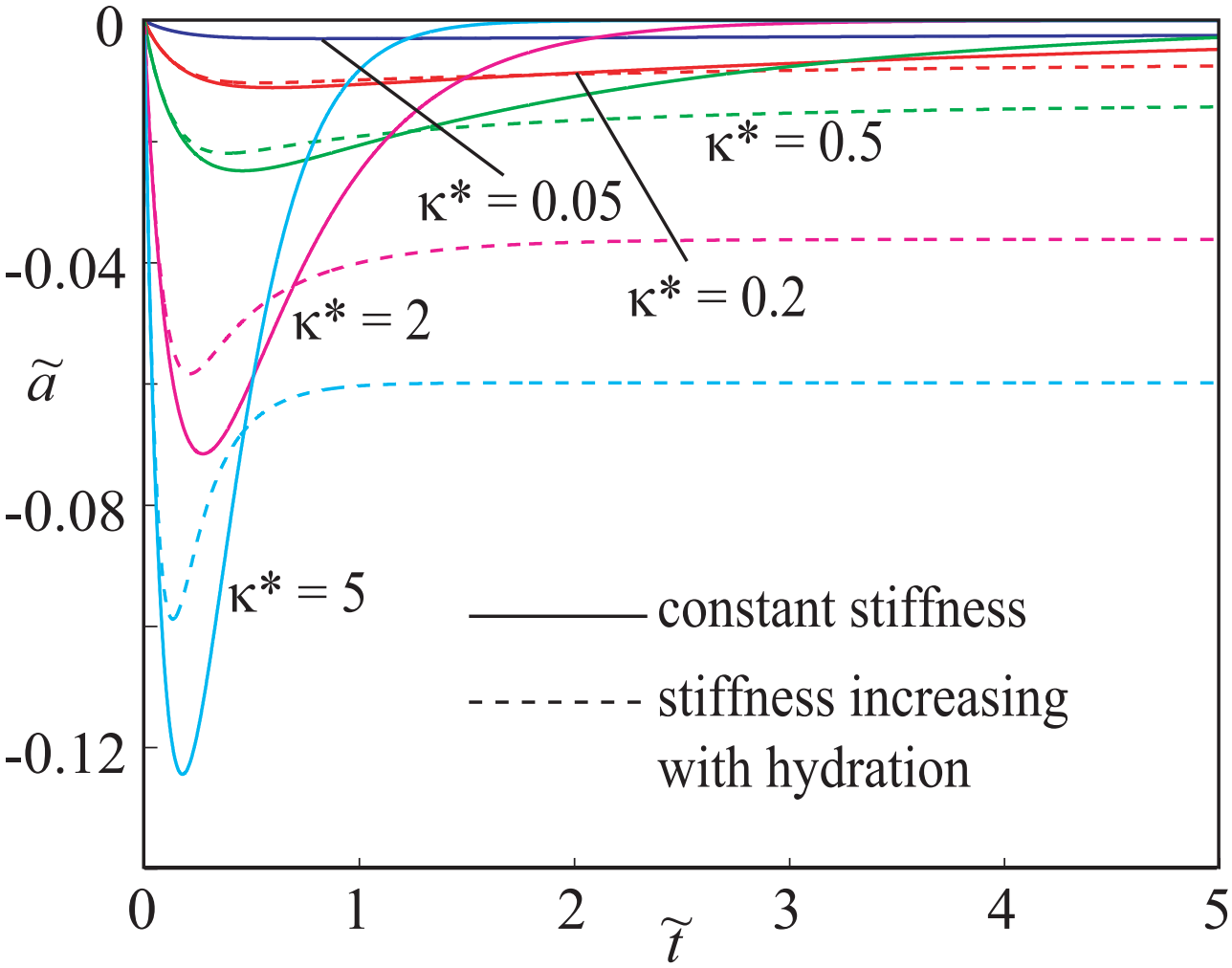

axisymmetric analysis: displacement at free-draining boundary

hydrating cement becomes stiffer as it hydrates - time-dependent ratio of moduli - displacements trapped

UNIVERSITY OF DUNDEE

Increased stiffness on hydration

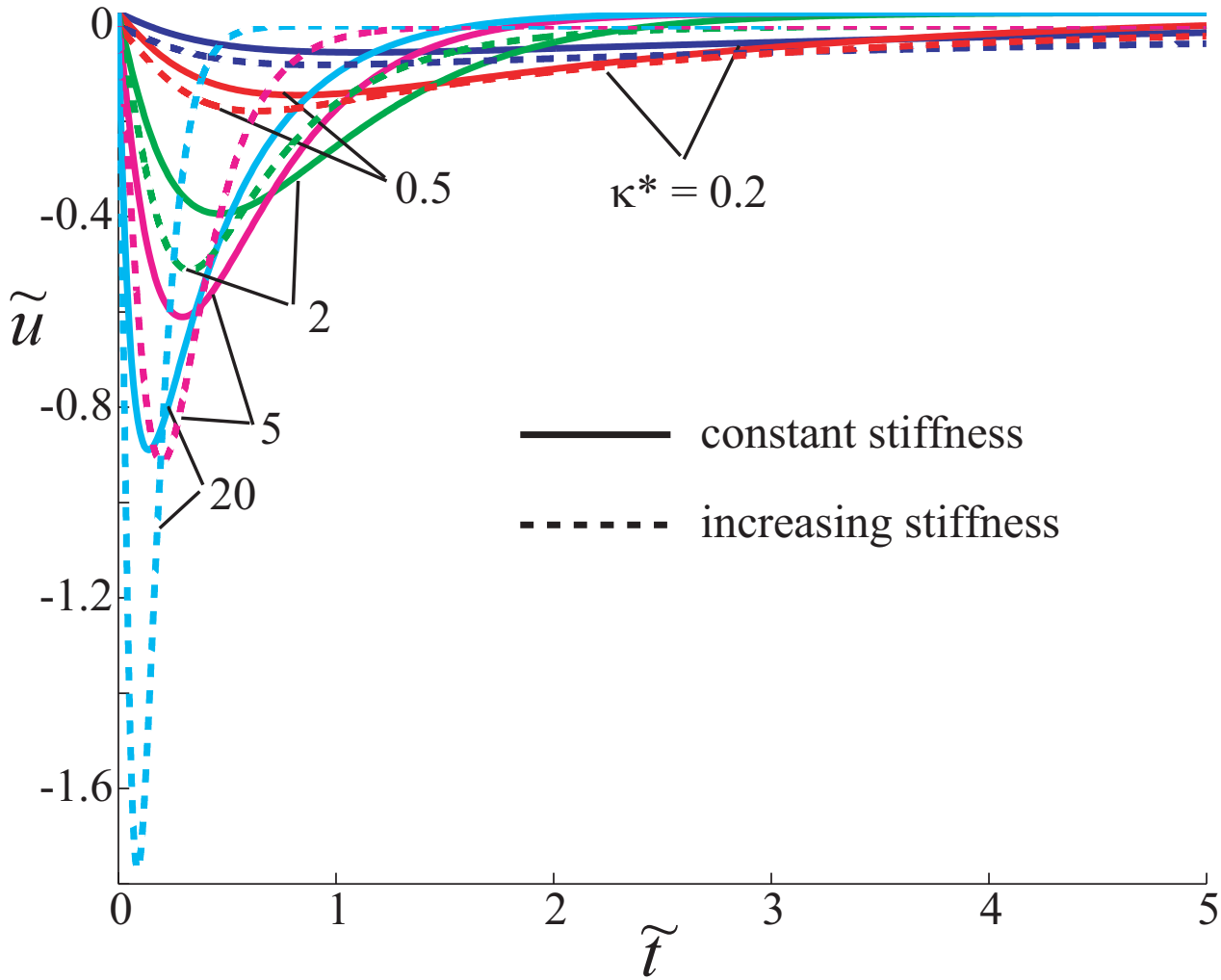

one-dimensional analysis; pore pressure at impermeable boundary

UNIVERSITY OF DUNDEE

Increased stiffness on hydration

stiffness increases by x5

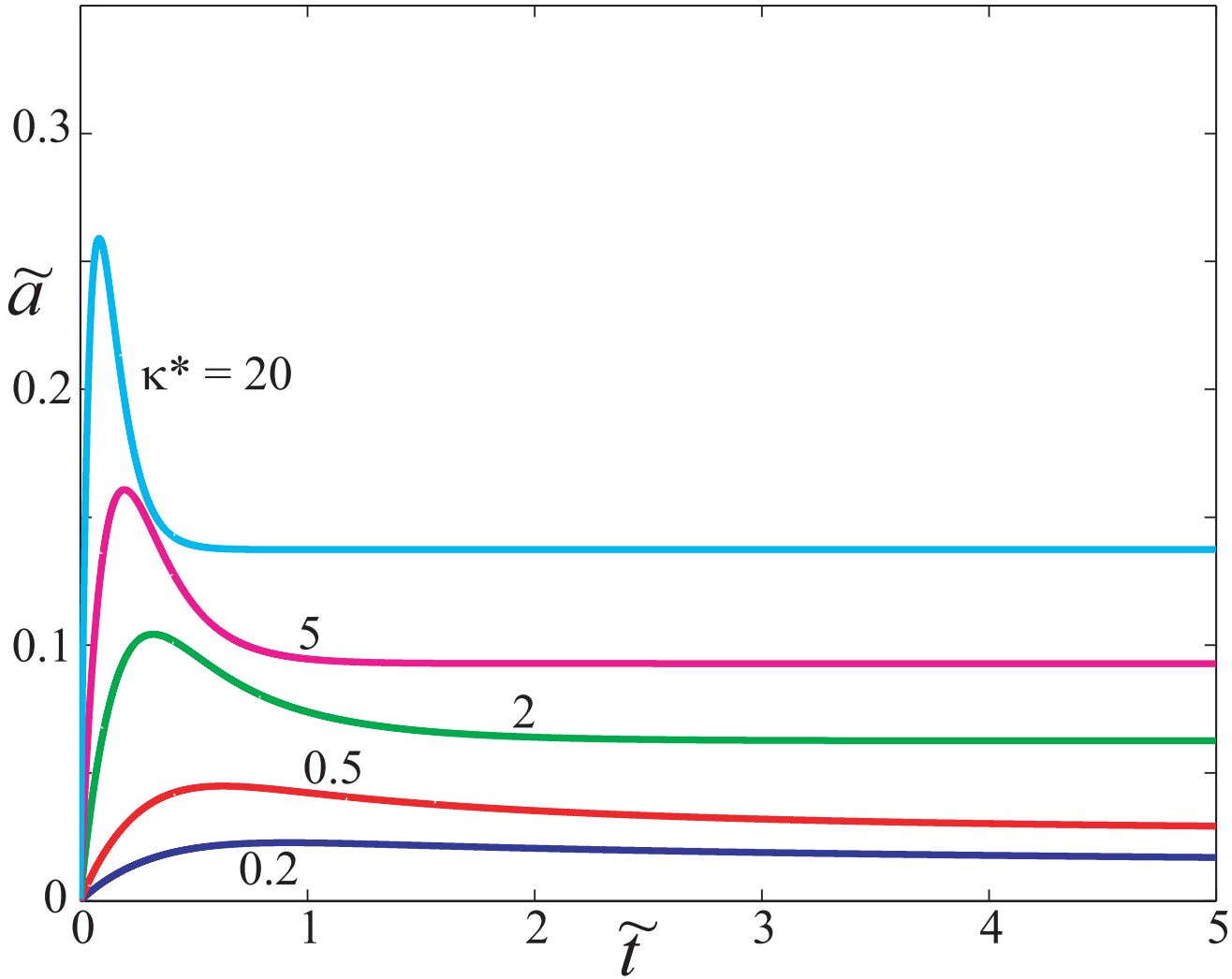

one-dimensional analysis; displacement at free boundary

UNIVERSITY OF DUNDEE

Less is more

- introduction
- consolidation analysis using parabolic isochrones
- application to embankment on soft clay
- behaviour of hydrating cement/soil mixture
- pipeline-seabed interaction
- conclusion

UNIVERSITY OF DUNDEE

sliding of pipeline on soft soil layer

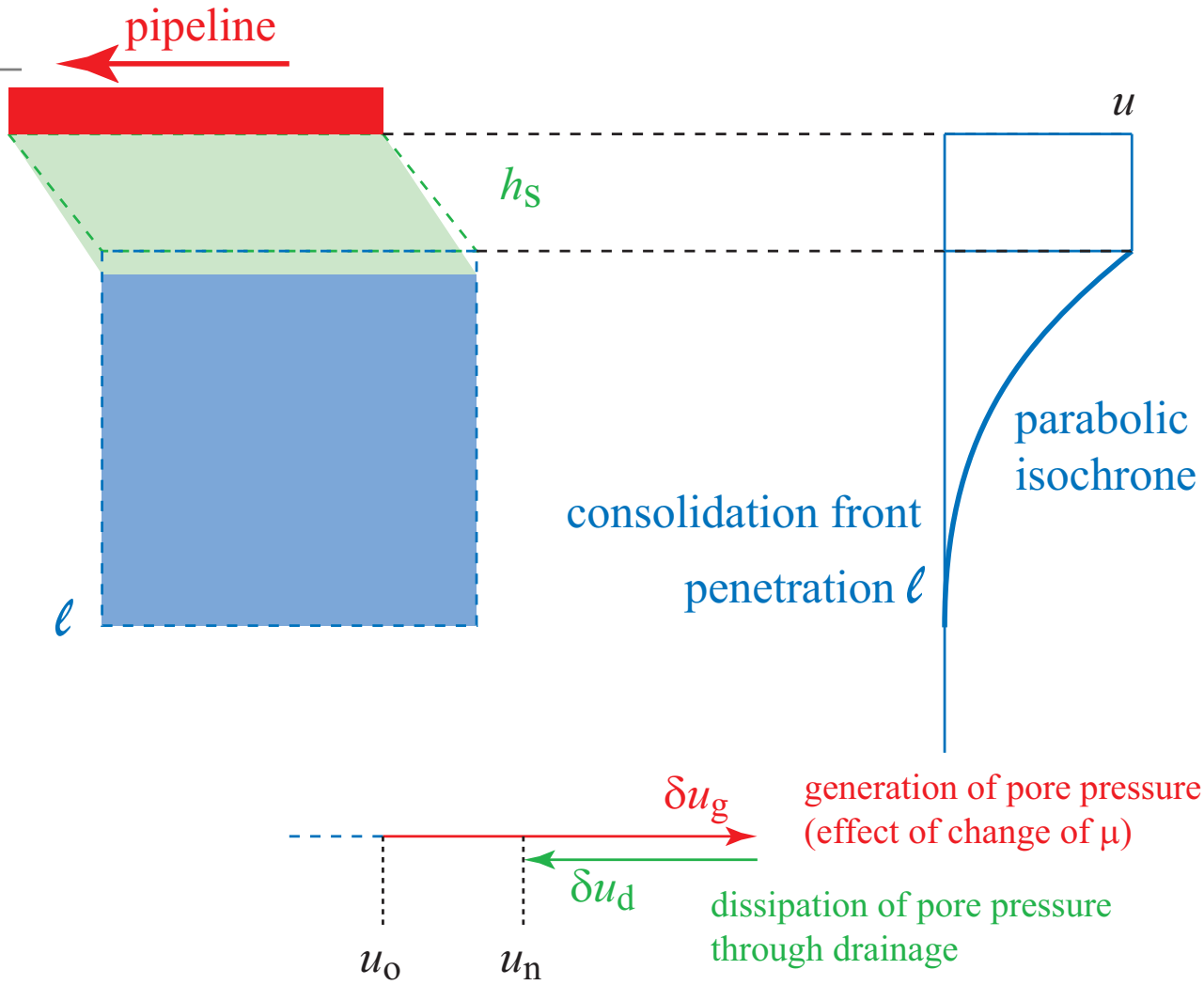

$$\delta u = u_n - u_o = \delta u_g - \delta u_d$$

- sliding of pipeline on soft layer

sliding of pipeline on soft soil layer

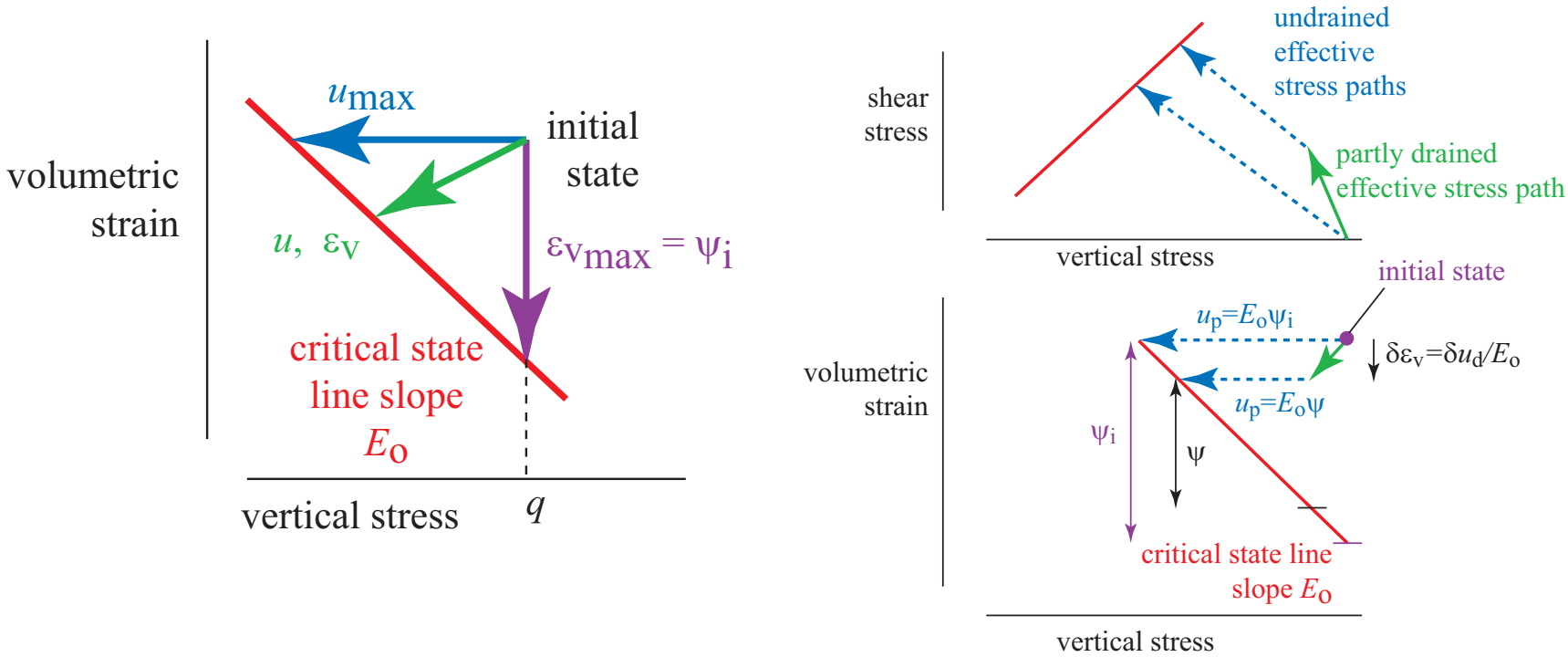

- critical state line locally **linear**: modulus E
- partial drainage; effective stress path

sliding of pipeline on soft soil layer

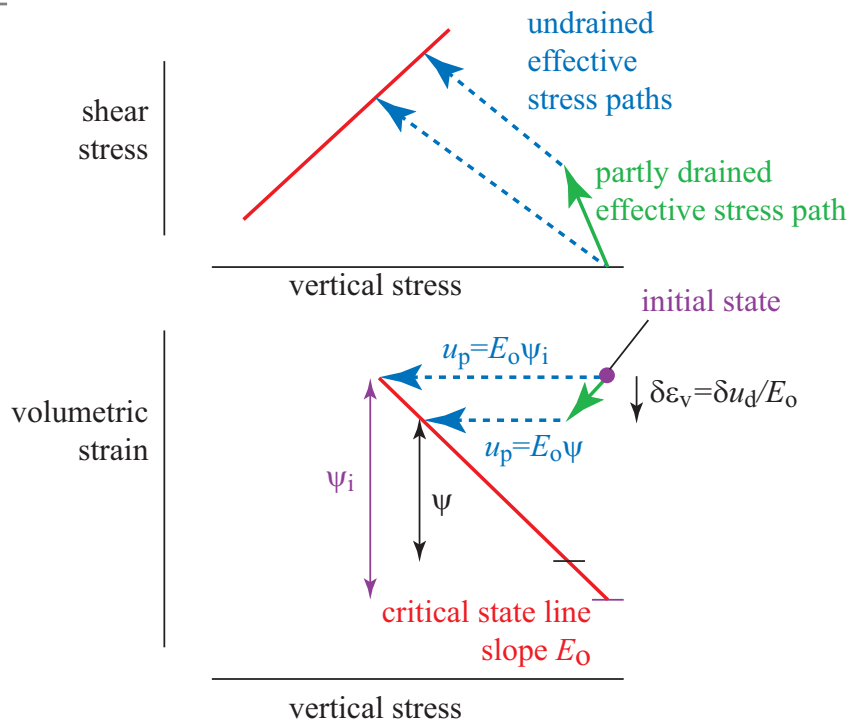

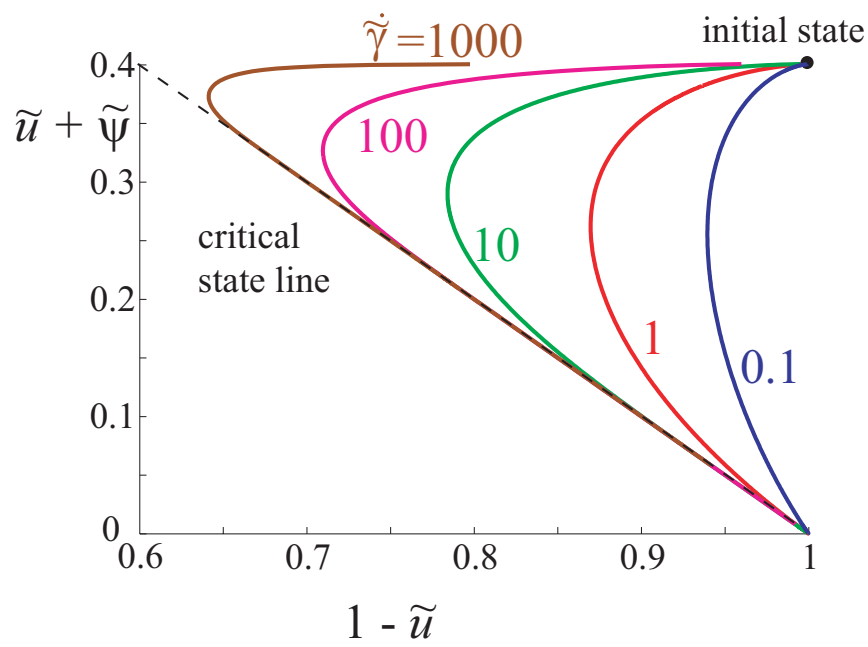

- time increment δt
- potential pore pressure generation in shearing δu_g
- pore pressure dissipation through drainage into soil beneath δu_d

UNIVERSITY OF DUNDEE

three unknowns:

- $\delta\varepsilon_v$ the compression of the slip layer
- δu the eventual change in pore pressure in the slip layer
- ℓ the depth to which the parabolic iscohrone extends into the soil

ensure compatibility between three governing physical mechanisms:

- mechanical response of the sheared soil
- the flow of water across the boundary
- the expansion of the underlying soil to maintain the overall constant volume condition

UNIVERSITY OF DUNDEE

shearing model

$$\tilde{\mu} = \frac{\tilde{\gamma}}{1+\tilde{\gamma}}; \quad \tilde{\tau} = \tilde{\mu}(1-\tilde{u}) = \frac{\tilde{\gamma}(1-\tilde{u})}{1+\tilde{\gamma}}$$

effect of strain rate

$$\tilde{\mu_f} = 1 + \zeta \log_{10} \frac{\dot{\tilde{\gamma}}}{\dot{\tilde{\gamma}}_r}$$

pore pressure parameter:

$$\tilde{a} = a\mu_f = \frac{\tilde{\psi}}{(1-\tilde{\mu})(1-\tilde{u}) - \tilde{\psi}} \qquad (1)$$

UNIVERSITY OF DUNDEE

sliding of pipeline on soft soil layer

$$\frac{\mathrm{d}\tilde{u}}{\mathrm{d}\tilde{t}} = \frac{\tilde{a}\tilde{\ell}(1-\tilde{u})(1-\tilde{\mu})^2\dot{\tilde{\gamma}} - 2\tilde{u}}{\tilde{\ell}(1+\tilde{a}\tilde{\mu})}$$

$$\frac{\mathrm{d}\tilde{\psi}}{\mathrm{d}\tilde{t}} = -\frac{\mathrm{d}\tilde{u}_g}{\mathrm{d}\tilde{t}} = \tilde{a}\frac{(1-\tilde{u})(1-\tilde{\mu})^2\dot{\tilde{\gamma}} + 2\tilde{\mu}(\tilde{u}/\tilde{\ell})}{1+\tilde{a}\tilde{\mu}}$$

$$\frac{\mathrm{d}\tilde{\ell}}{\mathrm{d}\tilde{t}} = \frac{6}{\tilde{\ell}} - \frac{\tilde{a}\tilde{\ell}}{\tilde{u}}\frac{(1-\tilde{u})(1-\tilde{\mu})^2\dot{\tilde{\gamma}}}{1+\tilde{a}\tilde{\mu}} + \frac{2}{1+\tilde{a}\tilde{\mu}}$$

sequence of operation:

$\delta\tilde{t} \to \delta\tilde{\gamma} \to \delta\tilde{\mu}$; $\delta\tilde{t} \to \delta\tilde{u}_d$;

$\delta\tilde{\mu}$ and $\delta\tilde{u}_d \to \delta\tilde{u}_g$; $\delta\tilde{u} \to \delta\tilde{\ell}$; $\delta\tilde{u}_g \to \delta\tilde{\psi}$

UNIVERSITY OF DUNDEE

sliding of pipeline on soft soil layer

$$\tilde{\delta} = \delta G_o / h_s \mu_f q = \tilde{\gamma} = G_o \gamma / \mu_f q = \tilde{v}\tilde{t} = \tilde{\delta}$$

$$\tilde{t} = c_v t / h_s^2$$

$$\tilde{v} = v G_o h_s / \mu_f q c_v = \tilde{\delta} / \tilde{t}$$

$$\dot{\tilde{\gamma}} = \tilde{\gamma} / \tilde{t} = h_s^2 G_o \dot{\gamma} / \mu_f q c_v$$

$$\tilde{\mu} = \mu / \mu_f$$

$$\tilde{\mu_f} = \mu_f / \mu_{fo}$$

$$\tilde{\psi} = E_o \psi / q$$

$$\tilde{\tau} = \tau / \mu_f q$$

$$\tilde{u} = u / q$$

$$\tilde{\ell} = \ell / h_s$$

dimensionless groups to ensure general applicability of analyses

UNIVERSITY OF DUNDEE

sliding of pipeline on soft soil layer

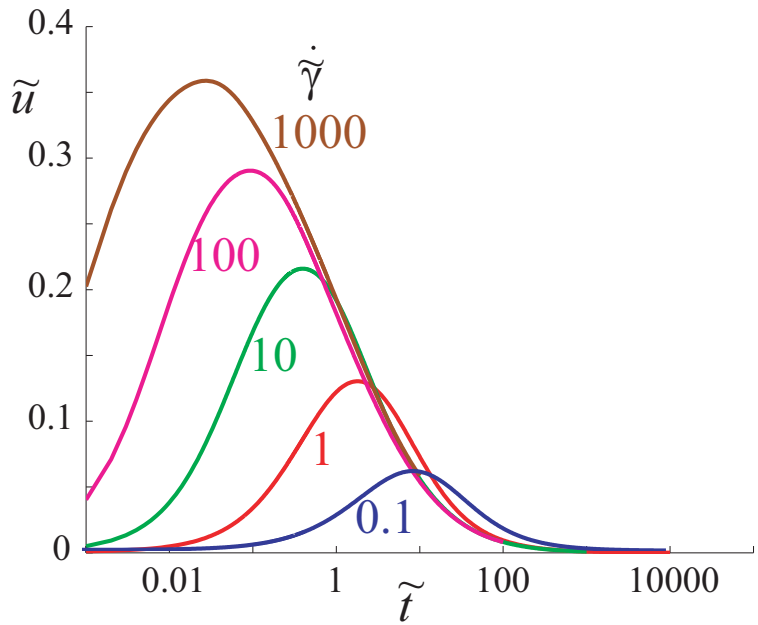

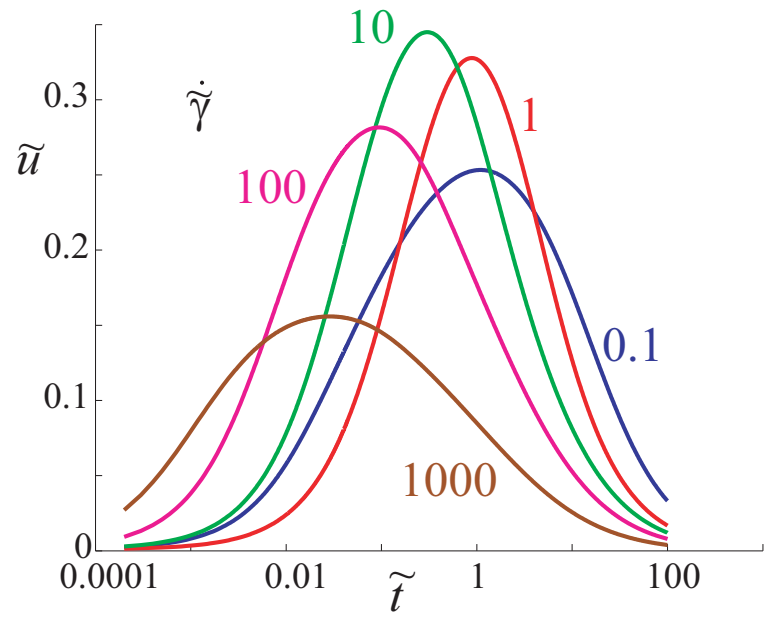

strain rate effect on pore pressure ... but does strain rate shift csl? ... equivalent to changing initial state parameter

rate↑⇒ csl↑? ⇒ equivalent to $\psi_i \downarrow$

$\dot{\tilde{\gamma}} = 0.1$, 1, 10, 100, 1000 ⇒ $\tilde{\psi}_i = 0.99$, 0.79, 0.59, 0.39, 0.19

UNIVERSITY OF DUNDEE

sliding of pipeline on soft soil layer

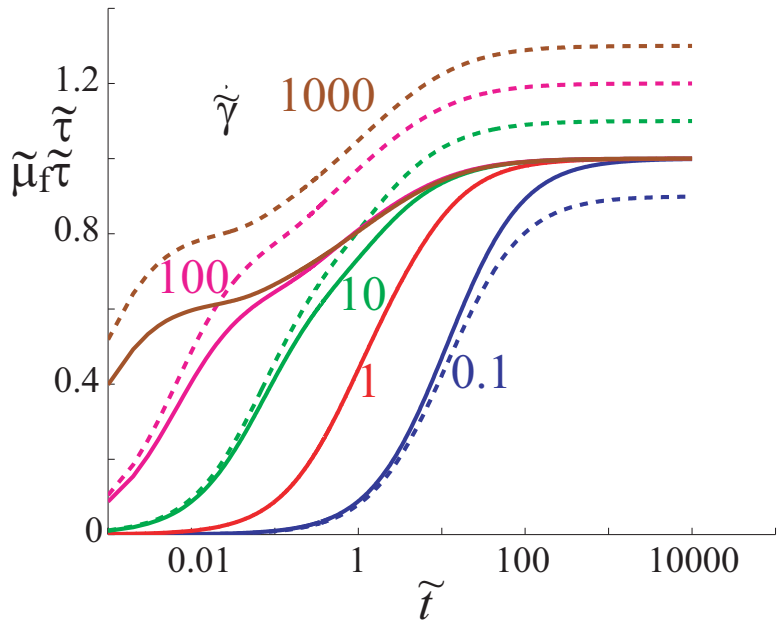

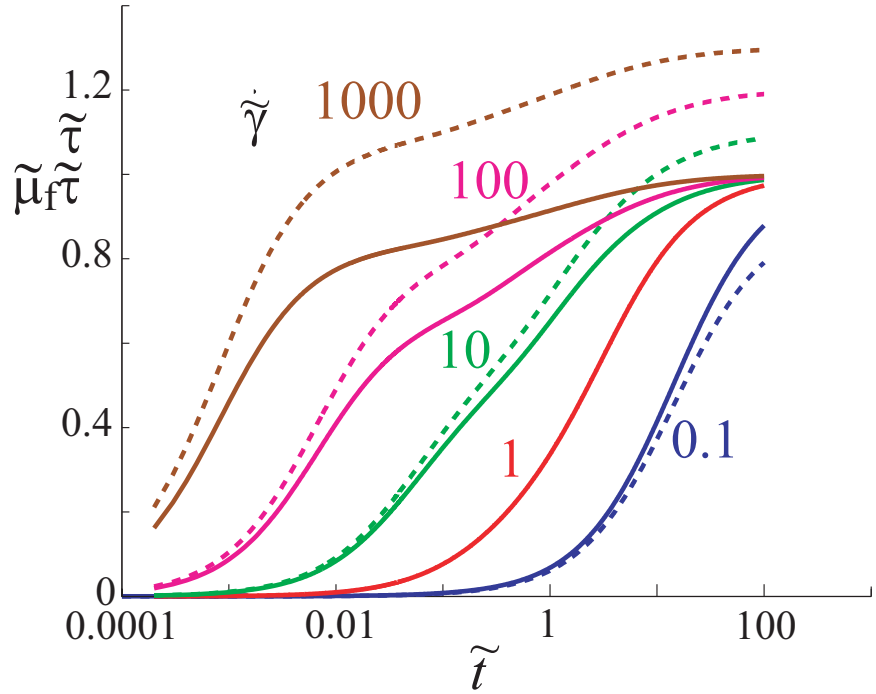

strain rate effect on shear stress - rate affects only failure stress ratio

if rate↑⇒ csl↑? ⇒ equivalent to ψ_i ↓:

$\dot{\tilde{\gamma}} = 0.1$, 1, 10, 100, 1000 ⇒ $\tilde{\psi}_i = 0.99$, 0.79, 0.59, 0.39, 0.19

UNIVERSITY OF DUNDEE

sliding of pipeline on soft soil layer

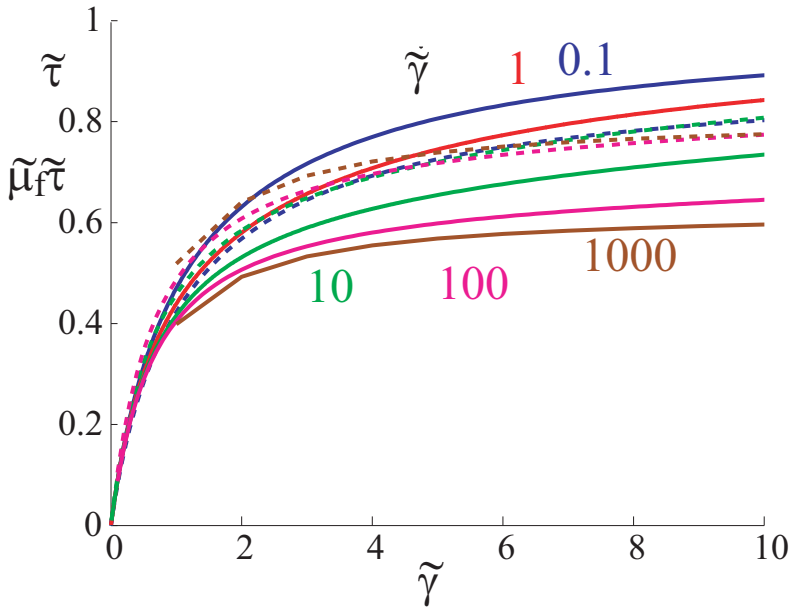

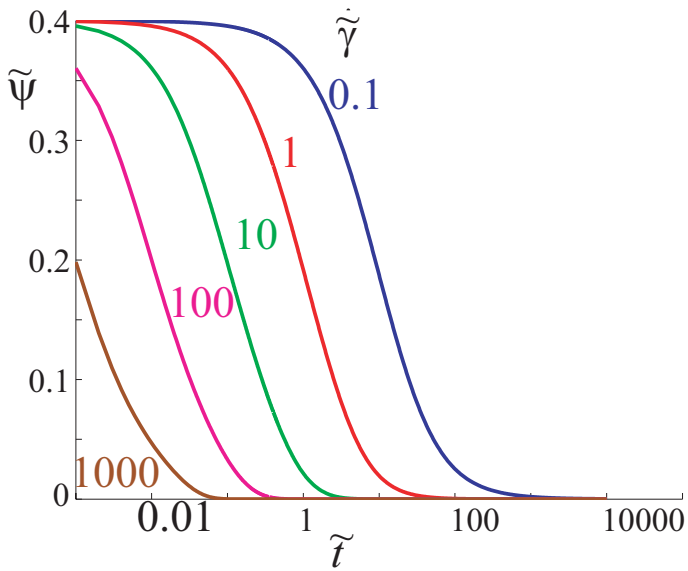

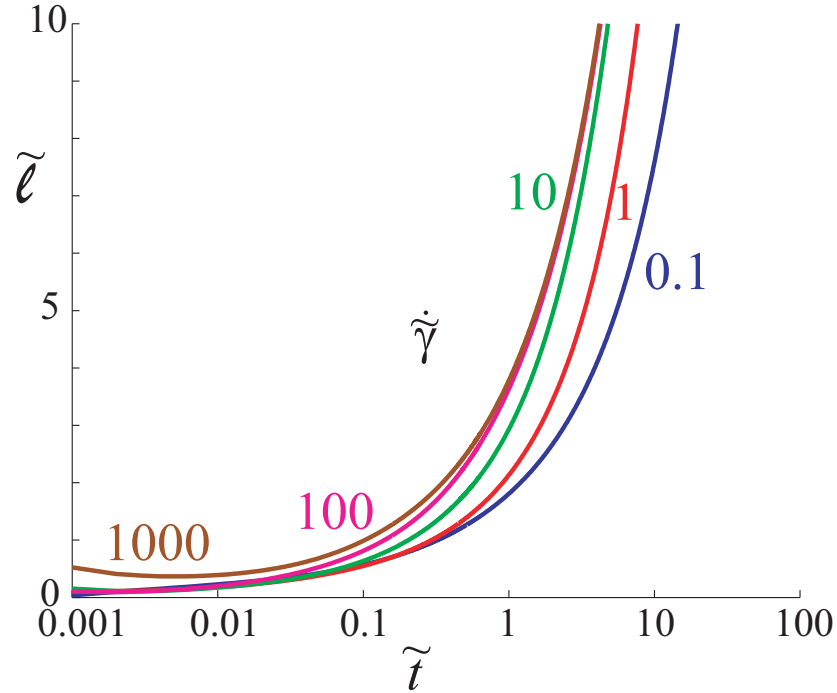

variation of shear stress, state parameter, and penetration of consolidation (swelling) front into underlying soil

UNIVERSITY OF DUNDEE

Less is more

- introduction
- consolidation analysis using parabolic isochrones
- application to embankment on soft clay
- behaviour of hydrating cement/soil mixture
- pipeline-seabed interaction
- conclusion

UNIVERSITY OF DUNDEE

Hydration of cement paste: Conclusions

- exact solutions *can* be obtained - FE sledge hammer not always necessary
- nondimensional approach widens applicability of solution
- parabolic isochrones provide a simple approximate solution - mechanisms clearly incorporated
- finite difference solution allows solution for complex problems

UNIVERSITY OF DUNDEE

Less is more: Step 0: Conclusions

Mathematics and civil engineering education

- A fully competent engineer must understand the mathematics necessary (but not sufficient) as the basis for making decisions and for communicating with other engineers, especially across disciplines.
- Most engineers will find it easier to learn and grasp engineering principles if they are previously familiar with the underlying mathematics.

UNIVERSITY OF DUNDEE

Mathematics and civil engineering education

- Exceptional people may well be able to perceive sound engineering solutions before they understand why - this is the way civil engineers worked mid 19th century - but to impose this order on the majority at the present day would be a handicap.
- Greyness correlates positively with narrowness of interest and shortness of vision ... not with high achievement in any particular discipline.

UNIVERSITY OF DUNDEE

Mathematics and civil engineering education

- I am reminded of the talking parrot. The concept of ‘pretty’ is limited to pronunciation rather than an attractive mate and who is ‘Polly’ anyway?
- The inability to use the back of an envelope to estimate an answer, to assess the effect of a changed input parameter on the result, reduces the engineer to the level of parrots, reproducing calculations with no understanding.

David Beadman of Bachy Soletanche : *New Civil Engineer* (1 Jun 2000)

UNIVERSITY OF DUNDEE

Step Zero

Step Zero of any modelling – especially finite element or centrifuge modelling – is to **write down the answer** *before* you switch on your computer, open the operating manual, design your experiment and instrumentation, etc.

This vital step can be supported by 'back of the envelope' calculations which must capture the essence of the mechanics of the problem.

Write down the answer!

UNIVERSITY OF DUNDEE

Less is more: Step 0

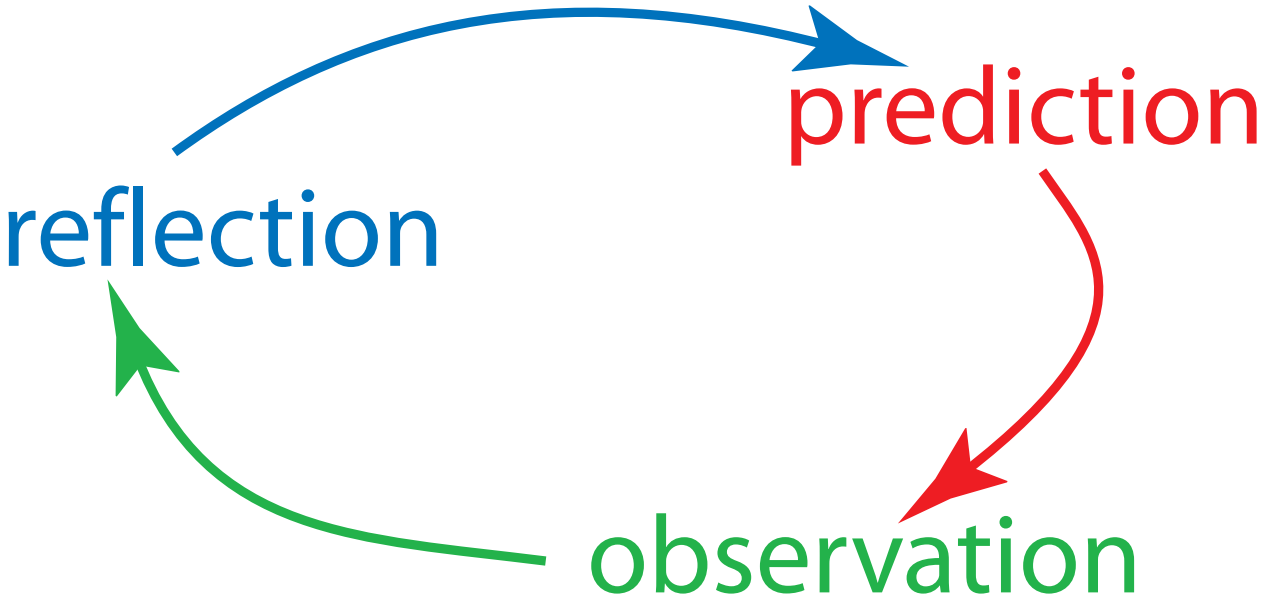

- before you switch on the computer...
- ...write down the answer!
- always start with *prediction*
- if subsequent *observation* unexpected...
- *reflection* required to improve *prediction* (understanding)

UNIVERSITY OF DUNDEE

Less is more: Step 0

- simplified problems
- or ‘system’ level description
- hand calculations - exact solutions?
- seeking confidence in predictions
- treat numerical output with caution unless corroborated

UNIVERSITY OF DUNDEE

Less is more: Step 0

- first order modelling
- adequate complexity
- what characteristics of response do we think are important (essential)?
- stiffness nonlinearity, strength/density, softening, anisotropy
- rate effects, history dependence, cementation, bond breakage
- particle breakage, particle erosion, non-monotonic loading, infinite repetitions

UNIVERSITY OF DUNDEE

Less is more: Step 0

- simple analysis
- reasonable assumptions for unknown quantities
- inclusion of essential features
- dimensionless groups

Coupled chemical shrinkage and consolidation: some benchmark solutions

David MUIR WOOD[1] and James DOHERTY[2]

[1]Division of Civil Engineering, University of Dundee and Centre for Offshore Foundation Systems, University of Western Australia

(E-mail: d.muirwood@dundee.ac.uk)

[2]School of Civil and Resource Engineering, University of Western Australia

(E-mail: james.doherty@uwa.edu.au)

Abstract

Mixtures of cement and mine waste are used as backfill in underground mines to provide support, which enables increased mineral extraction. Unlike most cemented material, the properties of mine backfill are relied upon immediately after cement is added and the material deposited underground. It is not just the properties of the final cemented product but also the behaviour of cemented backfill during the hydration process that is important. During the hydration process, the backfill experiences chemically induced volume changes. These volume changes can lead to the development of effective stresses, which control the loads generated on barricade walls and the subsequent stability of unsupported faces.

Although the processes that interact during cement hydration appear complex, the governing equation can be derived in terms of a small number of dimensionless parameter groups. The equation is simply the diffusion equation with a time-dependent source/sink term for which an analytical solution can be obtained under certain simplifying geometries. Approximate solutions can be obtained using a technique of analysis in which the mode shape of the spatial pore pressure

variation is assumed. Such solutions provide benchmarks for simplified problems against which results of finite element modelling (for example) can be compared in order to confirm that the controlling mechanisms have been correctly identified.

Keywords: self-desiccation, consolidation, dimensional analysis, numerical analysis, mine backfill

Introduction: Step 0

Confronted by a complex geotechnical problem involving chemical shrinkage, flow and mechanical deformation, it is almost inevitable that a commercial finite element (or equivalent) program will be sought to obtain a detailed solution. If we see the problem as complex then it is likely that the computer program will also see the problem as complex. The computer will usually chug through to a result and the engineer's task is to convince himself and his client that this is indeed the correct result. There is a necessary discipline to numerical modelling which may be described as 'Step 0' (**?**): before you reach for the computer program, open the manual, turn on the computer - write down the answer! The logic is clear: if you do not have an idea about the likely magnitude, direction etc of the eventual deformation, support force, pore pressure, then you will be unable to recognise when the computer is leading you up a blind alley.

Step 0 is therefore about 'back-of-the-envelope' calculations demonstrating a clear idea of the mechanisms governing the problem. If the computer result differs significantly from the prior rough estimate then there must be a misunderstanding in your simple analysis or in the detailed computer analysis which evidently needs to be resolved iteratively.

Step 0 may seem daunting but it is concerned with order of magnitude estimates, breaking down complex systems into simpler parts and generating benchmark

results which can be used to check that the numerical analysis is on the right track before embarking on the analysis of problems which are beyond the reach of simple solutions.

This paper is concerned with the description of a problem which might initially appear to be too complex for such simple analyses.

In order to improve mineral extraction from deep mines, mixtures of mine waste and cement can be used to fill existing openings (stopes) so that, as the cement hydrates and develops strong bonds, the initially cohesionless material develops a strength which enables it to stand unsupported and to permit excavation of adjacent pillars. The hydration of the cement produces products with a volume which is typically less than the sum of the volumes of their constituents (water and cement).

Provided the backfill material is saturated, hydration volume change requires pore water movement with development of excess pore pressures and subsequent consolidation. If the hydrating mixture has a high permeability, pore fluid can flow under very low hydraulic gradients. This results in no appreciable change in pore pressure or effective stress. However, for low permeability materials, large hydraulic gradients may be required to generate the flow resulting in significant negative excess pore pressures and corresponding increases in effective stress.

This process has been referred to as 'self-desiccation' (**?**). The effective stress change as a result of self-desiccation has been shown to be significant in controlling both the short and long terms strength of backfill in underground mining operations and has a significant impact on the loads applied to barricade walls built to contain the backfill. In principle, the volume changes that accompany the process of self-desiccation would also have significant influence on the lateral stresses that are generated in a bored pile, where the hydrating material is again kinematically confined by the surrounding soil.

This paper is concerned with the generation of bench-mark results for a problem involving the chemical volume change during hydration of cement-soil (or cement-tailings) mixtures and the associated consolidation and flow within the material (assumed saturated). Writing the governing equation in terms of dimensionless quantities makes the solution applicable to an infinite range of real problem dimensions and material properties. Although the problem appears complicated, it can be encapsulated in a rather familiar governing partial differential equation for which exact solutions exist for certain simple geometries. It will be shown how approximate solutions can be obtained by applying an understanding of the governing mechanisms at the system level rather than the element level. The solutions are used to validate a numerical procedure for simulating the impact of chemical volume change of more complex boundary value problems.

Hydration of cement: one-dimensional conditions

We make the usual continuum assumption that, although we are dealing with a particulate material, our boundary value applications are sufficiently large that we can ignore the fluctuations in stresses and displacements that occur at scales of the order of a few particle sizes. The governing equations are written in incremental form, describing what happens in a time increment δt.

There will in general be a volume change associated with the hydration process. There will typically be seepage flow into and out of the element driven by Darcy's Law. Supposing for simplicity that the total stress on the element is constant, then a change of pore pressure will imply a change of effective stress and hence a change in volume of the soil/aggregate/cement/hydration products. Compressibility of the pore water may also be included in the balance of volumetric effects (Fig 1) and this leads to the appropriate governing equation.

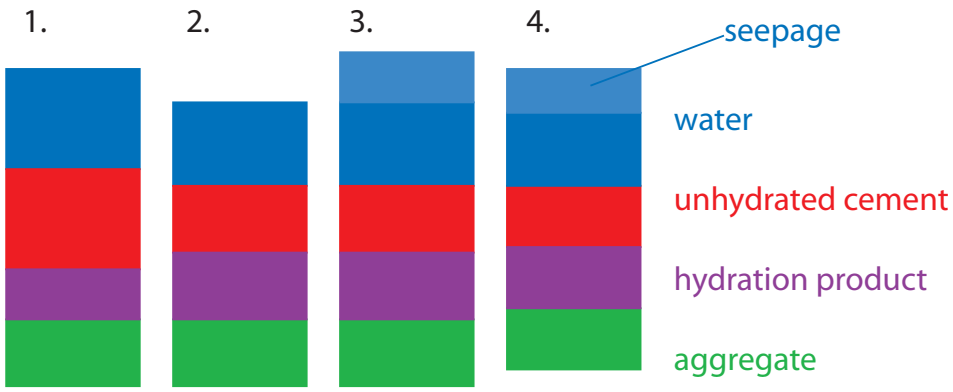

1. initial state
2. volume of hydration products increases; : volume of cement and water decreases
3. volume change resulting from seepage flow
4. pore pressure change: change in effective stress; compression of solid skeleton, compression of pore water

Fig. 1: Volume changes in hydrating element

The current degree of hydration $\zeta = 1 - \mu_{cc}$ where $\mu_{cc} = M_c/M_{co}$ is the ratio of current mass of unhydrated cement and original mass of (unhydrated) cement in the mixture. The rate of hydration decreases as the current degree of hydration heads towards completion:

$$\frac{\mathrm{d}\zeta}{\mathrm{d}t} = \kappa(1-\zeta) = -\frac{\mathrm{d}\mu_{cc}}{\mathrm{d}t}; \quad \zeta = 1 - \exp(-\kappa t) = 1 - \mu_{cc} \tag{1}$$

where κ is a parameter controlling the rate of hydration.

The ratio of the masses of water δM_{wh} and cement $\delta M_c = M_{co}\delta\mu_{cc}$ that combine to form the hydration products is constant $\lambda = \delta M_{wh}/\delta M_c$. The specific gravity of the cement is G_c and the typical specific gravity of the hydration products is G_h. The volume of hydration products is $-(1+\lambda)\delta\mu_{cc}M_{co}/G_h\rho_w$ and the volume of the constituent water and cement is $-(1/G_c + \lambda)\delta\mu_{cc}M_{co}/\rho_w$, where ρ_w is the density of water and the negative sign is required because the mass of unhydrated cement is decreasing. With total volume V of a representative element, the initial

volume fraction of cement $v_{co} = M_{co}/G_c\rho_w V$. The rate of volume loss of hydration products (which is the rate of creation of space in the hydrating element) is:

$$\delta V_h = \kappa\omega v_{co}\exp(-\kappa t)V\delta t \tag{2}$$

where

$$\omega = 1 - \frac{G_c}{G_h} + \lambda\left(G_c - \frac{G_c}{G_h}\right) \tag{3}$$

Typical values might be $G_c \sim 3.1$, $G_h \sim 2.3$, $\lambda \sim 0.25$, $\omega \sim 0.1$.

Equation (2) can be integrated to get the change in volume within an element since the beginning of hydration

$$\Delta V_h(t) = \omega\nu_{co}V[1 - \exp(-\kappa t)] \tag{4}$$

Previous researchers (**?** summarised by **??**, and **?**) express the chemical shrinkage after complete hydration using a parameter described as the 'efficiency of hydration' (E_h) expressed in units of volume/mass. The parameter ω is a dimensionless form of E_h representing volume loss after complete hydration as a proportion of the original volume of cement.

The increase in volume of water resulting from seepage according to Darcy's Law:

$$\delta V_{ws} = V\left[\frac{k}{\rho_w g}\frac{\partial^2 u}{\partial x^2}\right]\delta t \tag{5}$$

where k is permeability and g is acceleration due to gravity.

If we assume that the aggregate-water-cement mixture has a one-dimensional stiffness $E_o = E(1-\nu)/[(1+\nu)(1-2\nu)]$ then, if the pore pressure in the element changes while the total stress σ remains constant, there will be a change in effective stress σ' resulting from the change in pore pressure, $\delta\sigma' = -\delta u$ leading

to compression straining of the element:

$$\delta\epsilon_x = \frac{\delta\sigma'}{E_o} = -\frac{\delta V_E}{V} \tag{6}$$

If the bulk modulus K_w of the pore water is finite then there will also be a change in volume of the pore water δV_w resulting from the change in pore water pressure:

$$\delta V_w = nV\delta u/K_w \tag{7}$$

where n is the porosity of the mixture. The remaining components - aggregate, cement - are essentially incompressible; straining of the mixture implies straining of the 'soil skeleton' which is the void space available for the fluid component - which for the saturated mixture is just the water.

There will then be a balance between the increase in void space due to cement hydration, the loss of volume due to change in effective stress, the gain in volume of water from seepage, and the reduction in volume of the compressed water:.

$$\delta V_h - \delta V_E - \delta V_{ws} - \delta V_w = 0 \tag{8}$$

$$\kappa\omega\nu_{co}\exp(-\kappa t) - \frac{k}{\rho_w g}\frac{\partial^2 u}{\partial x^2} + \frac{1}{E_o}\frac{\partial u}{\partial t} + \frac{n}{K_w}\frac{\partial u}{\partial t} = 0 \tag{9}$$

We can combine the last two terms by writing $\frac{1}{E^*} = \frac{1}{E_o} + \frac{n}{K_w}$, or else treat the pore fluid as incompressible for the present, recognising that the consequence of finite pore fluid compressibility will be to produce a small decrease in compressibility.

We define a coefficient of consolidation $c_v = kE^*/\rho_w g$; for hydration of a finite layer of thickness H we introduce a dimensionless coordinate $\tilde{x} = x/H$, a dimensionless time $\tilde{t} = c_v t/H^2$, a dimensionless rate of hydration $\kappa^* = \kappa H^2/c_v$, and a dimensionless pore pressure $\tilde{u} = u/E^*\omega\nu_{co}$. Our governing equation then

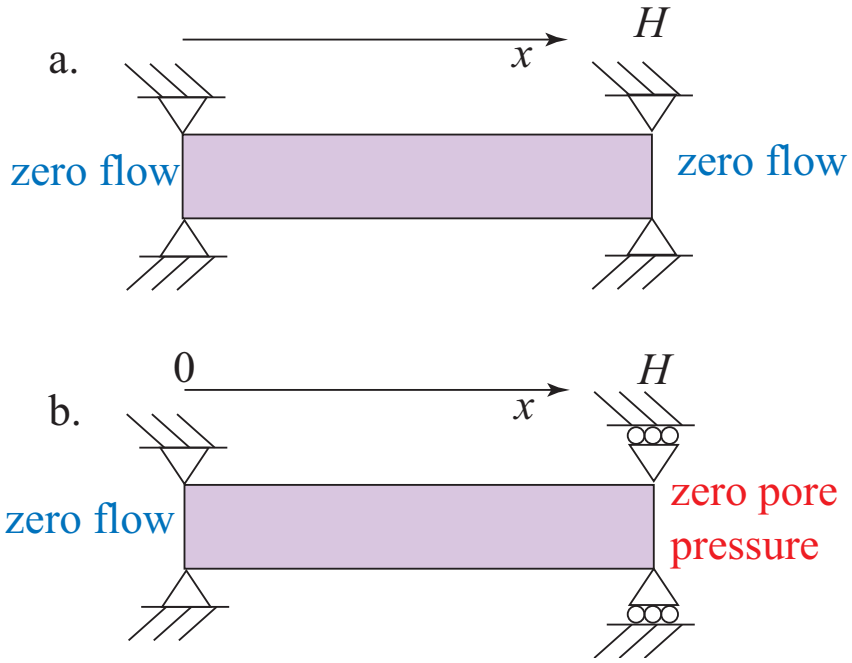

Fig. 2: One-dimensional problem definition: (a) element with no drainage at either end; (b) element with drainage at one end

becomes:

$$\kappa^* \exp(-\kappa^* \tilde{t}) - \frac{\partial^2 \tilde{u}}{\partial \tilde{x}^2} + \frac{\partial \tilde{u}}{\partial \tilde{t}} = 0 \tag{10}$$

In the absence of cement hydration ($\kappa^* = 0$) this is the familiar consolidation or diffusion equation. In the presence of cement hydration the first term acts as a sink term - attempting to remove water from the element (all elements) as a known function of time.

Kaczmarek and Hueckel (1998), for example, tackle a broader problem including effects of chemical concentration gradients as limiting factors for the reaction dynamics whereas we suppose that in the weak mixes that are used in mine backfill there is no lack of reaction constituents. We use this configuration as a vehicle for exploring available solutions of a problem with some realism. Through the introduction of dimensionless groups we have defined the problem in terms of one variable $\tilde{u}$ varying with position $\tilde{x}$ and time $\tilde{t}$ with just one single controlling

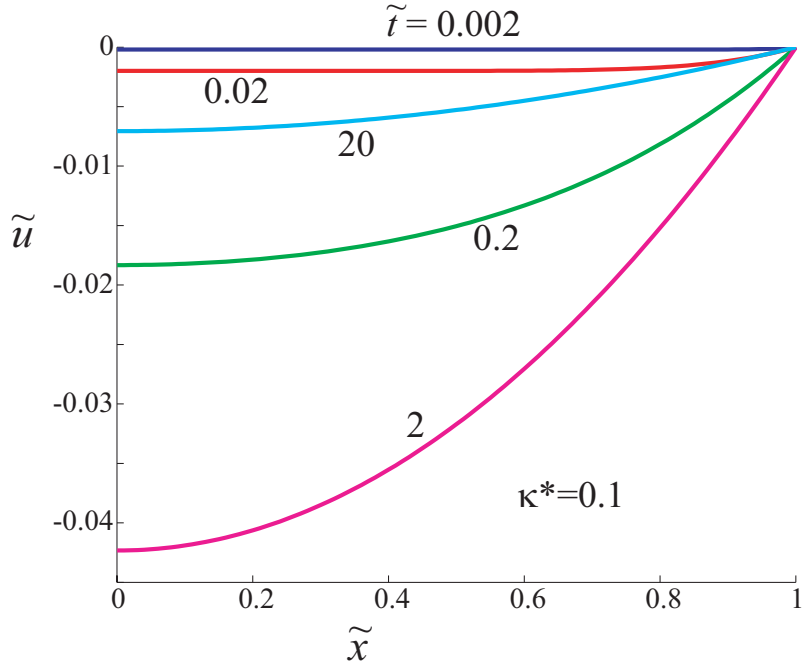

Fig. 3: One-dimensional flow: isochrones of $\tilde{u}$ ($\kappa^* = 0.1$)

parameter κ^*.

Finite layer with impermeable boundaries

For an initially uniform mixture with no drainage at the ends (Fig 2a), there will be no flow of water and the one-dimensional element will be undrained: $\partial^2\tilde{u}/\partial\tilde{x}^2 = 0$. Then

$$\frac{\mathrm{d}\tilde{u}}{\mathrm{d}\tilde{t}} = -\kappa^* \exp(-\kappa^*\tilde{t}) \tag{11}$$

$$\tilde{u} = \exp(-\kappa^*\tilde{t}) - 1 \tag{12}$$

and as $\tilde{t} \to \infty$, $\tilde{u} \to -1$ because the reduction in volume of the hydration products increases the void space available and a pore suction is necessary in order to compress the soil skeleton to compensate. This case provides a limiting case against which to compare results of analysis of more complex problems: (12) represents an upper limit on the pore pressure that can be generated). In fact,

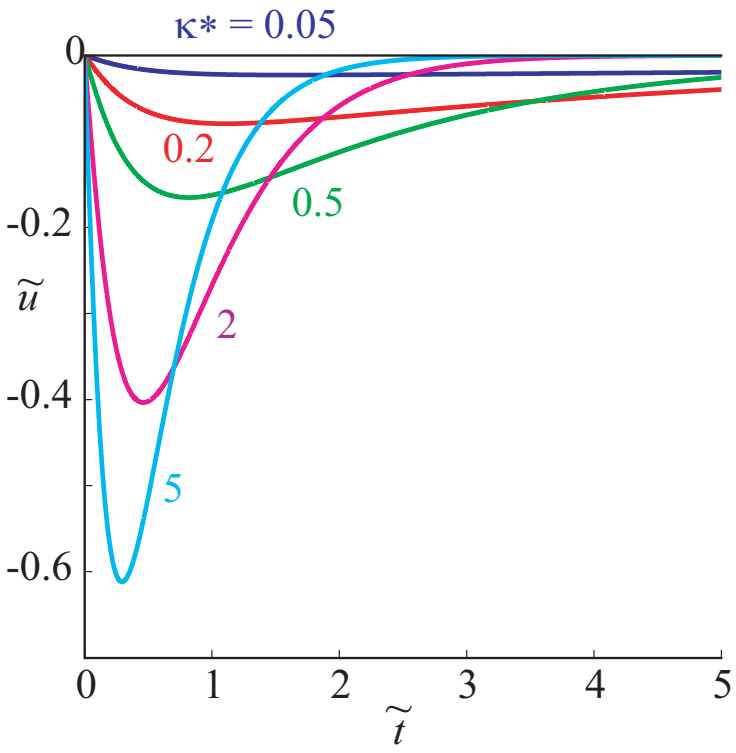

Fig. 4: One-dimensional flow: variation of normalised pore pressure $\tilde{u}$ at impermeable boundary $\tilde{x} = 0$ with normalised time $\tilde{t}$

with a permeable boundary (as analysed in the next section) the presence of the drainage boundary is only gradually felt through the hydrating concrete away from this boundary. Deprived of this feeling the pore pressure increases initially as $\tilde{u} \approx -\kappa^* \tilde{t}$.

Finite layer with one impermeable boundary

For a finite one-dimensional layer with no drainage at one end, and no pore pressure at the other (Fig 2b), the boundary conditions can be written: $\mathrm{d}\tilde{u}/\mathrm{d}\tilde{x} = 0$ at $\tilde{x} = 0$ and $\tilde{u} = 0$ at $\tilde{x} = 1$. With free drainage at $\tilde{x} = 1$ we expect $\tilde{u} \to 0$ as $\tilde{t} \to \infty$. The remaining boundary condition is an initial condition: at time $\tilde{t} = 0$, $\tilde{u} = 0$ for $0 < \tilde{x} < 1$.

?(p131) give the solution to the diffusion equation with a general time dependent source:

$$-A(\tilde{t}) - \frac{\partial^2 \tilde{u}}{\partial \tilde{x}^2} + \frac{\partial \tilde{u}}{\partial \tilde{t}} = 0 \tag{13}$$

as

$$\tilde{u} = \frac{4}{\pi} \sum_{m=0}^{\infty} \left\{ \frac{(-1)^m}{2m+1} \cos\left[(2m+1)\frac{\pi}{2}\tilde{x}\right] \int_0^{\tilde{t}} A(\tau) \exp\left[-\pi^2(2m+1)^2(\tilde{t}-\tau)/4\right] \mathrm{d}\tau \right\} \tag{14}$$

We have $A(\tilde{t}) = -\kappa^* \exp(-\kappa^* \tilde{t})$ so that:

$$\begin{aligned} \tilde{u} =& \frac{4\kappa^*}{\pi} \sum_{m=0}^{\infty} \frac{(-1)^{m+1}}{2m+1} \cos\left[(2m+1)\frac{\pi}{2}\tilde{x}\right] \times \\ & \times \frac{1}{[\pi^2(2m+1)^2/4 - \kappa^*]} \left\{ \exp[-\kappa^* \tilde{t}] - \exp[-\tilde{t}(\pi^2(2m+1)^2)/4] \right\} \end{aligned} \tag{15}$$

Isochrones of normalised pore pressure variation with time through the one-dimensional system are shown in Fig 3.

At the impermeable boundary $\tilde{x} = 0$ and the normalised pore pressure is:

$$\tilde{u} = \frac{4\kappa^*}{\pi} \sum_{m=0}^{\infty} \frac{(-1)^{m+1}}{(2m+1)[\pi^2(2m+1)^2/4 - \kappa^*]} \left\{ \exp[-\kappa^* \tilde{t}] - \exp[-\tilde{t}(\pi^2(2m+1)^2)/4] \right\} \tag{16}$$

The variation of normalised pore pressure at the impermeable boundary is shown in Fig 4.

As the hydration occurs, and pore pressures develop, deformations will occur. Since it is assumed that the total (axial) stress remains constant, the axial strains will be directly related to the changes in pore pressure, which correspond to the changes in effective stress, through the one-dimensional stiffness E_o. The displacements $a(x)$ through the layer can be calculated by numerical integration of the pore pressure $\tilde{u}$, setting the displacement to zero at the impermeable boundary

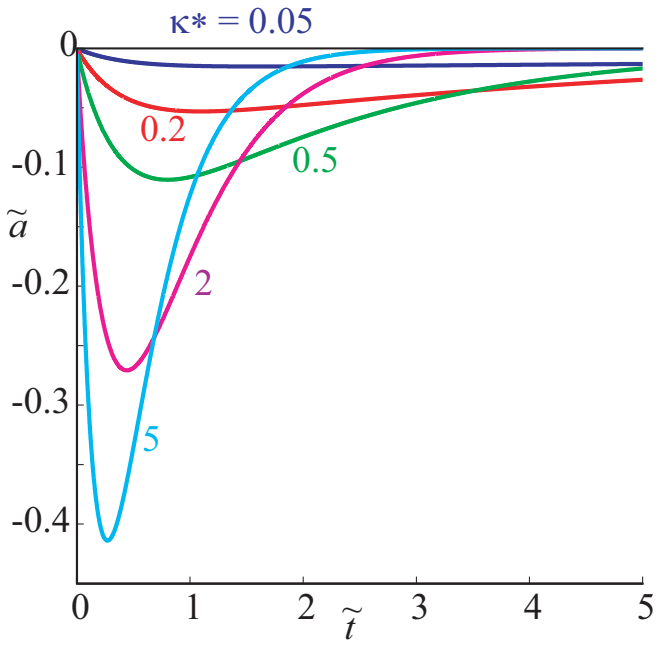

Fig. 5: One-dimensional flow: variation of normalised displacement $\tilde{a}$ at free boundary $\tilde{x} = 1$ with normalised time $\tilde{t}$

$\tilde{x} = 0$.

$$\begin{aligned}\tilde{a} =& \frac{a}{H\omega\nu_{co}}\frac{E_o}{E^*} = \int_0^{\tilde{x}} \tilde{u}\mathrm{d}\tilde{x} \\ =& \frac{8\kappa^*}{\pi^2}\sum_{m=0}^{\infty}\frac{(-1)^{m+1}}{(2m+1)^2}\sin\left[(2m+1)\frac{\pi}{2}\tilde{x}\right]\times \\ &\times\frac{1}{[\pi^2(2m+1)^2/4-\kappa^*]}\left\{\exp[-\kappa^*\tilde{t}]-\exp[-\tilde{t}(\pi^2(2m+1)^2)/4]\right\}\end{aligned} \tag{17}$$

At the free end of the layer $\tilde{x} = 1$ and the displacement is:

$$\tilde{a} = -\frac{8\kappa^*}{\pi^2}\sum_{m=0}^{\infty}\frac{\left\{\exp[-\kappa^*\tilde{t}]-\exp[-\tilde{t}(\pi^2(2m+1)^2)/4]\right\}}{(2m+1)^2[\pi^2(2m+1)^2/4-\kappa^*]} \tag{18}$$

Displacements are shown in Fig 5 for the free end of the layer, $\tilde{x} = 1$.

There are various limiting regimes of response. For $\tilde{t} \approx 0$, movement of pore

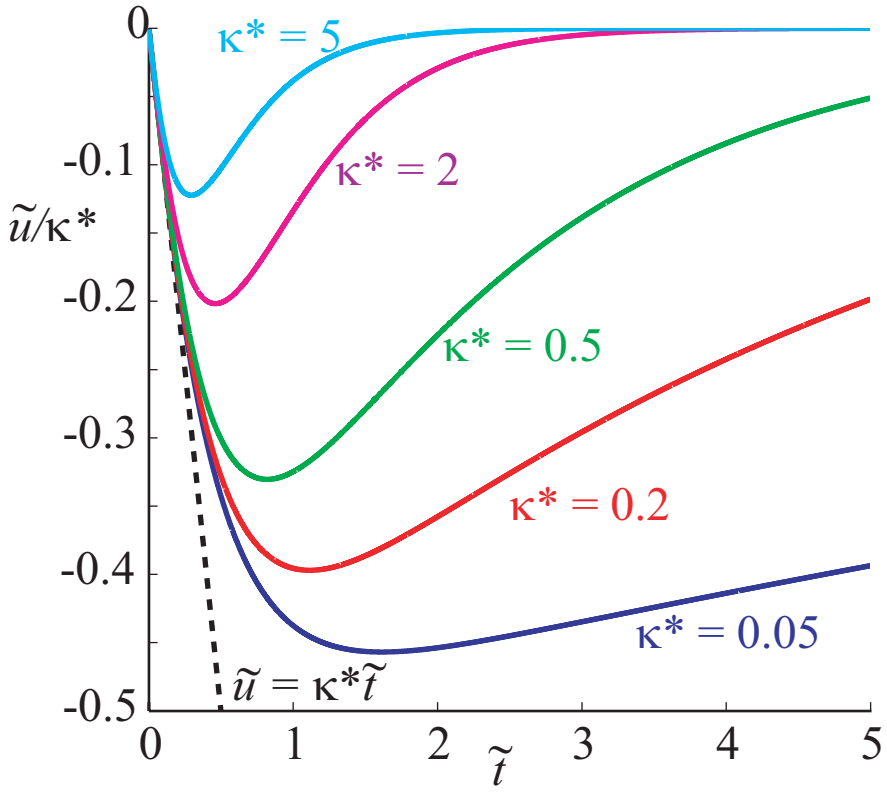

Fig. 6: One-dimensional flow: variation with normalised time $\tilde{t}$ of pore pressure $\tilde{u}/\kappa^*$ at impermeable boundary $\tilde{x} = 0$

water is restricted and the governing equation (10) becomes:

$$\kappa^* + \frac{\mathrm{d}\tilde{u}}{\mathrm{d}\tilde{t}} = 0; \quad \Rightarrow \quad \tilde{u} = -\kappa^* \tilde{t} \tag{19}$$

Plotting $\tilde{u}/\kappa^*$ with time at $\tilde{x} = 0$ (Fig 6) confirms this response as a limit to the pore pressure generation.

If the rate of hydration (indicated by the value of κ^*) is extremely high then the maximum pore pressure generated will approach the maximum possible pore pressure $\tilde{u} \to 1$ (Fig 4). In the limit the hydration and consolidation processes become completely uncoupled and the consolidation equation is applied to the classical problem of dissipation of an initial uniform pore pressure. This dissipation occurs in two stages: first the presence of the drainage boundary is gradually

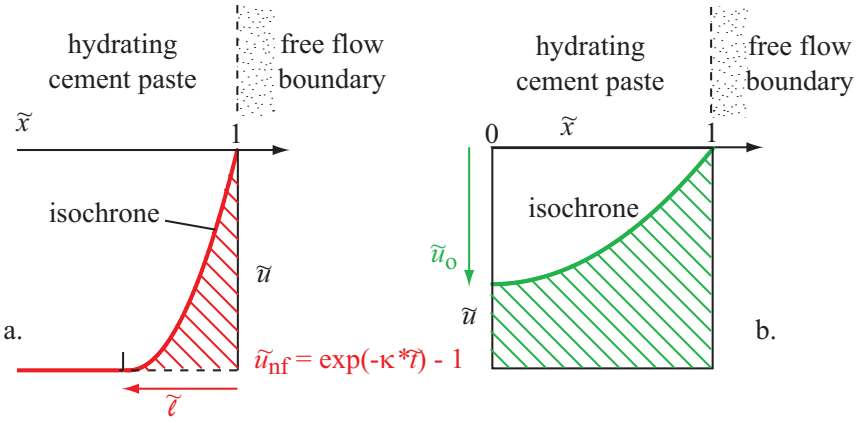

Fig. 7: One-dimensional flow: parabolic pore pressure isochrone (a) as effect of free flow boundary is felt further into hydrating backfill; and (b) as pore pressure at $\tilde{x} = 0$ is eliminated by flow.

felt at greater distances into the consolidating material. For our layer of thickness H the presence of the draining boundary is felt at a time $\tilde{t} \approx 1/16$ (**?**), (**?**). The no-flow pore pressure is $\tilde{u}_{nf}$ (12). The consolidation is then dominated by the first harmonic. The first term of the series solution (15) with $\tilde{x} = 0$ describes the dissipation of the pore pressure at the impermeable boundary:

$$\tilde{u} = -\frac{4}{\pi} \left\{ \exp[-(\pi^2 \tilde{t})/4] \right\} \tag{20}$$

Approximate solution using parabolic isochrones

The approximate solution that can be developed using the method of parabolic isochrones assumes simple geometry - a constant mode shape - for the isochrones of pore pressure (Fig 3) (**?**) (instead of using the full complex analytical expression (15)) and then applies the known physical constraints at the *system* level rather than at the level of the infinitesimal element. There are two phases of the system response.

In the first phase, the effect of the drainage boundary at $\tilde{x} = 1$ penetrates

gradually into the layer (Fig 7a). The typical pore pressure isochrone for this regime assumes a parabolic form for the variation of pore pressure from the no-flow limit $\tilde{u}_{nf}$ to zero at the drainage boundary at time $\tilde{t}$. The area above the isochrone shown shaded in Fig 7a indicates the combined change in effective stress - and hence change in volume - that has occurred at the present instant of time as a result of hydration shrinkage and flow. The *rate* at which this volume is changing must match the rate of flow out of the system which is governed by the slope of the isochrone at $\tilde{x} = 1$. Hence, from the geometry of the parabola:

$$\frac{\mathrm{d}[\tilde{u}_{nf}\tilde{\ell}/3]}{\mathrm{d}\tilde{t}} = \frac{2\tilde{u}_{nf}}{\tilde{\ell}} \tag{21}$$

$$\tilde{\ell}\frac{\mathrm{d}\tilde{\ell}}{\mathrm{d}\tilde{t}} = 6 + \frac{\tilde{\ell}^2\exp(-\kappa^*\tilde{t})}{\exp(-\kappa^*\tilde{t}) - 1} \tag{22}$$

Writing

$$M = \frac{\exp\left[-\kappa^*\left(\tilde{t}_j + \Delta\tilde{t}/2\right)\right]}{\exp\left[-\kappa^*\left(\tilde{t}_j + \Delta\tilde{t}/2\right)\right] - 1}; \quad \tilde{\ell}_{j+1} = \tilde{\ell}_j + \Delta\tilde{\ell} \tag{23}$$

$$\Delta\tilde{\ell}^2 + 2\frac{\tilde{\ell}_j\left(1 - M\Delta\tilde{t}\right)}{1 - M\Delta\tilde{t}/2}\Delta\tilde{\ell} - \frac{2\left(6 + M\tilde{\ell}_j^2\right)\Delta\tilde{t}}{1 - M\Delta\tilde{t}/2} = 0 \tag{24}$$

and $\Delta\tilde{\ell}$ can be found from the positive root of this quadratic equation.

In the second phase of response, the drainage front has reached the impermeable boundary at $\tilde{x} = 0$ (Fig 7b) and the balance between the rate of flow at $\tilde{x} = 1$ and the rate of change of the area under the parabolic isochrone (shaded in Fig 7b) which is controlled by the pore pressure $\tilde{u}_o$ at $\tilde{x} = 0$ now implies:

$$\frac{\mathrm{d}}{\mathrm{d}\tilde{t}}[\tilde{u}_{nf} - \tilde{u}_o + \tilde{u}_o/3] = -\kappa^*\exp(-\kappa^*\tilde{t}) - \frac{2}{3}\frac{\mathrm{d}\tilde{u}_o}{\mathrm{d}\tilde{t}} = 2\tilde{u}_o \tag{25}$$

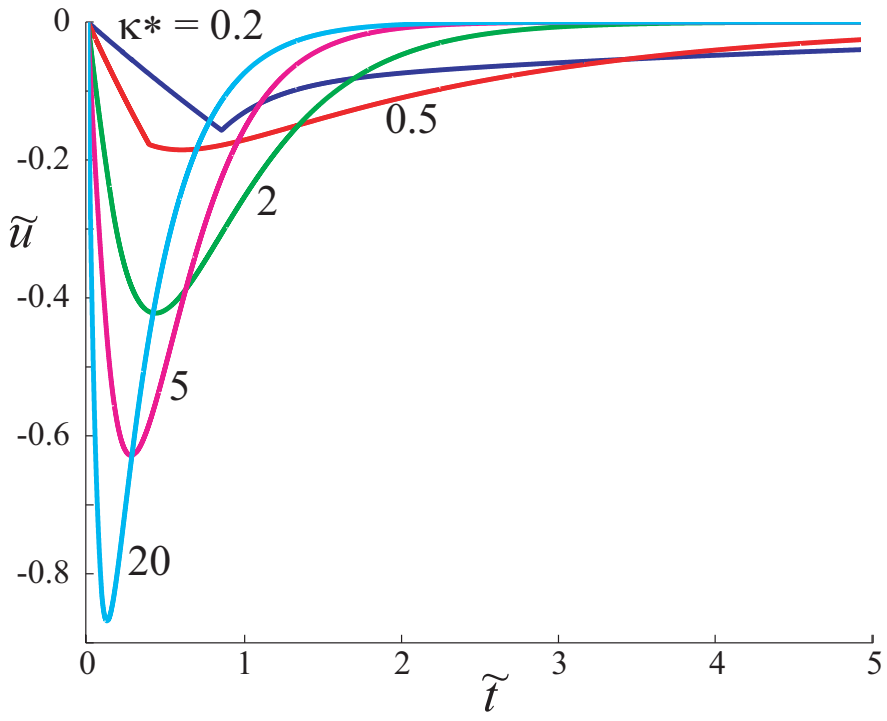

Fig. 8: One-dimensional flow: approximate analysis using parabolic isochrones: pore pressure at $\tilde{x} = 0$

Writing $\tilde{u}_{j+1} = \tilde{u}_j + \Delta\tilde{u}$

$$\Delta\tilde{u} = -\frac{3\left[\tilde{u}_j + (\kappa^*/2)\exp(-\kappa^*(\tilde{t}_j + \Delta\tilde{t}/2))\right]\Delta\tilde{t}}{1 + 3\Delta\tilde{t}/2} \tag{26}$$

The shrinkage of the hydrating cemented fill is still occurring so that the consequent continuing reduction (*increasing* negative magnitude) of $\tilde{u}_{nf}$ is competing against the effect of pore water flow (trying to *reduce* the negative magnitude of $\tilde{u}_{nf}$). The variation of pore pressure at $\tilde{x} = 0$ deduced from this approximate parabolic isochrone solution is shown in Fig 8.

The displacements calculated from the parabolic isochrone approximation are shown in Fig 9. With low values of κ^* the approximation is perhaps a little too coarse but the correspondence between exact and approximate values is really rather close (compare Figs 4 and 8 and Figs 5 and 9).

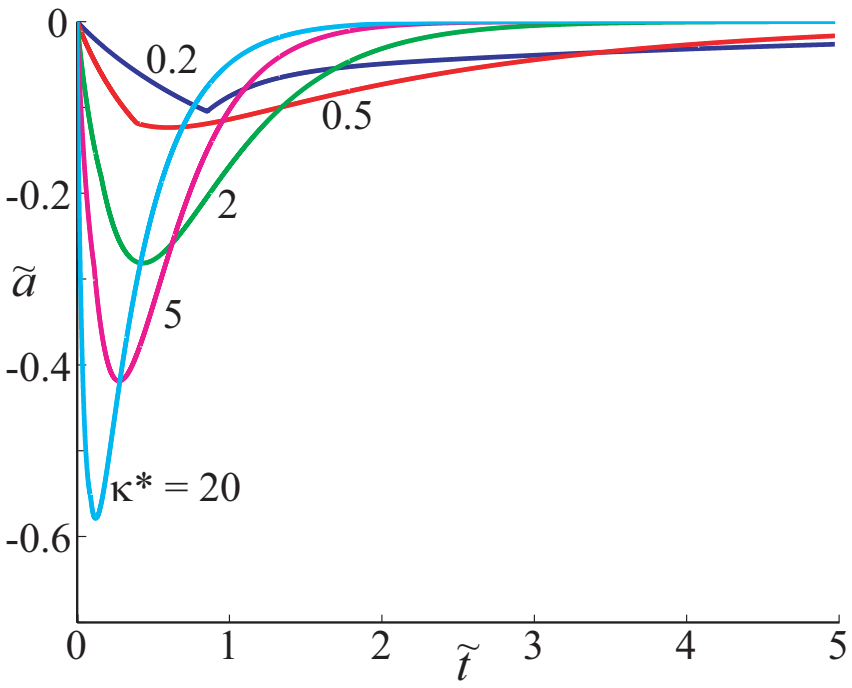

Fig. 9: One-dimensional flow: approximate analysis using parabolic isochrones: displacement at $\tilde{x} = 1$

Axisymmetric self-desiccation and consolidation

Under conditions of axial symmetry (Fig 10a), the only certain constraint is that the deformation occurs in plane strain with a vertical axis of symmetry. We have to combine elastic constitutive response, kinematic compatibility, and equilibrium. We assume that the elastic and permeability properties are constant with time and position.

From Hooke's Law, taking tensile stresses and strains as positive,

$$\sigma'_z = \mu(\sigma'_r + \sigma'_\theta) \tag{27}$$

and the corresponding change in mean effective stress

$$p' = (1 + \mu)(\sigma'_r + \sigma'_\theta)/3 \tag{28}$$

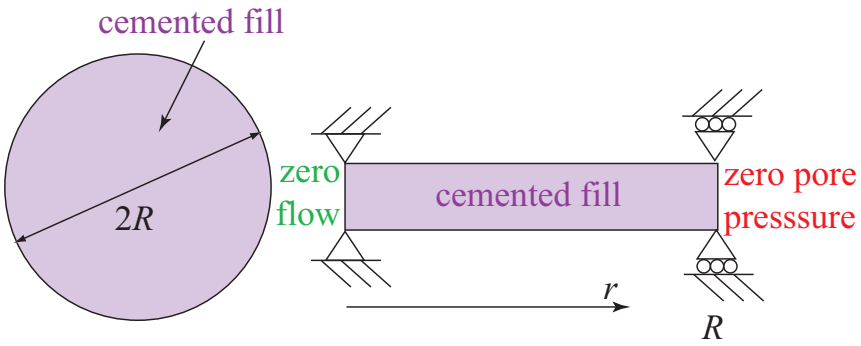

Fig. 10: Axisymmetric problem definition: cemented fill radius R

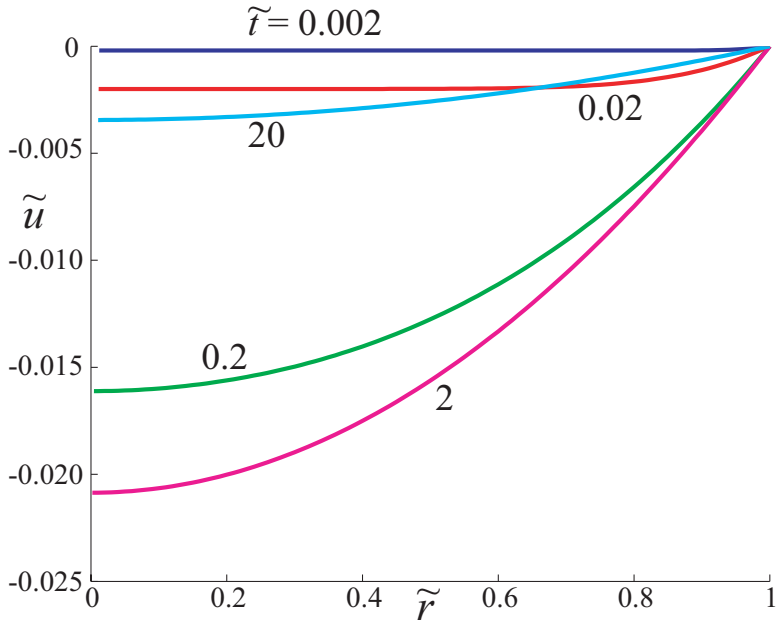

Fig. 11: Axisymmetric flow: isochrones of $\tilde{u}$ ($\kappa^* = 0.1$)

also from Hooke's law, with the value of σ'_z from (27) and the stiffness formulation

$$\begin{aligned} E\epsilon_r &= \sigma'_r - \mu\sigma'_\theta - \mu^2(\sigma'_r + \sigma'_\theta) = (1+\mu)[(1-\mu)\sigma'_r - \mu\sigma'_\theta]; \\ E\epsilon_\theta &= \sigma'_\theta - \mu\sigma'_r - \mu^2(\sigma'_r + \sigma'_\theta) = (1+\mu)[(1-\mu)\sigma'_\theta - \mu\sigma'_r] \end{aligned} \tag{29}$$

or alternatively using the compliance formulation

$$\begin{aligned} \sigma'_r &= \frac{E}{(1+\mu)(1-2\mu)}[(1-\mu)\epsilon_r + \mu\epsilon_\theta] \\ \sigma'_\theta &= \frac{E}{(1+\mu)(1-2\mu)}[(1-\mu)\epsilon_\theta + \mu\epsilon_r] \end{aligned} \tag{30}$$

Then

$$\sigma'_\theta + \sigma'_r = \frac{E}{(1+\mu)(1-2\mu)}(\epsilon_r + \epsilon_\theta) = \frac{3p'}{1+\mu} = \frac{E}{(1+\mu)(1-2\mu)}\epsilon_v \tag{31}$$

Kinematic compatibility links the components of strain through the incremental outward radial displacement a

$$\epsilon_r = \frac{\mathrm{d}a}{\mathrm{d}r}; \quad \epsilon_\theta = \frac{a}{r}; \quad \Rightarrow \quad \epsilon_r = \frac{\mathrm{d}(r\epsilon_\theta)}{\mathrm{d}r} \tag{32}$$

$$\epsilon_v = \epsilon_r + \epsilon_\theta = \frac{\mathrm{d}a}{\mathrm{d}r} + \frac{a}{r} = \frac{1}{r}\frac{\mathrm{d}(ar)}{\mathrm{d}r} \tag{33}$$

From (32) and (29):

$$\sigma'_\theta - \sigma'_r = r\mu\frac{\mathrm{d}\sigma'_r}{\mathrm{d}r} - r(1-\mu)\frac{\mathrm{d}\sigma'_\theta}{\mathrm{d}r} \tag{34}$$

Equilibrium produces a link between total stresses - or effective stresses with pore pressure. With tensile stresses positive and pore pressure a positive pressure, we

write $\sigma_r = \sigma'_r - u$ (and similarly for circumferential stress).

$$\begin{aligned} \sigma_\theta - \sigma_r &= r\frac{\mathrm{d}\sigma_r}{\mathrm{d}r} \\ \sigma'_\theta - \sigma'_r &= r\frac{\mathrm{d}\sigma'_r}{\mathrm{d}r} - r\frac{\mathrm{d}u}{\mathrm{d}r} \end{aligned} \tag{35}$$

$$\begin{aligned} -r\frac{\mathrm{d}u}{\mathrm{d}r} &= r\mu\frac{\mathrm{d}\sigma'_r}{\mathrm{d}r} - r(1-\mu)\frac{\mathrm{d}\sigma'_\theta}{\mathrm{d}r} - r\frac{\mathrm{d}\sigma'_r}{\mathrm{d}r} \\ &= -\frac{E(1-\mu)}{(1+\mu)(1-2\mu)}r\frac{\mathrm{d}}{\mathrm{d}r}(\epsilon_\theta + \epsilon_r) = -rK_1\frac{\mathrm{d}\epsilon_v}{\mathrm{d}r} \end{aligned} \tag{36}$$

with the controlling stiffness parameter being

$$K_1 = \frac{E(1-\mu)}{(1+\mu)(1-2\mu)} \tag{37}$$

The equation of flow links volumetric strain with pore pressure gradient

$$\frac{\partial \epsilon_v}{\partial t} = \frac{k}{\gamma_w}\frac{1}{r}\frac{\partial}{\partial r}\left(r\frac{\partial u}{\partial r}\right) \tag{38}$$

The volumetric strain rate arising from the hydration shrinkage is $\kappa\omega\nu_{co}\exp(-\kappa t)$ and the compressibility of the pore water gives an additional term $(n/K_w)\partial u/\partial t$ so that the balance of volumetric strains gives

$$\kappa\omega\nu_{co}\exp(-\kappa t) - \frac{k}{\gamma_w}\frac{1}{r}\frac{\partial}{\partial r}\left(r\frac{\partial u}{\partial r}\right) + \frac{\partial \epsilon_v}{\partial t} + \frac{n}{K_w}\frac{\partial u}{\partial t} = 0 \tag{39}$$

we have

$$K_1 r\frac{\partial \epsilon_v}{\partial r} = r\frac{\partial u}{\partial r} \tag{40}$$

$$\kappa\omega\nu_{co}\exp(-\kappa t) - \frac{kK_1}{\gamma_w}\frac{1}{r}\frac{\partial}{\partial r}\left(r\frac{\partial \epsilon_v}{\partial r}\right) + \frac{\partial \epsilon_v}{\partial t} + \frac{n}{K_w}\frac{\partial u}{\partial t} = 0 \tag{41}$$

where K_1 is the stiffness and k the permeability of the cemented fill.

Normalising $c_v = kK_1/\gamma_w$, $\tilde{r} = r/R$, $\tilde{t} = c_v t/R^2$, $\kappa^* = \kappa R^2/c_v$: $\tilde{\epsilon} = \epsilon_v/\omega\nu_{co}$, $\tilde{u} = u/K_1\omega\nu_{co}$

$$\kappa^* \exp(-\kappa^* \tilde{t}) - \frac{1}{\tilde{r}} \frac{\partial}{\partial \tilde{r}} \left(\tilde{r} \frac{\partial \tilde{\epsilon}}{\partial \tilde{r}} \right) + \frac{\partial \tilde{\epsilon}}{\partial \tilde{t}} + \frac{K_1 n}{K_w} \frac{\partial \tilde{u}}{\partial \tilde{t}} = 0 \tag{42}$$

We might neglect the final term, or incorporate its influence by reducing slightly the value of K_1.

The governing equation is now written in terms of the volumetric strain (instead of pore pressure) and we have made no constraining assumption apart from plane strain and isotropic elasticity. To determine pore pressure from volumetric strain we note that

$$\frac{\partial \tilde{\epsilon}}{\partial \tilde{r}} = \frac{\partial \tilde{u}}{\partial \tilde{r}}; \quad \Rightarrow \quad \tilde{u}(\tilde{r}) = \tilde{\epsilon}(\tilde{r}) + \Gamma \tag{43}$$

where Γ is a constant of integration calculated to give zero pore pressure at a drainage boundary. For the plain cylinder of cemented fill, $\tilde{u} = 0$ at $\tilde{r} = 1$ so that $\Gamma = -\tilde{\epsilon}_1$ and

$$\tilde{u} = (\tilde{\epsilon} - \tilde{\epsilon}_1) \tag{44}$$

To determine incremental displacement we integrate (33)

$$a = \frac{1}{r} \int_0^r r \epsilon_v \mathrm{d}r; \quad \tilde{a} = \frac{a}{R\omega\nu_{co}} = \frac{1}{\tilde{r}} \int_0^{\tilde{r}} \tilde{r} \tilde{\epsilon} \mathrm{d}\tilde{r} \tag{45}$$

noting that $\tilde{a} = 0$ at $\tilde{r} = 0$.

?(p204) give the solution to the axisymmetric diffusion equation for heat flow with zero initial and surface temperature and heat production proportional to $\exp(\kappa^* t)$ per unit time and unit volume for $t > 0$. We can adapt this solution for our problem to give the radial and time variation of normalised volumetric

strain:

$$\tilde{\epsilon} = -\exp[-\kappa^* \tilde{t}] \left\{ \frac{\mathrm{J}_0[\tilde{r}\kappa^{*1/2}]}{\mathrm{J}_0[\kappa^{*1/2}]} - 1 \right\} + 2\kappa^* \sum_{n=1}^{\infty} \frac{\exp[-R_n^2 \tilde{t}]\mathrm{J}_0[\tilde{r}R_n]}{R_n(R_n^2 - \kappa^*)\mathrm{J}_1[R_n]} \tag{46}$$

where R_n are the positive roots of $\mathrm{J}_0[x] = 0$ and J_0 and J_1 are Bessel functions of the first kind of order zero and 1 respectively.

At the centre, $\tilde{r} = 0$,

$$\tilde{\epsilon} = -\exp(-\kappa^* \tilde{t}) \left\{ \frac{\mathrm{J}_0[0]}{\mathrm{J}_0[\kappa^{*1/2}]} - 1 \right\} + 2\kappa^* \sum_{n=1}^{\infty} \frac{\exp(-R_n^2 \tilde{t})\mathrm{J}_0[0]}{R_n(R_n^2 - \kappa^*)\mathrm{J}_1[R_n]} \tag{47}$$

with $\mathrm{J}_0[0] = 1$.

At the boundary of the hydrating material $\tilde{r} = 1$

$$\tilde{\epsilon}_1 = 2\kappa^* \sum_{n=1}^{\infty} \frac{\exp[-R_n^2 \tilde{t}]\mathrm{J}_0[R_n]}{R_n(R_n^2 - \kappa^*)\mathrm{J}_1[R_n]} \tag{48}$$

Hence

$$\begin{aligned} \tilde{u} = &-\exp[-\kappa^* \tilde{t}] \left\{ \frac{\mathrm{J}_0[\tilde{r}\kappa^{*1/2}]}{\mathrm{J}_0[\kappa^{*1/2}]} - 1 \right\} \\ &+ 2\kappa^* \sum_{n=1}^{\infty} \frac{\exp[-R_n^2 \tilde{t}]\left[\mathrm{J}_0[\tilde{r}R_n] - \mathrm{J}_0[R_n]\right]}{R_n(R_n^2 - \kappa^*)\mathrm{J}_1[R_n]} \end{aligned} \tag{49}$$

The central pore pressure is shown as a function of time in Fig 12.

In order to deduce the radial displacements from the computed volumetric strains we use (45).

$$\tilde{a} = \frac{1}{\tilde{r}} \int_0^{\tilde{r}} \tilde{r}\tilde{\epsilon} \mathrm{d}\tilde{r} \tag{50}$$

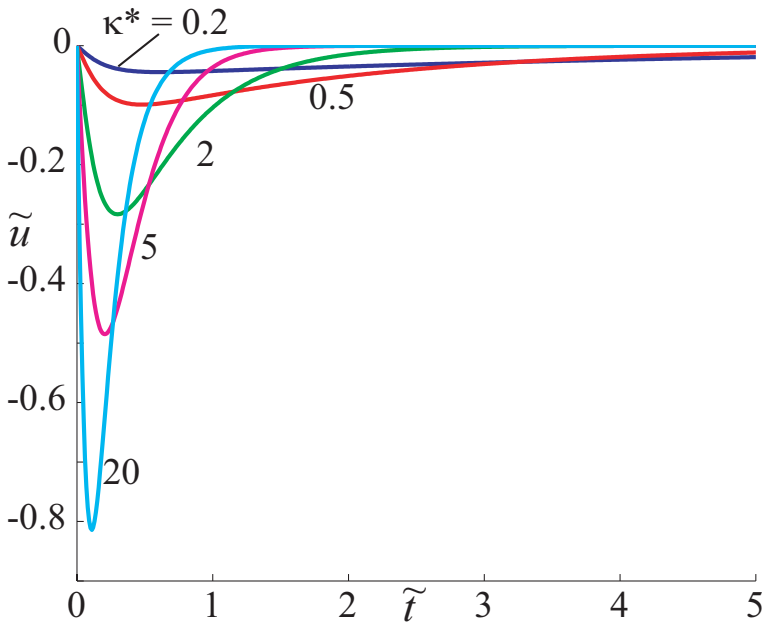

Fig. 12: Axisymmetric flow: variation of normalised pore pressure $\tilde{u}$ at impermeable boundary $\tilde{r} = 0$ with normalised time $\tilde{t}$

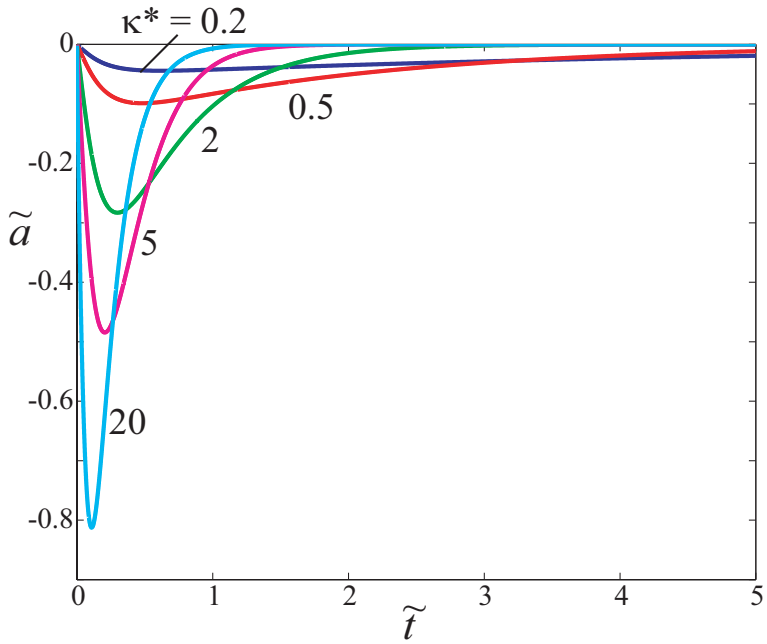

Fig. 13: Axisymmetric flow: variation of normalised displacement $\tilde{a}$ at free boundary $\tilde{r} = 1$ with normalised time $\tilde{t}$

and deduce after some manipulation that the displacement is:

$$\tilde{a} = -\exp[-\kappa^* \tilde{t}] \left\{ \frac{\mathrm{J}_1[\tilde{r}\kappa^{*1/2}]}{\kappa^{*1/2}\mathrm{J}_0[\kappa^{*1/2}]} - \frac{\tilde{r}}{2} \right\} + 2\kappa^* \sum_{n=1}^{\infty} \frac{\exp(-R_n^2 \tilde{t})\mathrm{J}_1[\tilde{r}R_n]}{R_n^2(R_n^2 - \kappa^*)\mathrm{J}_1[R_n]} \tag{51}$$

The displacement at the centre $\tilde{r} = 0$ is zero. The displacement at the outer boundary $\tilde{r} = 1$ is:

$$\tilde{a} = -\exp[-\kappa^* \tilde{t}] \left\{ \frac{\mathrm{J}_1[\kappa^{*1/2}]}{\kappa^{*1/2}\mathrm{J}_0[\kappa^{*1/2}]} - \frac{1}{2} \right\} + 2\kappa^* \sum_{n=1}^{\infty} \frac{\exp(-R_n^2 \tilde{t})}{R_n^2(R_n^2 - \kappa^*)} \tag{52}$$

The radial displacement at the outer boundary is shown as a function of time in Fig 13.

Finite difference solution for increasing stiffness with hydration time

The analytical solution of (10) can only be obtained for simple boundary conditions and constant material parameters. A finite difference formulation can be used to find solutions for a wider range of problems. The one-dimensional problem lends itself to a central difference formulation in space and time. With time step $\Delta\tilde{t}$ and position step $\Delta\tilde{x}$, and with subscript n referring to position and superscript j referring to time, (10) becomes for the one-dimensional problem:

$$\begin{aligned} &\kappa^* \exp(-\kappa^*[\tilde{t}^j + \tilde{t}^{j+1}]/2) - \\ &-\frac{1}{2}\left[\frac{\tilde{u}_{n-1}^{j+1} - 2\tilde{u}_n^{j+1} + \tilde{u}_{n+1}^{j+1}}{\Delta\tilde{x}^2} + \frac{\tilde{u}_{n-1}^{j} - 2\tilde{u}_n^{j} + \tilde{u}_{n+1}^{j}}{\Delta\tilde{x}^2}\right] + \frac{\tilde{u}_n^{j+1} - \tilde{u}_n^{j}}{\Delta\tilde{t}} = 0 \end{aligned} \tag{53}$$

This is equivalent to calculating the finite difference expressions at the time $\tilde{t}^j + \Delta\tilde{t}/2$. This leads to a set of simultaneous equations for $\tilde{u}_i^{j+1}$:

$$\begin{aligned} &-\frac{\beta}{2}\tilde{u}_{n-1}^{j+1} + (1+\beta)\tilde{u}_n^{j+1} - \frac{\beta}{2}\tilde{u}_{n+1}^{j+1} \\ &\quad = \frac{\beta}{2}(\tilde{u}_{n-1}^{j} + \tilde{u}_{n+1}^{j}) + (1-\beta)\tilde{u}_n^{j} - \kappa^* \exp(-\kappa^*[\tilde{t}^j + \tilde{t}^{j+1}]/2)\Delta\tilde{t} \end{aligned} \tag{54}$$

where $\beta = \Delta\tilde{t}/\Delta\tilde{x}^2$.

For the axisymmetric problem the corresponding finite difference formulation of the governing equation (42) in terms of volumetric strain is:

$$\begin{aligned} &-\frac{\beta}{2}\left[1 - \frac{\Delta\tilde{r}}{2\tilde{r}}\right]\tilde{\epsilon}_{n-1}^{j+1} + (1+\beta)\tilde{\epsilon}_n^{j+1} - \frac{\beta}{2}\left[1 + \frac{\Delta\tilde{r}}{2\tilde{r}}\right]\tilde{\epsilon}_{n+1}^{j+1} = \\ &= \frac{\beta}{2}\left[1 - \frac{\Delta\tilde{r}}{2\tilde{r}}\right]\tilde{\epsilon}_{n-1}^{j} + (1-\beta)\tilde{\epsilon}_n^{j} + \frac{\beta}{2}\left[1 + \frac{\Delta\tilde{r}}{2\tilde{r}}\right]\tilde{\epsilon}_{n+1}^{j} \\ &- \kappa^* \exp(-\kappa^*[\tilde{t}^j + \tilde{t}^{j+1}]/2)\Delta\tilde{t} \end{aligned} \tag{55}$$

For both problems the resulting set of equations has the form:

$$\boldsymbol{M}\tilde{\boldsymbol{\epsilon}}^{j+1} = \boldsymbol{d} \tag{56}$$

where the matrix $\boldsymbol{M}$ is tridiagonal. The equations resulting from (55) have the form:

$$\boldsymbol{M} = \begin{pmatrix} b_1 & c_1 & 0 & 0 & 0 & 0 & 0 \\ a_2 & b_2 & c_2 & 0 & 0 & 0 & 0 \\ 0 & a_3 & b_3 & c_3 & 0 & 0 & 0 \\ .. & .. & .. & .. & .. & .. & .. \\ 0 & 0 & 0 & a_{n-2} & b_{n-2} & c_{n-2} & 0 \\ 0 & 0 & 0 & 0 & a_{n-1} & b_{n-1} & c_{n-1} \\ 0 & 0 & 0 & 0 & 0 & a_n & b_n \end{pmatrix} \begin{pmatrix} \tilde{\epsilon}_1^{j+1} \\ \tilde{\epsilon}_2^{j+1} \\ \tilde{\epsilon}_3^{j+1} \\ .. \\ \tilde{\epsilon}_{n-2}^{j+1} \\ \tilde{\epsilon}_{n-1}^{j+1} \\ \tilde{\epsilon}_n^{j+1} \end{pmatrix} = \begin{pmatrix} d_1 \\ d_2 \\ d_3 \\ .. \\ d_{n-2} \\ d_{n-1} \\ d_n \end{pmatrix} \tag{57}$$

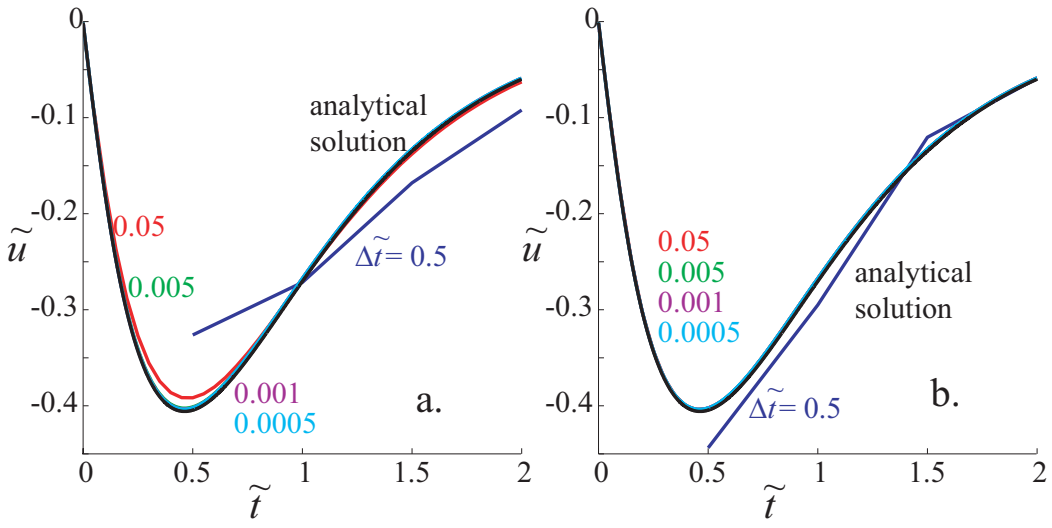

Fig. 14: Effect of timestep on accuracy of finite difference calculation: (a) incremental formulation; (b) single step formulation (54)

A solution can be obtained quite efficiently by the Thomas substitution method without the need for matrix inversion (?), (?). First forward substitution:

for $i = 1$ to $n - 1$;

$c_i = c_i/b_i$; $d_i = d_i/b_i$; $b_{i+1} = b_{i+1} - a_{i+1}c_i$; $d_{i+1} = d_{i+1} - a_{i+1}d_i$;

then backward substitution:

$\tilde{\epsilon}_n^{j+1} = d_n/b_n$;

for $i = n - 1$ to 1;

$\tilde{\epsilon}_i^{j+1} = d_i - c_i\tilde{\epsilon}_{i+1}^{j+1}$.

The effect of changing the step size for time in the finite difference solution is shown in Fig 14b. With large step size $\Delta\tilde{t} = 0.5$ the solution only matches the analytical solution very approximately. For smaller time steps $\Delta\tilde{t} = 0.05$, 0.005, 0.001 the result converges rapidly onto the analytical solution. For the present application step sizes $\Delta\tilde{x} = 0.02$ and $\Delta\tilde{t} = 0.0001$ have been used.

The finite difference solution can be applied to problems which do not admit of analytical solution. For example, in order to produce equations for which

analytical solutions are available we have restricted ourselves to hydration and consolidation with stiffness and permeability properties that do not change with time or position. In reality the stiffness of the cemented fill will increase as the hydration process continues (**?**). The permeability of the mixture controlling the rate of pore pressure movement may also change. The finite difference solution is readily adapted to include changes in stiffness (and permeability). For the hydrating concrete in the one-dimensional analysis we set $E^*/E_i^* = \xi(t)$:

$$\xi = \frac{E^*}{E_i^*} = 1 + (\xi_E - 1)\zeta = \xi_E - (\xi_E - 1)\exp(-\kappa^* \tilde{t}) \tag{58}$$

where E_i^* and E^* are the initial and current stiffnesses and ξ_E is the maximum increase in stiffness which occurs with completion of hydration, at infinite time.

We assume that the governing equation describes the *increments* of pore pressure that occur during the time increment. However, the Darcy flow will be controlled by the full gradient of pore pressure. We write $\tilde{u} = \tilde{u}_i + \delta\tilde{u}$ where $\tilde{u}_i$ is the pore pressure at the beginning of the time step. The governing equation (10) becomes:

$$\kappa^* \exp(-\kappa^* \tilde{t}) - \frac{\partial^2 \tilde{u}_i}{\partial \tilde{x}^2} - \frac{\partial^2 (\delta\tilde{u})}{\partial \tilde{x}^2} + \frac{1}{\xi}\frac{\partial(\delta\tilde{u})}{\partial \tilde{t}} = 0 \tag{59}$$

The coefficient of consolidation c_v is calculated for the initial stiffness E_i^* so that all the dimensionless definitions can be retained. The time dependent factor $E_i^*/E^* = 1/\xi$ must be applied to the time derivative.

The finite difference equation becomes:

$$\begin{aligned} &-\beta\delta\tilde{u}_{n-1}^{j+1} + (1/\xi + 2\beta)(\delta\tilde{u}_n^{j+1}) - \beta\delta\tilde{u}_{n+1}^{j+1} \\ &\quad = \beta(\tilde{u}_{i(n-1)}^{j} + \tilde{u}_{i(n+1)}^{j}) + \delta\tilde{u}_n^j - 2\beta\tilde{u}_{i(n)}^{j} - \kappa^* \exp(-\kappa^*[\tilde{t}^j + \tilde{t}^{j+1}]/2)\Delta\tilde{t} \end{aligned} \tag{60}$$

noting that $\delta\tilde{u}_n^j = 0$ by definition. The increments of pore pressure that are cal-

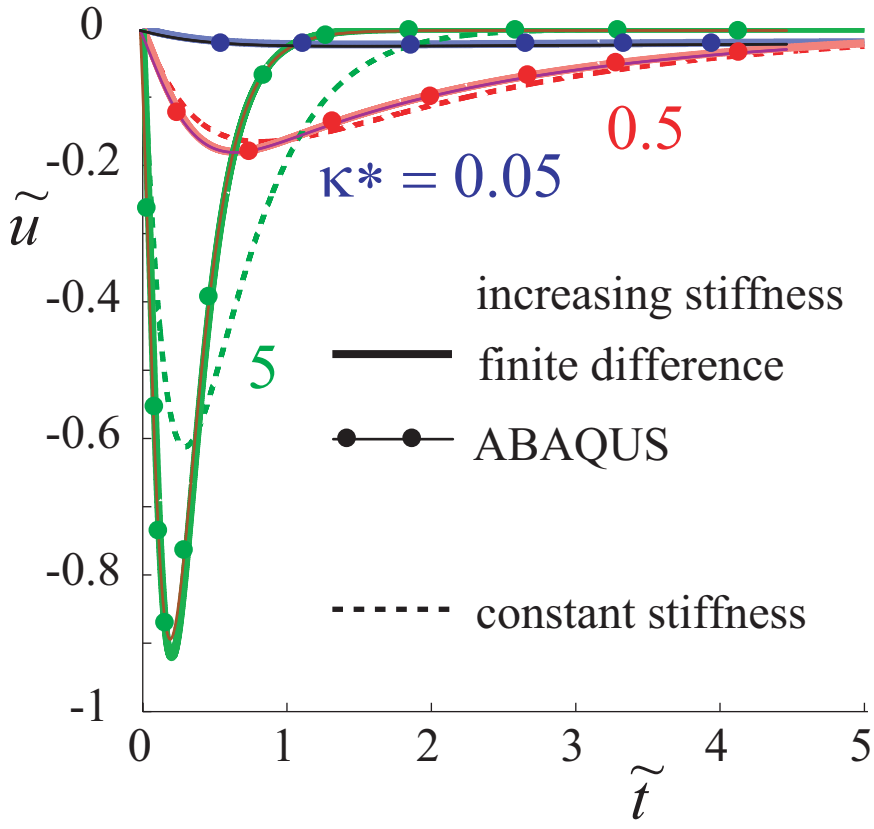

Fig. 15: Variation of normalised pore pressure $\tilde{u}$ at the impermeable boundary $\tilde{x} = 0$ with normalised time $\tilde{t}$: dashed lines, constant stiffness; solid lines, stiffness increasing by factor $\xi_E = 5$ with hydration; dotted lines, ABAQUS calculation

culated in each time increment are added to the pre-existing pore pressures to be used as initial pore pressures for the subsequent time increment. The deformations are computed from the increments of pore pressure using the appropriate current stiffness. This procedure has been used to compute the development of pore pressures (Fig 15) and displacements (Fig 16) in a cemented fill whose stiffness increases by a factor $\xi_E = 5$ with full hydration (compare Fig 4). The displacements can be compared with those which were calculated for constant stiffness and shown in Fig 5. As hydration progresses, the stiffness increases with time (58), the maximum change in pore pressure increases (becomes more negative) and the maximum displacement at the free boundary is reduced. The volume

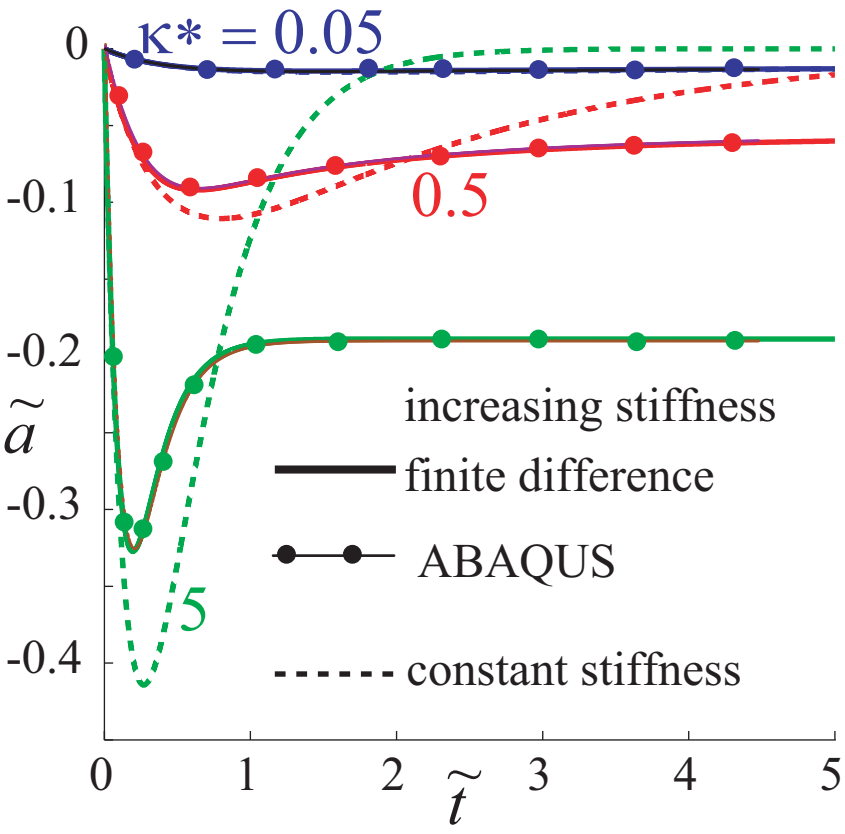

Fig. 16: Variation of normalised displacement $\tilde{a}$ at the permeable boundary $\tilde{x} = 1$ with normalised time $\tilde{t}$: dashed lines, constant stiffness; solid lines, stiffness increasing by factor $\xi_E = 5$ with hydration; dotted lines, ABAQUS calculation

change developing with hydration is not affected by the stiffness variation: with higher stiffness a given volume change generates a higher change of stress. With increasing time, the displacement is 'frozen' into the hydrating concrete whereas in the constant stiffness calculation the displacement returns to zero (Figs 16, 5). The frozen displacement represents a permanent locked-in shrinkage of the hydrated cemented fill.

Numerical modelling of coupled chemical shrinkage and consolidation

The analytical and approximate solutions presented above are restricted to one-dimensional and axisymmetric geometries. In order to model more general bound-

ary conditions, along with more general constitutive behaviour, a numerical solution is required. A numerical approach for simulating coupled chemical shrinkage and consolidation has been developed using the ABAQUS finite element software package (**?**). There are number of potential ways by which the chemical volume loss that occurs during cement hydration might be simulated. **?** imposes a strain on the pore fluid which is numerically equivalent to a chemical volume change. The change in porosity that occurs as a result of volumetric strains resulting from changes in mean effective stress is captured. However, the change in porosity that occurs as a result of the formation and growth of hydration products is not represented. However, this change in porosity is likely to be small for cement contents in the range of 3-6% that are most commonly used in mine backfill.

Such a procedure has been applied to simulate the one-dimensional problem (see Fig 2b) with chemical volume change. The problem was modelled with 30 8-noded plane strain finite elements. Repeated ABAQUS simulations have confirmed the theoretical deduction that the normalised pore pressure $\tilde{u}$ is controlled *only* by the parameter κ^*: dimensionless (normalised) numerical results were insensitive to the values of individual material parameters provided that the dimensionless parameter κ^* remained the same.

The results obtained from ABAQUS with the shrinkage simulation procedure for the one-dimensional problem and stiffness increasing with time are compared with the finite difference solution in Figs 15, 16. The calculated displacements and pore pressures show excellent agreement - they are essentially identical. The precise description of the peak of the pore pressure generation curve (Fig 15) is dependent on the size of the timestep size for the calculations.

Conclusions

This paper has tried to emphasise a number of key messages.

1. There is a need to be able to reduce apparently complex problems to their constituent parts in order to be able to make simple deductions about their expected response before embarking on an extensive programme of numerical analyses. This 'step zero' is an essential discipline to force the engineer to decide what physical mechanisms control the behaviour at element or basic system level. The results of subsequent numerical or physical modelling should be inspected to ensure that the understanding of the dominant mechanisms is indeed correct, and an iterative procedure may be required in order to provide a convergence of understanding and observation.

2. It will not always be possible to reduce complex problems to a simple conceptual model which can be used as part of the step 0 'back-of-the-envelope' prediction. However, careful consideration of the controlling mechanisms, combined with some simple but reasonable assumptions about the contributory parameters can lead to clear identification of dimensionless groups. Description of a problem in terms of dimensionless groups immediately generalises the problem and its solution. The solutions then possess an infinite range of applicability.

3. It may serendipitously be possible to obtain analytical solutions to the governing equations. More frequently it will be necessary to break down the problem further and to explore ways in which approximate solutions can be obtained. One method of solution might involve interpretation of the problem as a single system rather than as a collections of interconnected elements. The parabolic isochrone approach to approximate solution of consolidating systems builds on an assumed parabolic mode shape for the

isochrones of pore pressure. Such a technique finds a wide range of applications and can provide surprisingly accurate results.

4. It is not difficult to convert governing nonlinear partial differential equations into finite difference form for numerical solution. Such a finite difference approach does not require particularly complex programming but does extend the range of problems for which results can be obtained to provide benchmark comparisons for subsequent finite element analyses.

Acknowledgements

The first author is particularly grateful for the support of the Centre for Offshore Foundation Systems, University of Western Australia through the award of the Martin Fahey Visiting Fellowship during 2013. He also acknowledges the support of the Northern Research Partnership of Scottish universities at Dundee University.

The second author would like to acknowledge the support of Barrick Gold of Australia Ltd and Panoramic Resources Ltd through their sponsorship of an Australian Research Council linkage project (LP100200173) *Behaviour of cementing backfill in full scale mining stopes.*

References

Kaczmarek, M. & T. Hueckel (1998). Chemo-mechanical consolidation of clays: analytical solutions for a linearized one-dimensional problem. *Transport in Porous Media 32*, 49–74.

Shearing and consolidation: axial pipeline resistance?

Introduction

This note takes its inspiration from the model used by Randolph, White and Yan (2012) to describe the axial soil resistance of a pipeline on a deep seabed. The sliding of the pipeline is treated as a shearing process occurring on a thin interface of soil which can be described by a simple shear element which is capable of shearing and compression. This simple shear element is then coupled with an underlying compression (oedometer) element which maintains an overall constant volume condition by acting as a consolidation and drainage buffer in response to pore pressure changes and compressions in the interface layer. A consistent modelling approach is used to describe stiffness and strength and effects of rate of shearing. The contribution of the underlying oedometer element to consolidation is treated using the parabolic isochrone approximation.

Sliding of planar interface

The pipeline is assumed to be sitting and sliding on a thin planar interface layer of soil of thickness h_s. Shearing is concentrated in this interface layer, but the layer can also compress. Beneath this interface region is an 'infinite half space' of soil which acts as a drainage buffer for pore pressure changes in the interface and provides possibility only for one-dimensional compression. This provides a nice example of the description of a real problem using two 'one-dimensional' elements - one a simple shear element (which combines simple shear and one-dimensional compression) and the other a purely oedometric element.

1. Critical state line

Suppose that there is a critical state line which can be defined locally in relation to the initial state of the soil in terms of a 'state variable' $\psi_i = \varepsilon_{v_{max}}$ (which is the normal or volumetric strain required to bring the soil to the critical state at the current effective stress) and a stress level defined by the pipeline contact stress q. The compression of the soil is described by a one-dimensional stiffness E_o (Fig 1). This is equivalent to declaring the critical state line to be locally linear - consistent with the constant stiffness assumed for the analysis of consolidation - in terms of vertical strain and vertical stress. The maximum pore pressure that can be generated on sliding under constant volume conditions is then $u_{max} = E_o\psi_i$ and the link between actual pore pressure generation and actual vertical strain during partial drainage is $\varepsilon_v = [\psi_i - u/E_o]$.

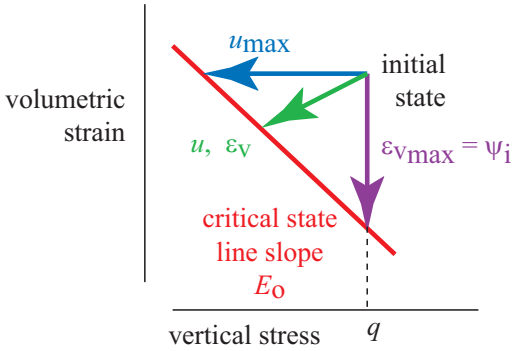

Fig. 1: Vertical strain and pore pressure development

2. Compression and consolidation

If vertical strain occurs within the interface of thickness h_s (Fig 2) (a vertical compression for $\psi_i > 0$), then there must be a compensating volumetric expansion of the nearby soil beneath in order to maintain an overall condition of constant volume. This expansion is associated with the advancing of a consolidation front into this soil as the pore pressure change at the boundary with the interface layer is felt to increasing depth. We assume a parabolic 'mode shape' for the pore pressure isochrone in this soil to a depth ℓ. The parabolic isochrone indicates that the average increase in pore pressure over the depth ℓ (decrease in effective stress) is one third of the change in pore pressure at the boundary. The resulting deformation is $u\ell/3E_o$. We also know for the consolidating soil that the *rate* at which water flows across the boundary with the interface layer $2(u/\ell)(k/\gamma_w)$ must balance the *rate* of volume expansion resulting from the reduction in effective stress described by the parabolic isochrone. Hence:

$$\frac{\mathrm{d}(u\ell)}{3E_o \mathrm{d}t} = \frac{2ku}{\ell\gamma_w} \Rightarrow \ell = \sqrt{12c_v t} \tag{1}$$

for constant pore pressure u, where the coefficient of consolidation $c_v = kE_o/\gamma_w$.

The deformation of the shearing layer is $h_s[\psi_i - u/E_o]$ so that

$$\frac{u\ell}{3E_o} = h_s\left[\psi_i - \frac{u}{E_o}\right] \Rightarrow \tilde{u} = \frac{\tilde{\psi}_i}{1+\sqrt{4\tilde{t}/3}} \tag{2}$$

where we introduce dimensionless groups $\tilde{t} = c_v t/h_s^2$ for time, $\tilde{u} = u/q$ for pore pressure and $\tilde{\psi} = E_o\psi/q$ for state variable. There is evidently a contradiction in writing this equation because we have assumed constant pore pressure in calculating the value of ℓ. We resolve this issue in the next section.

If the interface soil is trying to compress as it is sheared then the vertical strain will be (let us suppose) positive. For undrained or partially drained interface soil the pore pressure will be positive and water will flow down the pore pressure

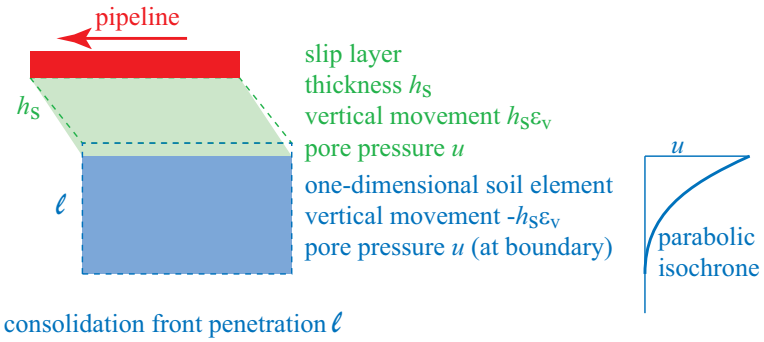

Fig. 2: Pipeline, interface and soil beyond

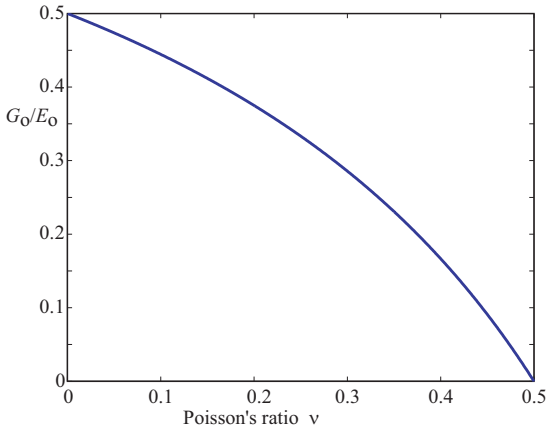

Fig. 3: Poisson's ratio and modulus ratio G_o/E_o.

gradient into the underlying soil. As time goes by the pore pressure at the interface reduces but the compression of the interface layer increases. We know that $\tilde{u} \leq 1$ since the pore pressure u cannot exceed the total normal stress q. This in turn implies a constraint that $\tilde{\psi} \leq 1$. The limiting value of pore pressure in undrained shearing is $E_o\psi$ so that for $\tilde{\psi} < 1$ the maximum value $\tilde{u} = \tilde{\psi} < 1$.

3. Stress:strain response

Next a hyperbolic relationship between mobilisation of shear stress ratio $\mu = \tau/\sigma'$ and strain γ is introduced:

$$\frac{\mu}{\mu_f} = \frac{G_o\gamma}{q\mu_f + G_o\gamma} \quad \tilde{\mu} = \frac{\tilde{\gamma}}{1+\tilde{\gamma}} \tag{3}$$

where μ_f is the ultimate stress ratio and G_o is an initial shear stiffness which might be related to E_o through some sort of Poisson's ratio (Fig 3):

$$\frac{G_o}{E_o} = \frac{E}{2(1+\nu)}\frac{(1+\nu)(1-2\nu)}{E(1-\nu)} = \frac{(1-2\nu)}{2(1-\nu)} \tag{4}$$

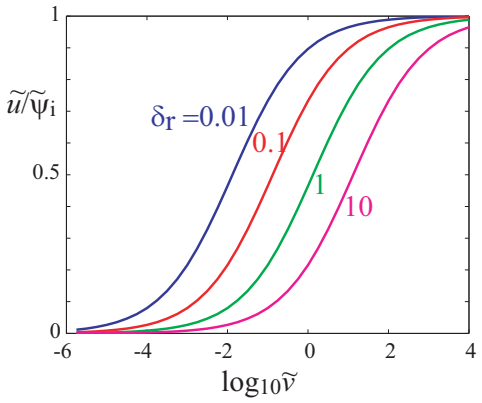

Fig. 4: Normalised pore pressure $\tilde{u}/\tilde{\psi}$ and velocity $\tilde{v}$

and a normalised shear strain emerges: $\tilde{\gamma} = G_o\gamma/\mu_f q$ where $\mu_f q/G_o$ is the elastic strain to reach the failure shear stress; and $\tilde{\mu} = \mu/\mu_f$. The current shear stress τ is proportional to current effective stress $q - u$:

$$\tau = \mu(q-u) \Rightarrow \tilde{\tau} = \tilde{\mu}(1-\tilde{u}) = \frac{\tilde{\gamma}(1-\tilde{u})}{1+\tilde{\gamma}} \tag{5}$$

with $\tilde{\tau} = \tau/\mu_f q$.

We have defined 'dimensionless' strain and time. Displacement $\delta = \gamma h_s$ and velocity $v = \delta/t$ so that $\tilde{\delta} = \delta G_o/h_s\mu_f q$ and $\tilde{v} = vG_o h_s/\mu_f q c_v$ so that $\tilde{v} = \tilde{\delta}/\tilde{t}$ and also $\tilde{\gamma} = \tilde{\delta} = \tilde{v}\tilde{t}$. The displacement is scaled not with the thickness of the slip layer h_s but with the displacement matching the elastic shear strain at failure. The velocity of sliding is scaled with this displacement and with a time emerging from the consolidation process. For a given displacement $\tilde{\delta}_r$, $\tilde{t} = \tilde{\delta}_r/\tilde{v}$ and

$$\frac{\tilde{u}}{\tilde{\psi}_i} = \frac{1}{1+\sqrt{4\tilde{\delta}_r/3\tilde{v}}} \tag{6}$$

and $\tilde{u}/\tilde{\psi}_i$ is plotted as a function of $\tilde{v}$ for $\tilde{\delta}_r = 0.01$, 0.1, 1, 10 in Fig 4.

The shear stress $\tilde{\tau}$ is plotted as a function of $\tilde{t}$ for different $\tilde{v} = 0.001$, 0.01, 0.1, 1, 10, 100 in Fig 5:

$$\tilde{\tau} = \frac{\tilde{v}\tilde{t}(1+\sqrt{4\tilde{t}/3}-\tilde{\psi}_i)}{(1+\tilde{v}\tilde{t})(1+\sqrt{4\tilde{t}/3})} \tag{7}$$

All the curves converge (in the logarithmic plot, Fig 5) as the strain increases - but of course failure $\tau = \tau_f$ can only be attained at infinite strain. The shear stress $\tilde{\tau}$ is also shown as a function of shear strain $\tilde{\gamma} = \tilde{v}\tilde{t}$ for the same values of $\tilde{v}$ (Fig 6). The curves are plotted for $\tilde{\psi}_i = 0.4$.

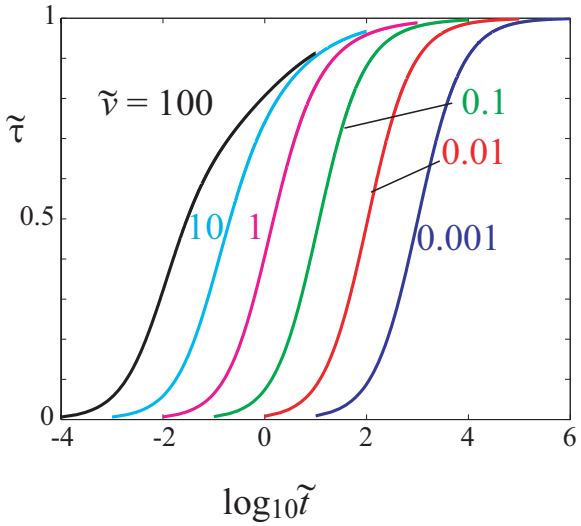

Fig. 5: Normalised shear stress and time

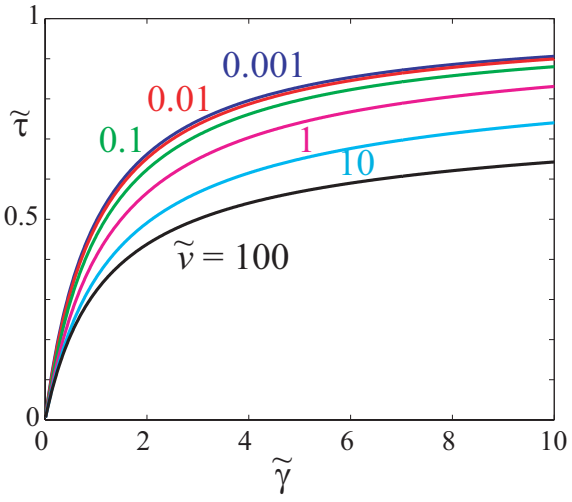

Fig. 6: Normalised shear stress and strain

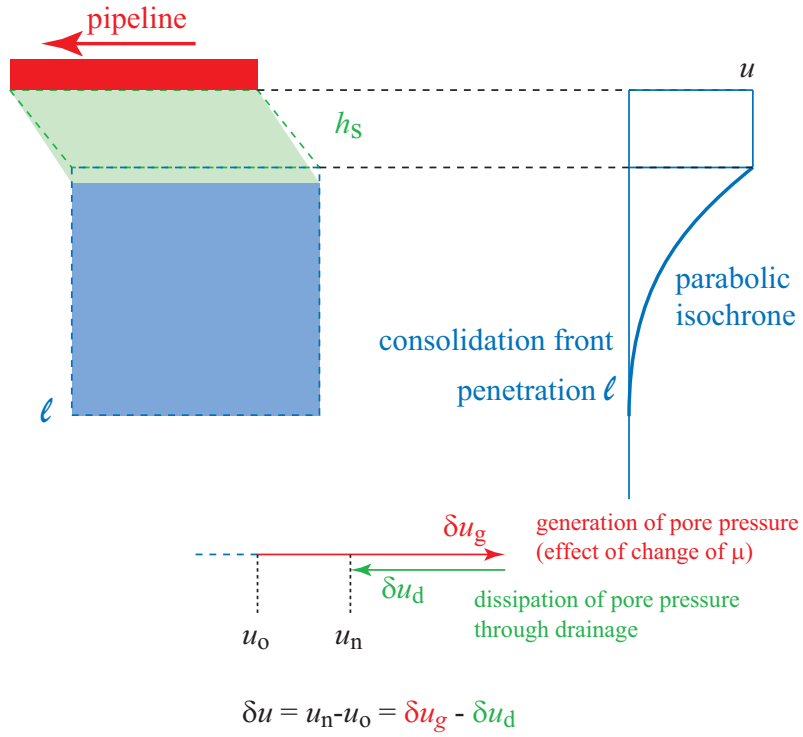

Fig. 7: Parabolic isochrone for pore pressure dissipation

Effect of strain rate

Observations at all scales suggest a dependence of resistance to shearing on the rate of shearing above that expected from the drainage and consolidation properties of the boundary between the sliding layer and the underlying soil. There are three timescales involved in the problem: one concerned with the rate of shearing, one concerned with the consolidation properties of the underlying sediment c_v, and the third concerned with the effect of strain rate on the constitutive response - the viscous properties of the soil.

We return to the problem analysed in the previous section but now include the variation of pore pressure. The pore pressure in the interface layer of thickness h_s is u (Fig 7): during any time increment, some of the potential pore pressure generation δu_g is dissipated δu_d through drainage into the underlying soil. The parabolic isochrone of pore pressure in the underlying soil has pore pressure magnitude u at the surface (boundary with the slip layer) and extends to a depth ℓ. The problem is evidently a little more complicated than the analysis of a typical load increment in an oedometer because we are concerned with events happening during a certain time increment δt in the history of the process of shearing. There are three unknowns: $\delta\varepsilon_v$ the compression of the slip layer; δu the eventual change in pore pressure in the slip layer; and ℓ the depth to which the parabolic

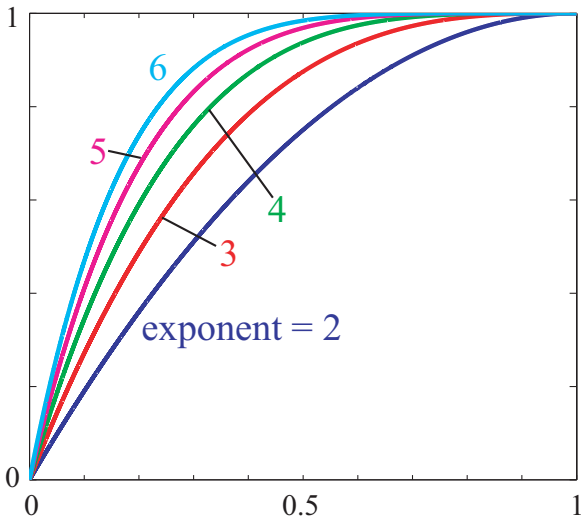

Fig. 8: Effect of value of exponent in (8) on shape of isochrone.

iscohrone extends into the soil. We have to ensure compatibility between three governing physical mechanisms: the mechanical response of the sheared soil; the flow of water across the boundary; and the expansion of the underlying soil to maintain the overall constant volume condition. The last two are the product of the parabolic isochrone; the first is the product of the constitutive model for the shearing soil.

1. Parabolic (or higher order) isochrones?

The choice of a parabolic shape for the isochrone is arbitrary: we could choose a more general power law relationship for the shape of the isochrone, and then generalise the expressions that have been obtained for the analysis of the build-up of pore pressure in the interface. For a power law with exponent n, the area under the convex face of the curve as a proportion of the area of the enclosing rectangle, representing the change in effective stress is $1/n + 1$:

$$\int_0^1 x^n \mathrm{d}x = \frac{1}{n+1} \tag{8}$$

and the slope of the tangent at $x = 1$ as a proportion of the diagonal of the enclosing rectangle, representing the flow rate across the boundary, is $1/n$:

$$\left.\frac{\mathrm{d}\left(x^n\right)}{\mathrm{d}x}\right|_{x=1} = n \tag{9}$$

We might choose to replace the parabolic isochrones with higher exponent curves - thus recognising that the tail of penetration of the consolidation front into the underlying soil under the steadily increasing load might be longer than for an instantly applied load (Fig 8). The factor 3/2 becomes $(n + 1)/n$. However, it

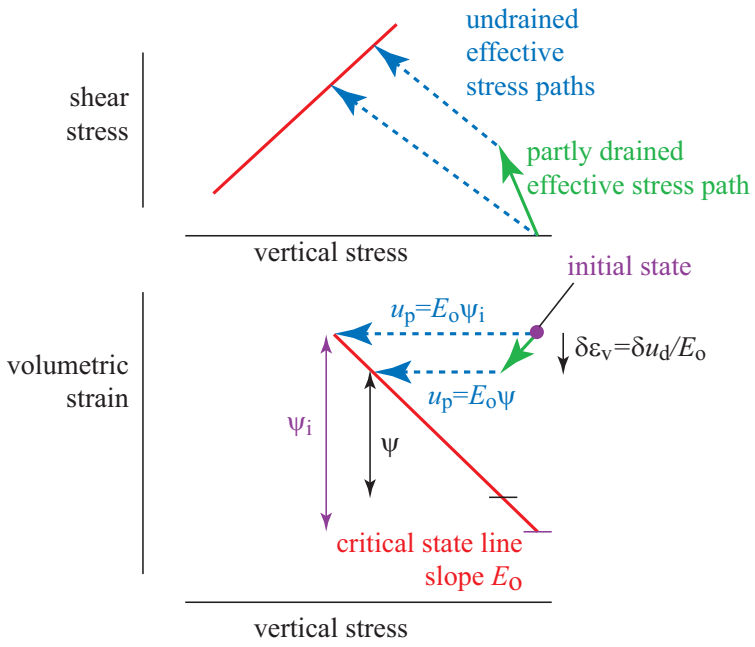

Fig. 9: Partial consolidation and critical state line.

turns out that, while the shape of the isochrone will affect the depth ℓ to which it reaches: $\ell \propto \sqrt{[n(n+1)]}$ the value of u is less influenced.

2. Rate-dependent constitutive model

A rather basic soil model is proposed with a few clear elements which can be readily modified in order to change the response. This is an extension of the shearing model described in (3). Incrementally:

$$\delta\tilde{\mu} = \frac{1}{(1+\tilde{\gamma})^2}\delta\tilde{\gamma} = (1-\tilde{\mu})^2\delta\tilde{\gamma} \tag{10}$$

In the absence of pore pressure the shear strength $\tau_f = \mu_f q$ so that $\mu_f q/G_o$ is the elastic strain required to reach the failure shear stress at constant normal stress q. Alternatively, when $\tilde{\gamma} = 1$, $\tilde{\mu} = 1/2$. The shear stress is $\tau/\mu_f q = \tilde{\tau} = \tilde{\mu}(1-\tilde{u})$. The shear stress is scaled with $\tau_f = \mu_f q$ which is the eventual shear stress reached when consolidation has removed all pore pressure generated through suppressed dilation.

The influence of rate of shearing on strength is achieved by making the frictional strength coefficient μ_f depend on strain rate $\dot{\gamma} = v/h_s$:

$$\mu_f = \mu_{fo}\left[1 + \zeta \log_{10}\frac{\dot{\gamma}}{\dot{\gamma}_r}\right] \quad \Rightarrow \quad \tilde{\mu_f} = 1 + \zeta \log_{10}\frac{\dot{\tilde{\gamma}}}{\dot{\tilde{\gamma}}_r} \tag{11}$$

If we adopt a typical rule of thumb that the strength increases by 10% for each log cycle of increase in strain rate, then $\zeta \sim 0.1$. If we impose a constant strain

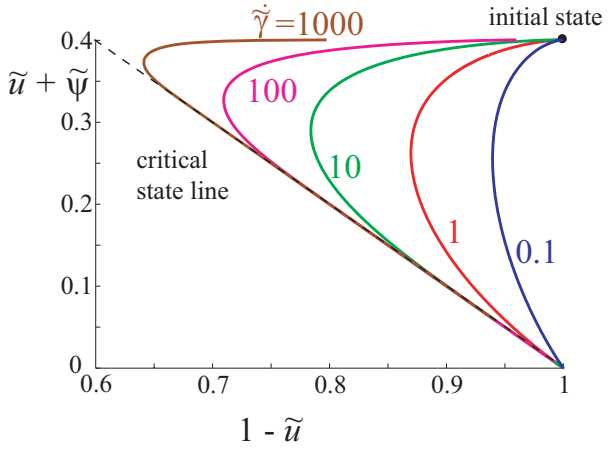

Fig. 10: State paths in compression plane for slip layer.

rate then $\tilde{\mu}_f$ is defined. Over a time step δt, $\delta\gamma = \dot{\gamma}\delta t$ and $\delta\mu$ is then determined from (10). We have added $\tilde{\mu_f} = \mu_f/\mu_{fo}$ and $\dot{\tilde{\gamma}} = \tilde{\gamma}/\tilde{t} = h_s^2 G_o \dot{\gamma}/\mu_f q c_v$. In this final expression. $\mu_f q/G_o$ is the elastic strain to reach the failure stress ratio and c_v/h_s^2 is a reference consolidation time.

We assume again that the critical state line is locally linear in a compression plane with normal stress and vertical (volumetric) strain (Fig 9). We are analysing a partially drained problem so that in any time increment there is some attempt at pore pressure generation through shearing together with some attempt at pore pressure dissipation through consolidation. We require a pore pressure generation model. The simplest assumption would be to propose that the undrained effective stress path is always linear from the present effective stress state to the critical state failure point (Fig 9). The initial stress state at the start of a time increment is $q-u, \mu(q-u)$ and the failure state is $q-u-E_o\psi, \mu_f(q-u-E_o\psi)$. This effectively defines a pore pressure parameter (of the improved type, separating effects of total stress and dilatancy):

$$a = -\frac{\delta\sigma'}{\delta\tau} = \frac{E_o\psi}{\mu_f(q-u-E_o\psi) - \mu(q-u)} = \frac{E_o\psi}{(\mu_f-\mu)(q-u) - \mu_f E_o\psi} \tag{12}$$

or

$$\tilde{a} = a\mu_f = \frac{\tilde{\psi}}{(1-\tilde{\mu})(1-\tilde{u}) - \tilde{\psi}} \tag{13}$$

The pore pressure generation is independent of the strain rate but is dependent on the prior volumetric compression of the interface layer which moves the state of the interface soil closer to the critical state line.

We can link pore pressure generation with increment of stress ratio which is directly dependent on the increment of shear strain. The combination of pore pressure generation δu_g and pore pressure dissipation δu_d gives us an eventual change of pore pressure and change in effective stress $\delta u = \delta u_g - \delta u_d = -\delta\sigma'$.

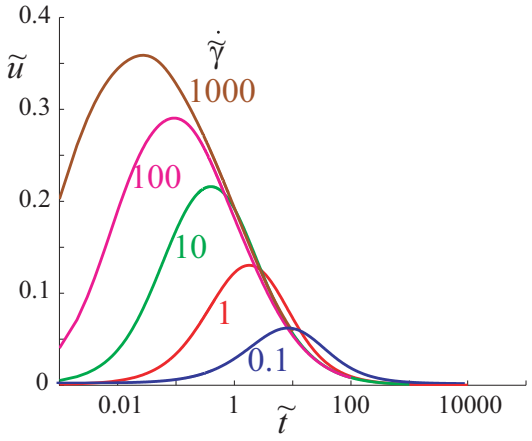

Fig. 11: Variation of pore pressure with time: effect of strain rate.

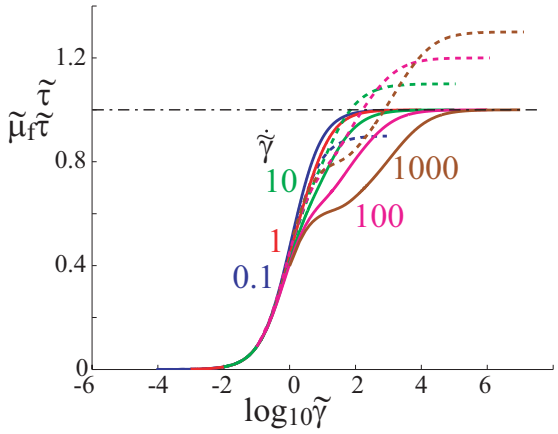

Fig. 12: Variation of $\tilde{\tau}$ (solid line) and $\tilde{\mu}_f\tilde{\tau}$ with $\tilde{\gamma}$: effect of strain rate.

For an increment of stress along the partially drained effective stress path, $\tau = \mu\sigma'$ so that

$$\delta\tau = \sigma'\delta\mu + \mu\delta\sigma' = \sigma'\delta\mu + \mu(\delta u_d - a\delta\tau) \Rightarrow \delta\tau = \frac{\sigma'\delta\mu + \mu\delta u_d}{1 + a\mu} \tag{14}$$

Since $\sigma' = q - u$

$$\delta u_g = \frac{a(\sigma'\delta\mu + \mu\delta u_d)}{1 + a\mu} \Rightarrow \delta\tilde{u}_g = \tilde{a}\frac{(1-\tilde{u})\delta\tilde{\mu} + \tilde{\mu}\delta\tilde{u}_d}{1 + \tilde{a}\tilde{\mu}} \tag{15}$$

with $\delta\tilde{\mu}$ from (10), $\delta\tilde{\gamma} = \dot{\tilde{\gamma}}\delta\tilde{t}$, $\tilde{u} = u/q$, $\tilde{\psi} = E_o\psi/q$.

The change in state parameter ψ arises from the generated change in pore pressure δu_g; the dissipation merely moves the state parallel to the critical state line

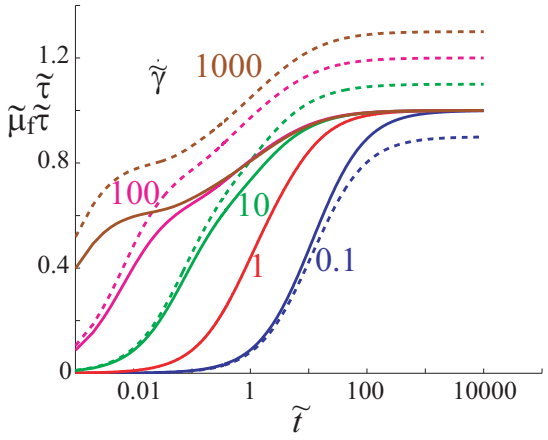

Fig. 13: Variation of $\tilde{\tau}$ (solid line) and $\tilde{\mu}_f\tilde{\tau}$ with $\tilde{t}$: effect of strain rate.

(Fig 9):

$$\delta\psi = -\frac{\delta u_g}{E_o} \quad \Rightarrow \quad \delta\tilde{\psi} = -\delta\tilde{u}_g = -(\delta\tilde{u} + \delta\tilde{u}_d) \tag{16}$$

There are three volumes which must be identical: the volume expelled from the interface layer; the volume transmitted through flow at the boundary between the interface layer and the underlying soil; and the volume change of the underlying soil resulting from the increase of pore pressure. All three components are controlled by the actual changes in pore pressure δu and in the geometry of the parabolic isochrone describing the penetration of the pore pressure into the underlying soil.

The compression of the interface layer is:

$$h_s\delta\varepsilon_v = h_s\delta u_d/E_o \tag{17}$$

The flow rate across the boundary must produce a volume change matching the compression of the interface layer of thickness h_s:

$$h_s\delta\varepsilon_v = \frac{2uk}{\ell\gamma_w}\delta t \tag{18}$$

$$\delta\tilde{u}_d = 2\frac{\tilde{u}}{\tilde{\ell}}\delta\tilde{t} \tag{19}$$

This must also match the expansion that can be computed from the area above the isochrone in the underlying soil:

$$h_s\delta\varepsilon_v = \frac{\delta(u\ell)}{3E_o} = \frac{u\delta\ell + \ell\delta u}{3E_o} \Rightarrow \delta\tilde{\ell} = 6\frac{\delta\tilde{t}}{\tilde{\ell}} - \tilde{\ell}\frac{\delta\tilde{u}}{\tilde{u}} \tag{20}$$

In sequence of operation: $\delta\tilde{t} \rightarrow \delta\tilde{\gamma} \rightarrow \delta\tilde{\mu}$ (10); $\delta\tilde{t} \rightarrow \delta\tilde{u}_d$ (19); $\delta\tilde{\mu}$ and $\delta\tilde{u}_d \rightarrow \delta\tilde{u}_g$ (15); $\delta\tilde{u} \rightarrow \delta\tilde{\ell}$ (20);$\delta\tilde{u}_g \rightarrow \delta\tilde{\psi}$ (16).

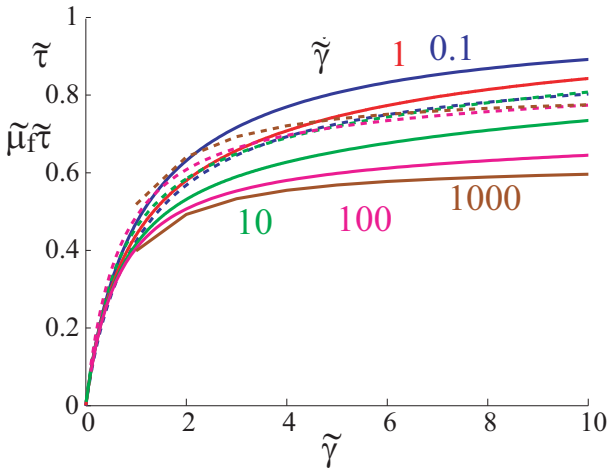

Fig. 14: Variation of $\tilde{\tau}$ (solid line) and $\tilde{\mu}_f\tilde{\tau}$ with $\tilde{\gamma}$: effect of strain rate.

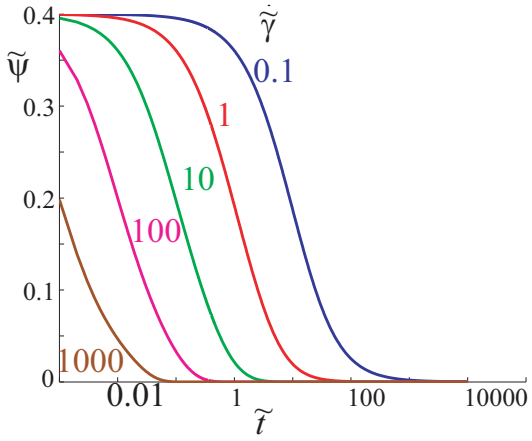

Fig. 15: Variation of $\tilde{\psi}$ with $\tilde{t}$: effect of strain rate.

$$\frac{\mathrm{d}\tilde{u}}{\mathrm{d}\tilde{t}} = \frac{\tilde{a}\tilde{\ell}(1-\tilde{u})(1-\tilde{\mu})^2\dot{\tilde{\gamma}} - 2\tilde{u}}{\tilde{\ell}(1+\tilde{a}\tilde{\mu})} \tag{21}$$

and

$$\frac{\mathrm{d}\tilde{\psi}}{\mathrm{d}\tilde{t}} = -\frac{\mathrm{d}\tilde{u}_g}{\mathrm{d}\tilde{t}} = \tilde{a}\frac{(1-\tilde{u})(1-\tilde{\mu})^2\dot{\tilde{\gamma}} + 2\tilde{\mu}(\tilde{u}/\tilde{\ell})}{1+\tilde{a}\tilde{\mu}} \tag{22}$$

$$\frac{\mathrm{d}\tilde{\ell}}{\mathrm{d}\tilde{t}} = \frac{6}{\tilde{\ell}} - \frac{\tilde{a}\tilde{\ell}}{\tilde{u}}\frac{(1-\tilde{u})(1-\tilde{\mu})^2\dot{\tilde{\gamma}}}{1+\tilde{a}\tilde{\mu}} + \frac{2}{1+\tilde{a}\tilde{\mu}} \tag{23}$$

Then finally the shear stress that is mobilised is $\tau = \mu(q-u)$ or $\tilde{\tau} = \tilde{\mu}(1-\tilde{u})$. The normalisations for the various variables that have been introduced are: $\tilde{u} = u/q$, $\tilde{t} = c_v t/h_s^2$, $\tilde{\mu} = \mu/\mu_f$, $\tilde{\ell} = \ell/h_s$, $\tilde{\gamma} = G_o\gamma/\mu_f q$, $\dot{\tilde{\gamma}} = h_s^2 G_o\dot{\gamma}/\mu_f q c_v$, $\tilde{\psi} = E_o\psi/q$, $\tilde{\tau} = \tau/\mu_f q$.

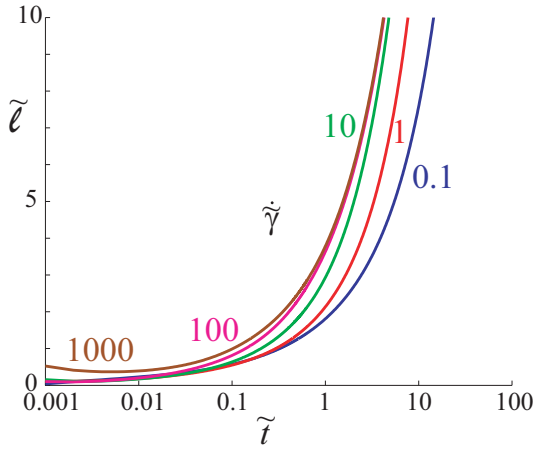

Fig. 16: Variation of $\tilde{\ell}$ with time.

The governing equations have been solved using a Runge-Kutta 4th order solution procedure, with a time step $\delta\tilde{t} = 0.001$.

Results and discussion

One set of parametric studies has varied the constant strain rate $\dot{\tilde{\gamma}}$ with constant initial state parameter $\tilde{\psi}_i = 0.4$. It is instructive to plot the paths followed in the compression plane $(1-\tilde{u}), (\tilde{u}+\tilde{\psi})$. As the strain rate increases so the initial response becomes more significantly undrained and the pore pressure builds up. However, the pore pressure eventually dissipates entirely bringing the state of the soil in the slip layer down the critical state line in the compression plane (up the critical state line in the stress plane) so that the eventual strength is inevitably $\tilde{\tau} = 1$ or $\tau = \mu_f q$. Because $\tilde{\tau}$ is scaled with μ_f and since the strain rate affects only μ_f the eventual value of $\tilde{\tau}$ is independent of strain rate. The pore pressure varies with time as shown in Fig 11 - the maximum pore pressure is dependent on the strain rate. The variation of shear stress - shown as both $\tilde{\tau}$ and $\tilde{\mu}_f\tilde{\tau}$ - with shear strain is shown in Fig 12 and with time in Fig 13: this latter figure is equivalent to Fig 5 but with allowance made for the variation of pore pressure. The variation of $\tilde{\tau}$ with $\tilde{\gamma}$ with the strain plotted on a linear axis is shown in Fig 14: this figure is equivalent to Fig 6. The variation of state variable $\tilde{\psi}$ with time is shown in Fig 15. The variation of $\tilde{\ell}$ with time is shown in Fig 16. Evidently the distance of penetration of the consolidation front into the soil beneath the slip layer becomes very large as the pore pressure falls towards zero but the product $\tilde{u}\tilde{\ell}$ has to be able to provide the necessary effective stress and volume changes.

The analysis has been presented in its barest form with the separate contributions to pore pressure generation and dissipation clearly identified. The dissipation is entirely controlled by the parabolic isochrone of pore pressure variation within the soil beneath the slip layer. The generation is controlled by the pore pressure parameter $\tilde{a}$. Pore pressure generation is seen as a reaction of a soil

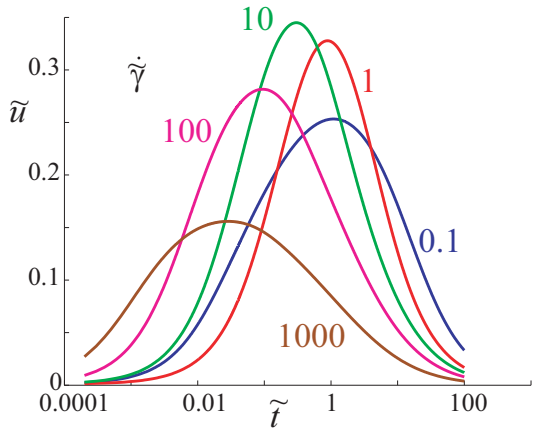

Fig. 17: Variation of $\tilde{u}$ with $\tilde{t}$: inclusion of effect of strain rate on initial $\tilde{\psi}$.

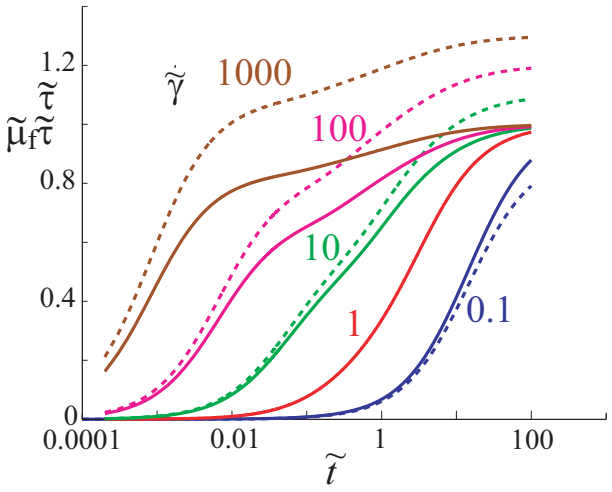

Fig. 18: Variation of $\tilde{\tau}$ (solid line) and $\tilde{\mu}_f\tilde{\tau}$ with $\tilde{t}$: inclusion of effect of strain rate on initial $\tilde{\psi}$.

which wants to change in volume while being constrained to maintain a constant volume either by an external prevention of drainage (closure of a tap on a triaxial apparatus) or by an inability of the permeability to permit the fluid flow and volume change which would be required to keep up with the rate of shearing of the soil. As the state of the soil approaches the critical state the desire to change in volume disappears and the mechanism of pore pressure dissipation will triumph over the now completed mechanism of pore pressure generation. The critical state provides a limit on the magnitude of pore pressure that can be generated so that the simple linear effective stress path that is used to compute the pore pressure parameter at each step (Fig 9) may not provide a bad representation of the pore pressure generation.

Rate of straining has been permitted only to change the maximum stress ratio μ_f. An increase in strain rate could lead to a raising of the critical state line in the

compression plane, with shearing continuing at a lower density, higher void ratio. This is equivalent to reducing the initial value of state variable $\tilde{\psi}_i$ with strain rate with the evident consequence that the pore pressure cannot rise so much and that the shear stress at any particular time will be consequently higher - there will therefore be two reinforcing effects on the shear stress that is generated although the eventual strength once pore pressure dissipation is complete should not change. Typical results are shown in Figs 17 and 18 assuming that $\dot{\tilde{\gamma}} = 0.1$, 1, 10, 100, 1000; that $\tilde{\psi}_i = 0.99$, 0.79, 0.59, 0.39, 0.19 correspondingly and that $\zeta = 0.1$, as previously. The pore pressures are shown in Fig 17 and the shear stresses in Fig 18.